LITERATURE REVIEW: INFLUENCE OF HEAT TREATMENTS ON ALUMINIUM

Abstract

Microstructure, defects such as porosities and residual stresses of alloy $AlSi_7Mg_{0,6}$ made by Powder Bed Fusion additive manufacturing presents significant differences as compared to material produced by casting technologies. The high cooling rate induces singular microstructures difficult to assess with classical thermodynamic diagrams. The aim of this literature review is to establish the state of the art in term of proposed thermal treatments; the consequence will be to assess what are the missing information to understand the influence of these treatments on microstructure, defects and residual stresses of the material.

DATE : 12/02/2019

REFERENCE : LIV-M-031-L6-480

Author(s)	*Function(s) & name(s)*	*Research Engineer*	*Jules BAROT*
		Research Engineer	*Jean-Marc AGULLO*
Checker(s)	*Function(s) & name(s)*	*Research Engineer*	*Jonathan HUGUES*
		Project Manager	*Céline LARIGNON*
		Quality Manager	*Stephane BENAZET*
Approver	*Function & name*	*R&T Manager*	*Simon PERUSIN*

Table of Contents

1 Accronyms 4
2 Introduction and objectives 4
3 Precipitation hardening mechanism 5
4 Microstructure evolution 10
5 Porosity 26
6 DTA/DSC profiles 29
7 Hardness 33
8 Tensile Properties 40
9 Fatigue behaviour 53
10 Impact resistance 62
11 Conclusion 63
12 Suggestion for new heat treatment 63
13 References 65

Revision Table

Issue	Date	modified §	Evolution summary	Modified by
1	12/02/2019	Creation		

1 Accronyms

LBM: Laser Beam Melting

LBMed: samples or parts manufactured by LBM

SRT: Stress Relief Treatment

HIP: Hot Isostatic Pressing

HIPed: samples or parts submitted to HIP

SHT: Solution Heat Treatment

AA: Artificial Ageing

2 Introduction and objectives

The objective of this literature review is to present available data concerning heat treatment of AlSi7Mg0.6 manufactured by LBM. At the present time, a classical thermal treatment, developed in the forties on cast alloys, is applied on parts produced by LBM by industrial people. Taking into account literature data, the objective of the present document is to suggest possible way to optimize thermal treatment and associated mechanical properties.

The current conventional treatment is composed of the following steps:

Stress Relief Treatment (SRT): 300°C – 2 hours

The SR is performed at the end of the manufacturing when the parts are still fixed on the base plate. After the SR, the support can be removed and no deformation is expected due to presence of residual stresses. This SR treatment is also performed on cast alloys just after the casting step.

Hot Isostatic Pressing (HIP): 500°C – 130 min

Like for cast materials, parts are generally submitted to HIP to reduce the size and the number of internal porosities. The objective is to improve Fatigue properties by limitation of sub-surface porosities which are detrimental to life time when the parts are submitted to cyclic stresses.

T6 treatment (AMS 2771)

- Solution Heat Treatment: 540°C – (4-8) hours,
- Water Quench: (20-30)°C,
- Artificial Ageing: 160°C – (2-10) hours.

Different improvements can be proposed by IRT for optimization of the following points:

1. Microstructure: consequence of the combination of each step (SHT, HIP, T6)
    a. To get a microstructure as homogeneous as possible,
    b. To get optimal repartition of semi-coherent precipitates responsible of the part hardening,
    c. To reduce microstructure disparities which could be responsible of a strong anisotropy in term of mechanical properties,
    d. To limit size and number of porosities which could be detrimental to Fatigue properties.
2. Deformation: consequence of HIP constraints and Quench effect
    a. To limit the amount of manufacturing internal stresses,
    b. To limit necessity of complex tooling and risk of shocks during HIP & quench step.
3. Mechanical properties: consequence of T6 treatment parameters
    a. To get an optimized set of parameters to maximize static properties,
    b. To get an acceptable elongation (> 5%) to minimize risks of parts failure in case of overloads,
    c. To maintain acceptable Fatigue properties at least comparable to the ones of cast materials.
4. Cost: consequence of the combination of each step (SHT, HIP, T6)
    a. To reduce the thermal treatment disadvantages in term of cost and cycle time.

The influence of each thermal treatment steps on the properties detailed here above will be developed in the present document.

3 Precipitation hardening mechanism

AlSi7Mg0.6 (AS7G06) is known as a precipitation hardening alloy. Its chemical composition gives its ability to form precipitates when heat treated in the right conditions, leading to improved mechanical properties.

In precipitation hardening, a conventional processed alloy is heated to a high enough temperature to solve a significant amount of an alloying element into solid solution. It is then rapidly cooled (quenched) to room temperature, maintaining alloying elements in the solution. On reheating to an intermediate temperature, the host metal rejects the alloying element in the form of fine semi-coherent precipitates which impede the movement of dislocations. As a consequence, these fine semi-coherent precipitate particles act as barriers to the motion of dislocations and provide resistance to slip, thereby increasing the strength and hardness [1].

Precipitation hardening is also known as age hardening or ageing, to indicate that the resulting strength increase develops with time.

A portion of a phase diagram for an alloy system that has the characteristics required for precipitation hardening is shown in Figure 1. Note that the solvent metal at the left-hand edge of the diagram can absorb much more of the solute metal at elevated temperature than it can at room temperature. When the alloy is heated to the solution heat treating temperature and held for a sufficient length of time, the solvent metal absorbs some of the solute metal. Then, when it is rapidly cooled to room temperature, atoms of the solute metal are trapped as a supersaturated solid solution in the solvent metal. On reheating to an intermediate ageing temperature, the supersaturated solution precipitates very fine particles that act as barriers to dislocation movement. Note the effects of different ageing temperatures, shown in Figure 1. If the metal is aged at too low a temperature (*T1* in figure 1), the precipitation process will be incomplete, and the desired strength will not be achieved, a condition known as underageing. On the other hand, ageing at too high a temperature (*T4* in figure 1) also results in lower-than-desired strength because the precipitate particles coarsen, and the alloy is now said to be overaged. Commercial heat treatments are closer to *T2 and T3* (in figure 1), in which the optimal strength can be obtained in a reasonable ageing time (See Figure 2). The alloy used in this example is one that requires classically artificial or elevated-temperature ageing. Some alloys will age satisfactorily at room temperature, a process called natural ageing. The typical ageing curve for T6 treatment generally used for AlSi7Mg0.6 is given in Figure 3 [1].

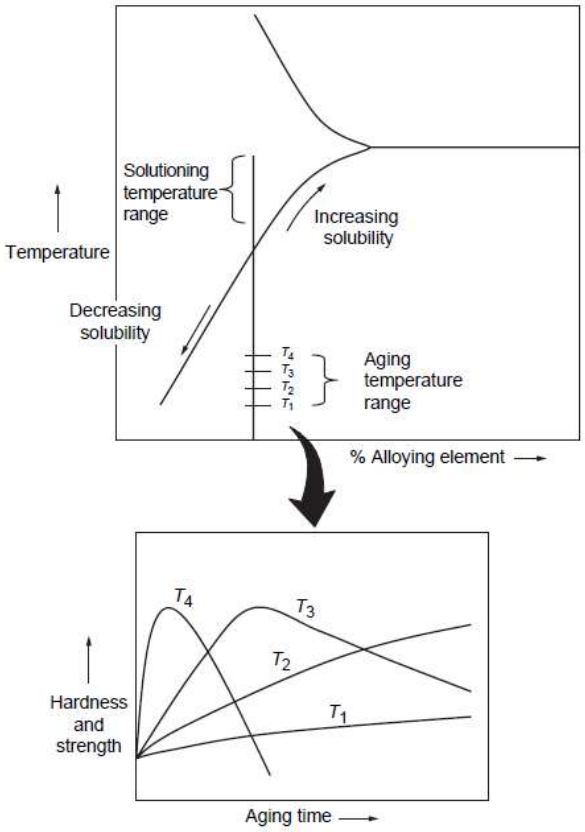

Figure 1: Partial binary aluminium phase diagram and typical precipitation-hardening heat treatment for aluminium [1]

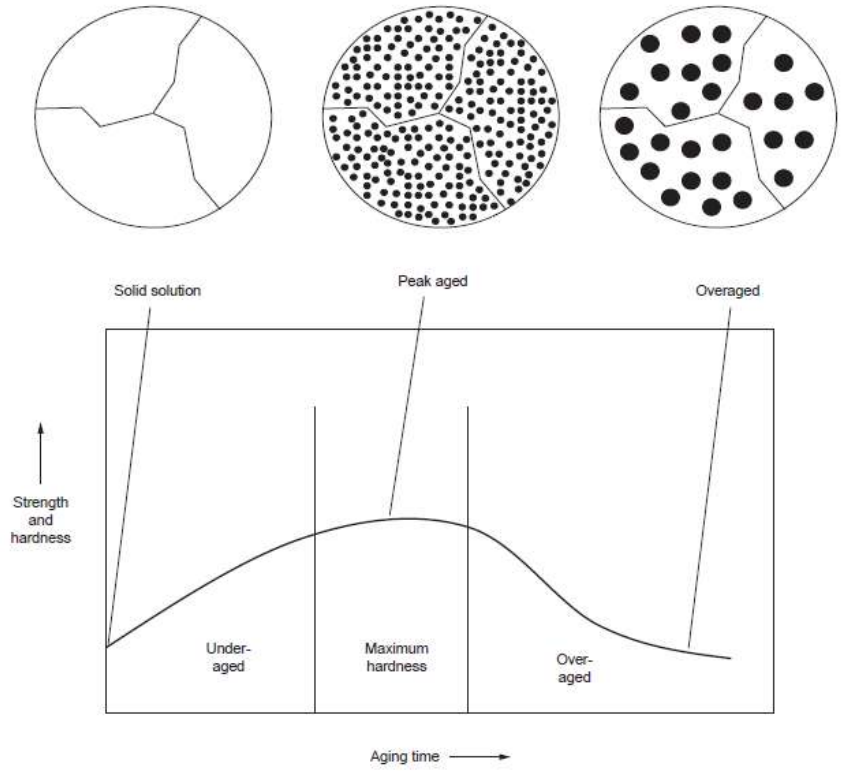

Figure 2: Typical ageing curve for aluminium alloys [1]

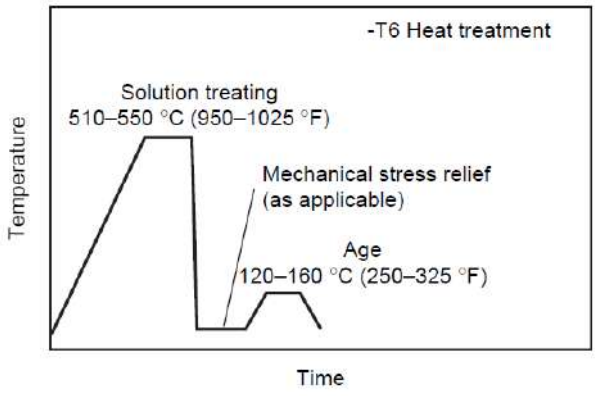

Figure 3: T6 treatment thermal cycle [1].

Note: the possibility to make a mechanical stress relief (Figure 3) is applicable only to wrought products and not to parts produced by additive manufacturing.

The ageing sequence of AlSi7Mg0.6 is given in Figure 4. Within the first stage of precipitation, solute atoms rearrange into very small clusters of atoms, called Guinier-Preston zones. These clusters have been observed independently by Guinier and Preston in 1938 using X-ray scattering. GP zones for Al-Si-Mg alloys are rod shaped and grow along the three <100> cube directions of the aluminium matrix. These needles are semi-coherent with the matrix (see Figure 5). They are coherent along their length which is along an aluminium <100> direction but there is a considerable mismatch within the direction perpendicular to the “cylindrical” interface between the needles and the matrix, which expands to accommodate it [2].

These needle range between 20 to 100 nm in length and are approximately 6 nm in diameter [3].

As ageing is performed, GP zones will grow and evolve in shape. Further growth of the needles leads to the formation of dislocation loops around them. This indicates that the needles have lost coherency along their length - a new

intermediate phase is formed (β'). These rods are still aligned along <100> directions. Even more ageing leads to the nucleation and growth of equilibrium precipitates of Mg_2Si (β). They are in the form of platelets lying in {100] planes [3]. These phases (β' and β) do not improve mechanical properties.

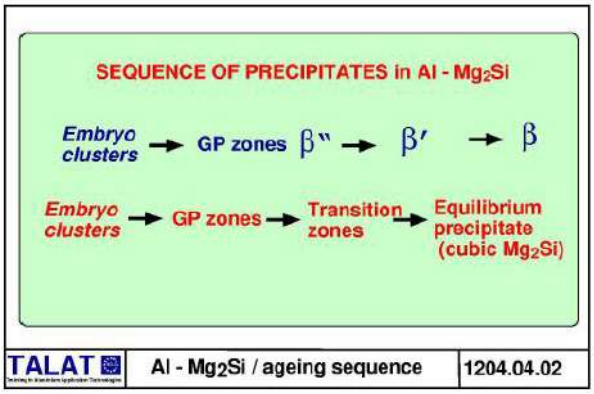

Figure 4: Al – Mg_xSi ageing sequence [2]. The composition of hardening precipitates was detailed in literature by Barlas [4] β'' (Mg_5Si_6) – β' ($Mg_{1,7}Si$) – β (Mg_2Si) – see morphologies in Figures 5 and 6

Due to the size of hardening precipitates, they can be evidenced only by SEM. Different sizes and shapes of precipitates, coming from [2], are showing in Figures 7 to 10.

Other studies relates also the typical size of hardening precipitates: (D. L. Zhang and Zheng 1996) observed β'' and β' precipitates on cast AlSi7Mg0.4 samples after T6 treatment (SHT: 14 h at 540°C / water quench: from 25°C to 95°C / ageing: 6 h at 170°C). β'' precipitates were 3 to 4 nm in diameter and 10 to 20 nm in length. β' precipitates were approximately 15 nm in diameter and 300 nm in length [5].

d

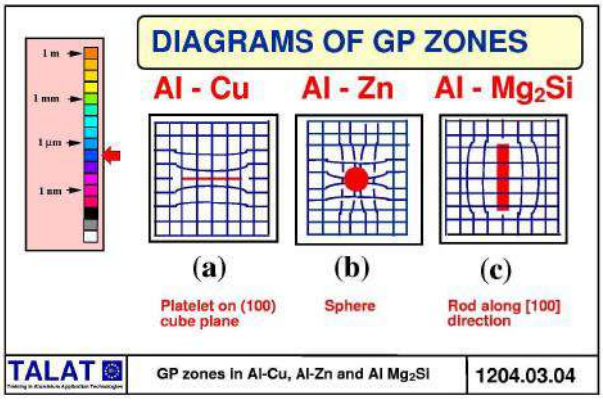

Figure 5: GP zones shapes for different Al-alloys [2]

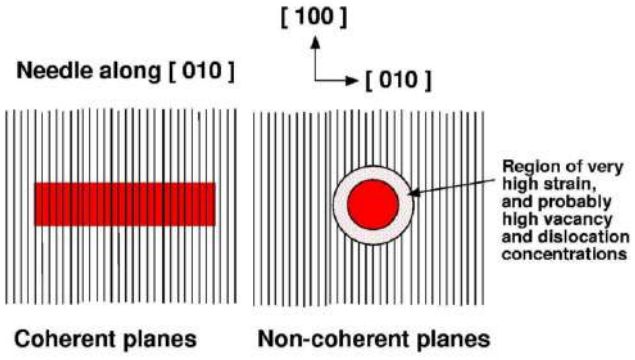

Figure 6: Coherency in a cubic lattice; section of a β'' precipitates [2]

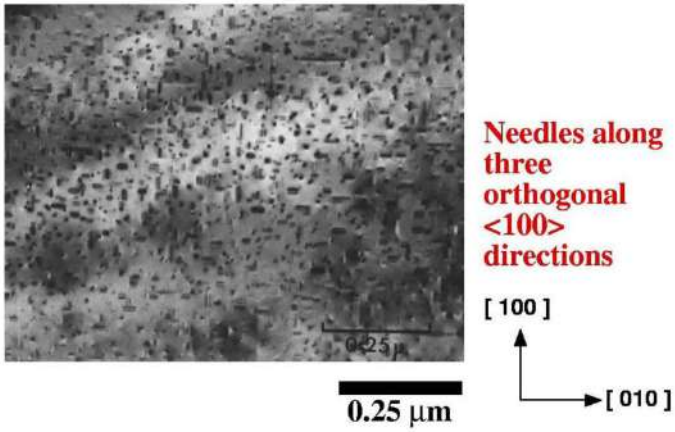

Figure 7: TEM of rod-shaped GP zones in Al-1.2Mg_2Si [2]

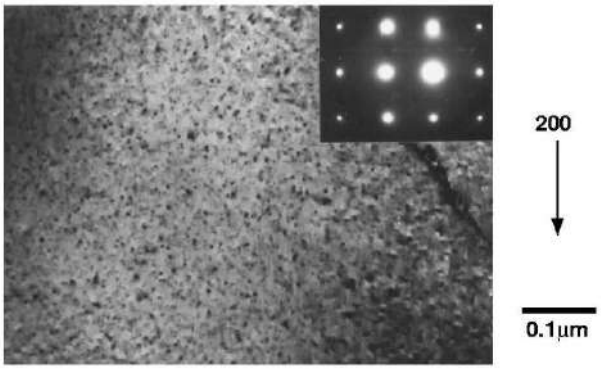

Figure 8: SHT at 530°C, water quenched and 24 h at 175 °C. Peak hardening. Al 6061 [2]

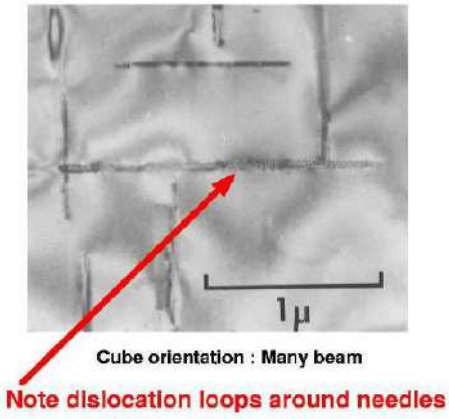

Figure 9: SHT 560 °C, water quench and AA at 250 °C for 30 minutes. Al-1.2wt% Mg_2Si. ϐ' precipitates [2]

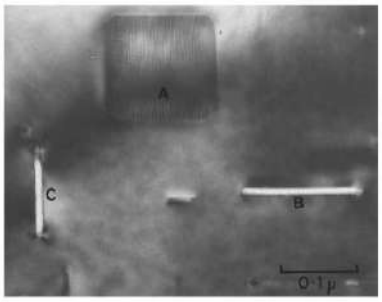

Figure 10: SHT 560 °C, water quench and AA at 250 °C for 120 minutes. Al-1.2wt% Mg_2Si. β precipitates [2]

Precipitation hardening is known from half a century and largely used in the industry. This is why it is generally the treatment of first interest when dealing with Al-Si-Mg alloys made by Laser Beam Melting. However, due to the typical homogeneous microstructure obtained in as-built component, commonly practised T6 may results in a not so much optimised microstructure and thus mechanical properties. The T6 treatment integrates numerous parameters concerning heating, quenching and aging; however, there is not a lot of data in literature to detail clearly what are the influence of each of these T6 parameters on the microstructure of obtained alloys.

4 Microstructure evolution

Fiocchi *et al.* studied the influence of thermal treatment at relevant temperatures identified by DSC analyses [6] on ALSi10Mg made by LBM. In Figure 11 are shown optical SEM micrographs of heat treated samples at 263°C, 294 °C and 320 °C for 30 min and 2 h. It can be observed that at 263 °C, the microstructure does not show significant differences compared to as-built microstructure and still show a cellular microstructure, whereas at 294°C, a sudden change is observed as the Si-enriched network is disrupted and spheroidisation occurs. At 320°C, Si particles coarsening is observed.

Higher temperature than 294 °C did not induce significant changes in the microstructure but in association with time, they still have an influence on the Si particle size as their number decreases and their size increases over time, as shown on Table 1. However, time (in the range tested) does not seem to have an additional significant influence on the microstructure as long as the temperature is lower than 263 °C, indeed for 30 min and 2 h, samples treated at this temperature display the same microstructure.

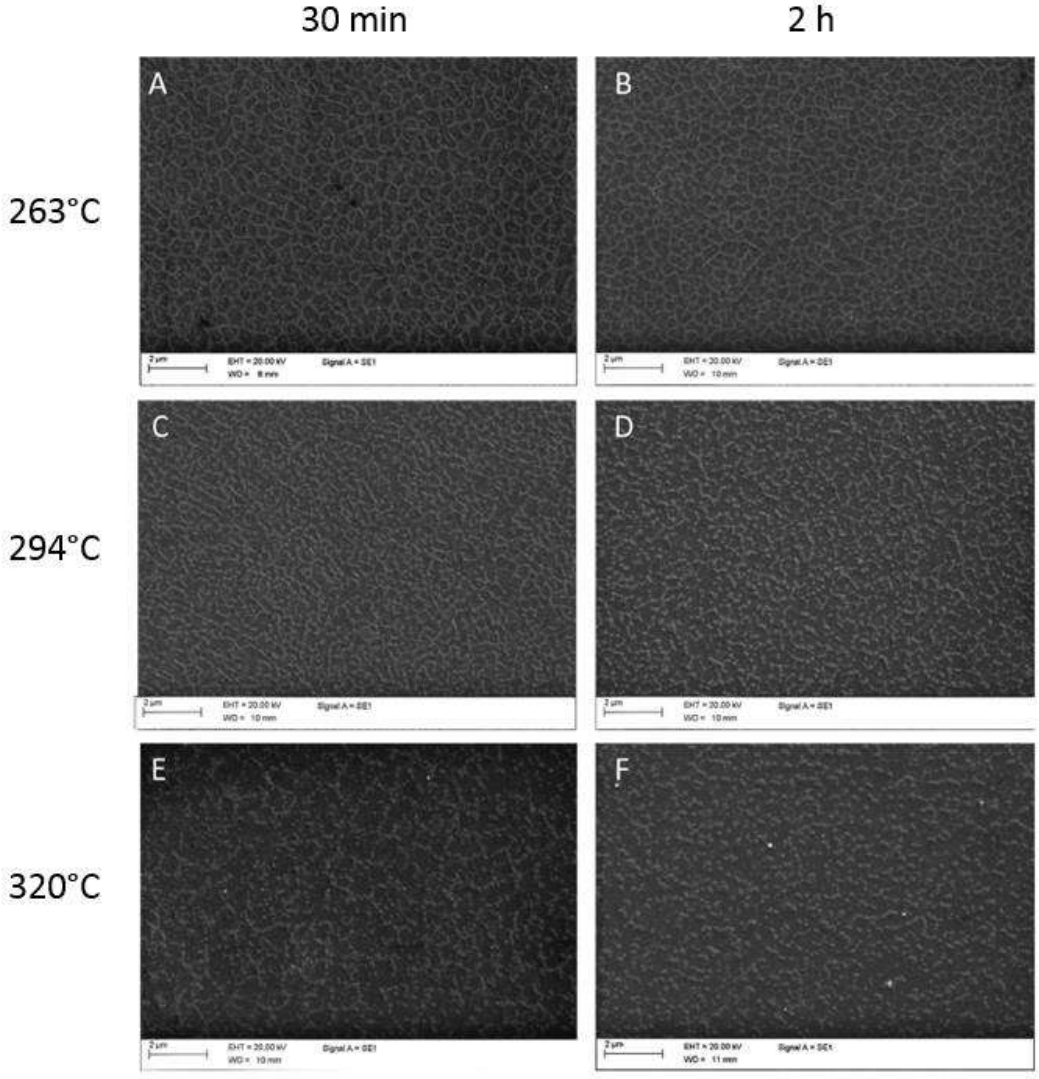

Figure 11: SEM micrographs of LBM built samples after heat treatment for 30 min at 263°C (a), 294 C (c), 320 C (e); after heat treatment for 2 h at 263 C (b), 294 C (d), 320 C (f) [6]

Table 1: Si particles density as function of heat treatment temperature and duration [6]

Treatment temperature	Si particles density (particles/µm²)	
	30 min	2 h
294 °C	13.0	12.0

320 °C	8.2	6.0

Kimura *et al.* [7] studied the influence of various annealing heat treatments (T5: heating without SHT similar to direct aging) at different temperature for a given time (5 h) (A356 alloy made by LBM). Microstructure evolution according to the temperature is presented in Figure 12 and Figure 13. As seen before, no significant change is observed at temperature below 300 C. Between 150 C and 250 C, the cellular microstructure is not changed and only the Si precipitation inside α-Al cells is observed with extremely small particles. On the other hand, at temperatures equal to or greater than 300°C, the cellular morphology is disrupted and Si appears in a form of particles which grow as the temperature is increased. At these temperatures, no differences in microstructure are visible between horizontal and vertical planes.

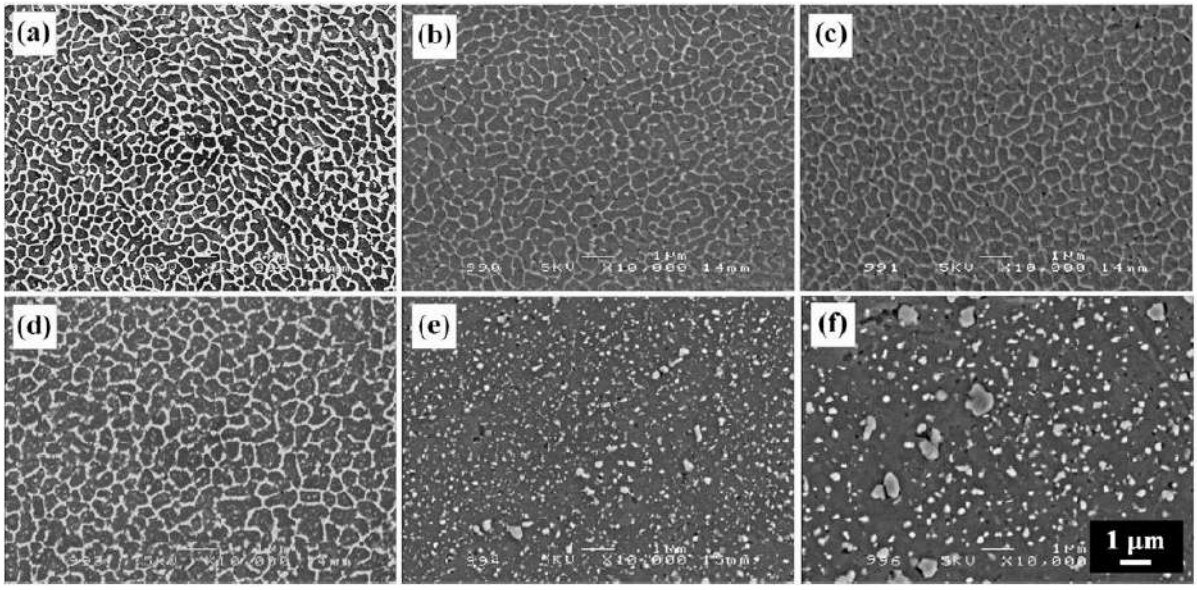

Figure 12: SEM images of the horizontal cross sections of (a) an as-fabricated LBM specimen and T5 LBM specimens annealed for 5 h at b) 150 °C, (c) 200 °C, (d) 250 °C, (e) 300 °C, and (f) 350 °C [7]

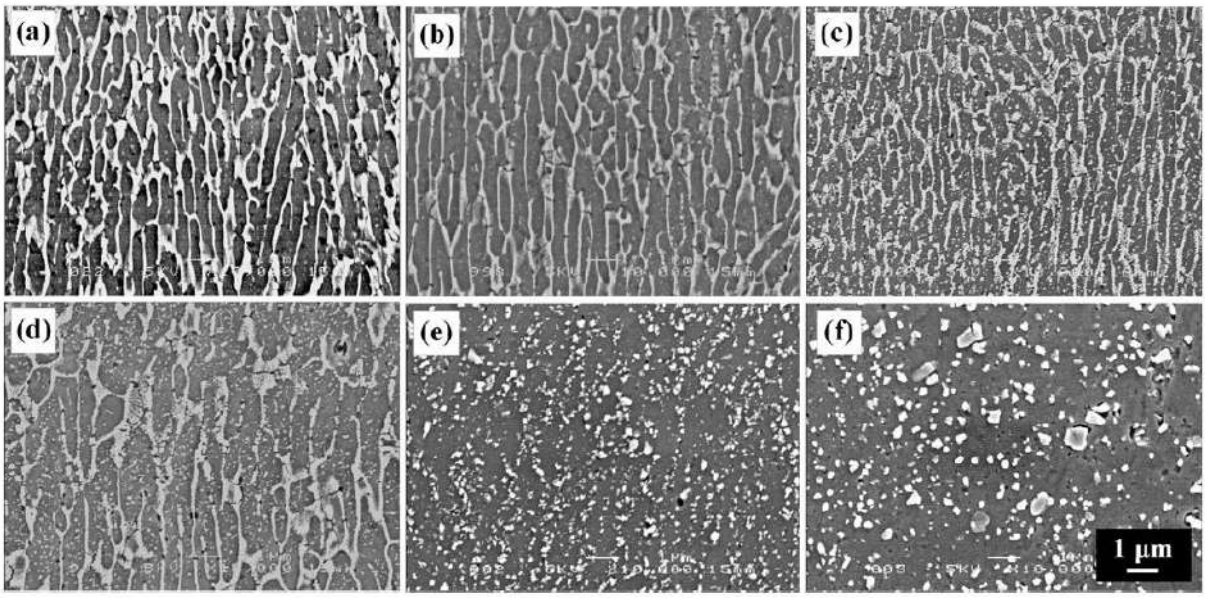

Figure 13: SEM images of the vertical cross sections of (a) an as-fabricated LBM specimen and T5 LBM specimens annealed for 5 h at (b) 150 °C, (c) 200 °C, (d) 250 °C, (e) 300 °C, and (f) 350 °C [7]

After a T6 treatment, Si particles are even coarser and no difference can be observed between horizontal and cross-sectional planes (Figure 14).

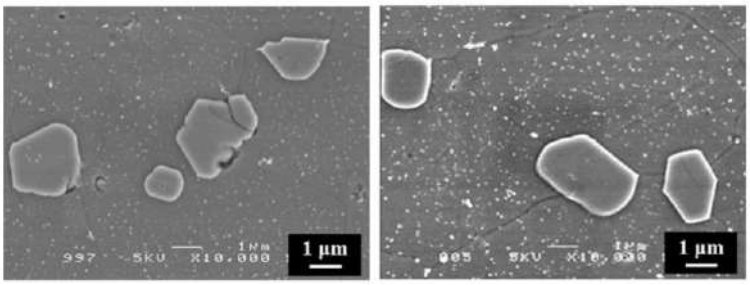

Figure 14: SEM images of the (a) horizontal and (b) vertical cross sections of AlSi7Mg0.3 T6 LBM specimen solution treated at 535 °C for 8 h and annealed at 155 °C for 6 h [7]

Yang *et al.* studied the impact of different heat treatments on AlSi7Mg0.6 by LBM (Table 2) [8].

Table 2: Heat treatment conditions applied in (Yang, Rometsch, Davies, et al. 2018) *[8]*

Condition	Heat Treatment	Details
A	As-built	Tested 1 week later (Natural ageing)
B	Direct Ageing	8 h @ 160 °C
C	Stress relief	2 h @ 300 °C
D	SR + T6	2 h @ 300 °C + SHT 1 h @ 543 °C + Polymer quench (PQ) + AA 8 h @ 160 °C
E	SR + T6	2 h @ 300 °C + SHT 3 h @ 543 °C + PQ + AA 8 h @ 160 °C
F	SR + T6	2 h @ 300 °C + SHT 8 h @ 543 °C + PQ + AA 8 h @ 160 °C

Microstructures for these different conditions are presented in Figure 15 and Figure 16. When directly aged, the eutectic network is preserved and only a precipitation of Si in α cells occurs. Whereas as already seen, when heat treated at 300 °C, the eutectic network is disrupted.

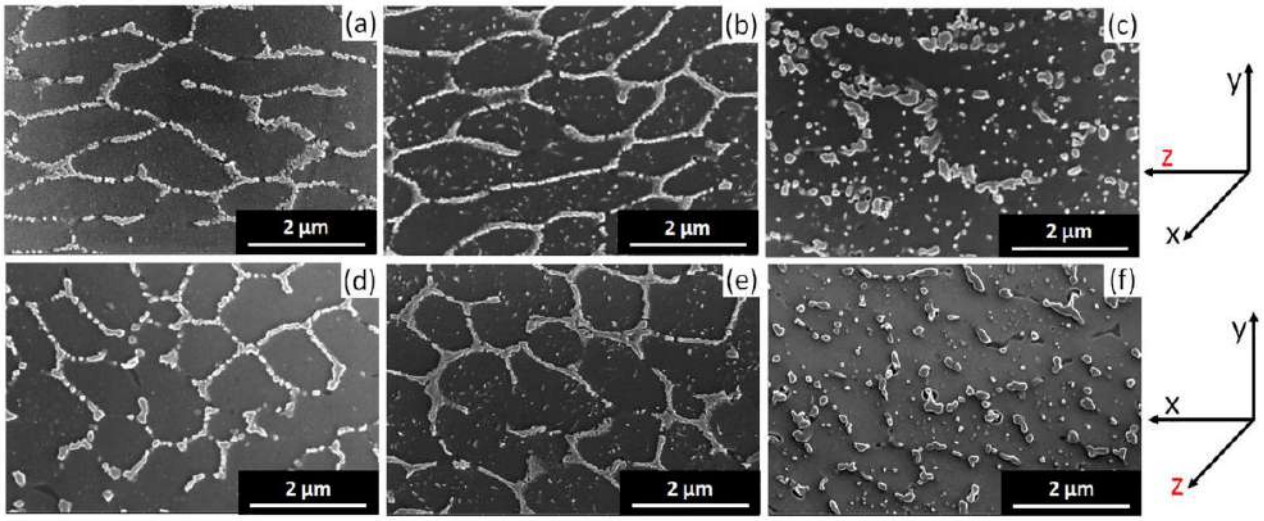

Figure 15: Secondary electron images showing microstructure of (a) and (d) for Condition A, (b) and (e) for Condition B, and (c) and (f) for Condition C on the vertical and horizontal sections, respectively [8].

T6 treatment leads to a totally different microstructure with large silicon precipitates and even iron intermetallic phases. There is no difference according to the observation plane. As the solution heat treatment time is increased, the size of the Si precipitates increases too.

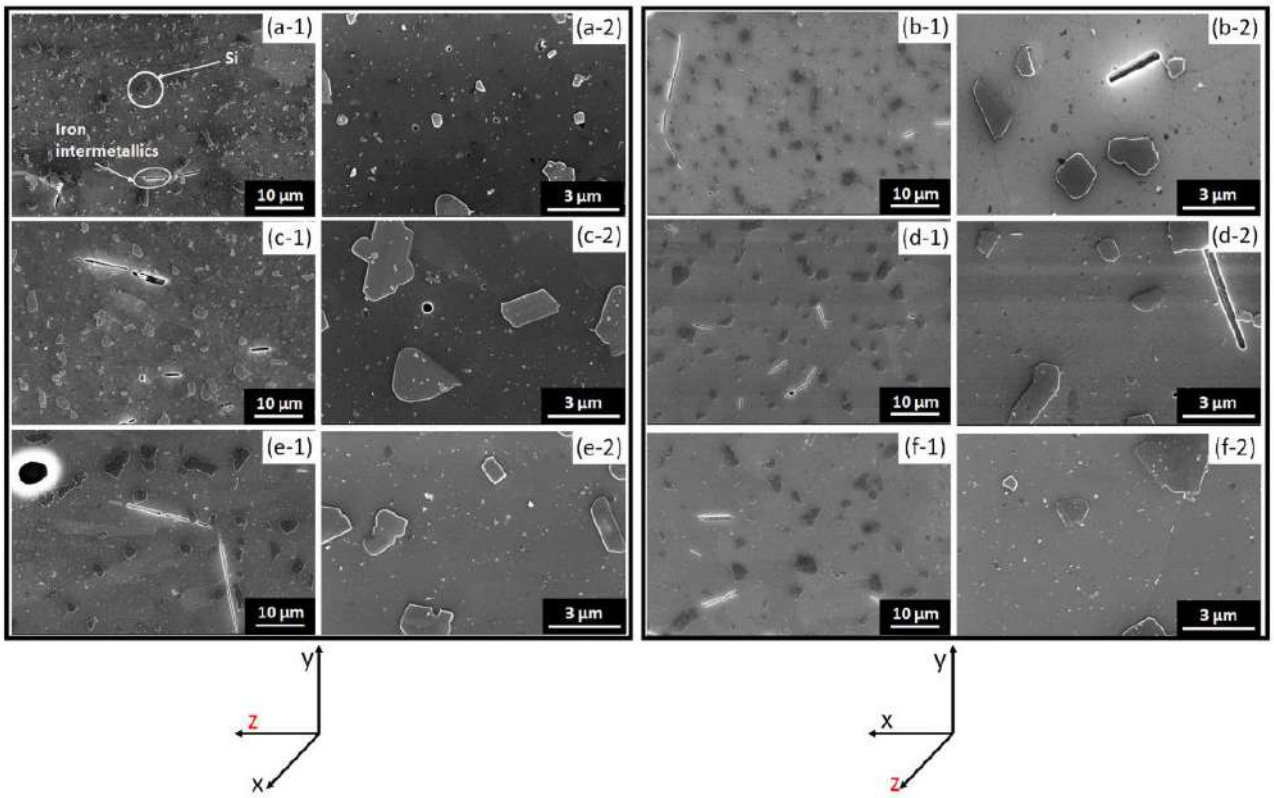

Figure 16: Secondary electron images showing microstructure of (a) and (b) for Condition D, (c) and (d) for Condition E, and (e) and (f) for Condition [8].

Figure 17 shows different texture effects of these different configurations. It is clear that although the microstructure changes according to the different heat treatments, where Si particles morphology evolves, the crystallographic structure remains unchanged. Although the grain structure does not change, mechanical properties are largely affected by the different heat treatments, showing that properties of LBMed Al-Si alloys do not derived from the grain structure but from the phase distribution and morphology.

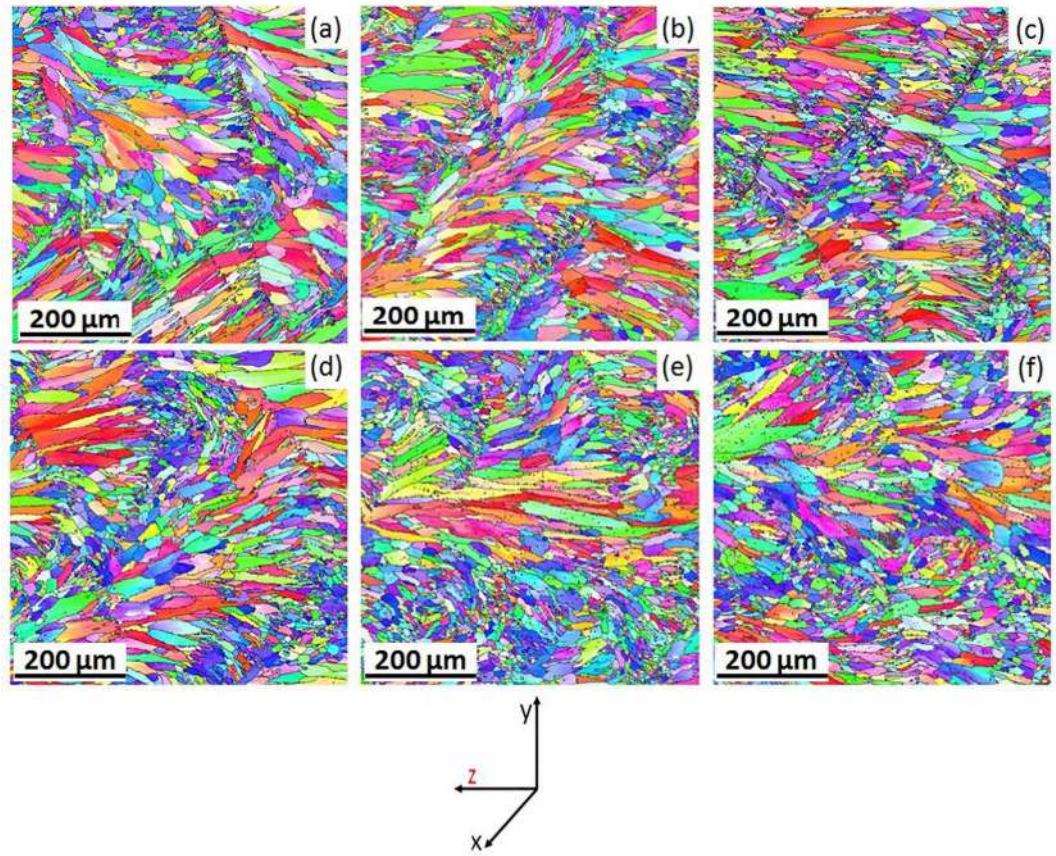

Figure 17: Microstructure reconstructed from inverse pole figures for Conditions (a) A, (b) B, (c) C, (d) D, (e) E, and (f) F, where the building direction (z) is parallel to the scale bar [8].

Li *et al.* studied the influence of solution heat treatment time at 500 °C on AlSi12 made by LBM [9]. The base plate was heated at 200 °C. Solution heat treatment of specimens was performed in air at 500 °C up to 4 h, followed by water quenching.

In Figure 18 is plotted the number of Si particles per µm² and their total area for different solution heat treatment time durations at 500 °C [9]. This graphs shows that the particle coarsening occurs rapidly and is complete after 2h. Particle coalescence and Ostwald ripening, where large particles grow at the expense of small ones are the two phenomena involved. Silicon is rejected from saturated α-Al and rearrange with eutectic Si to form large particles.

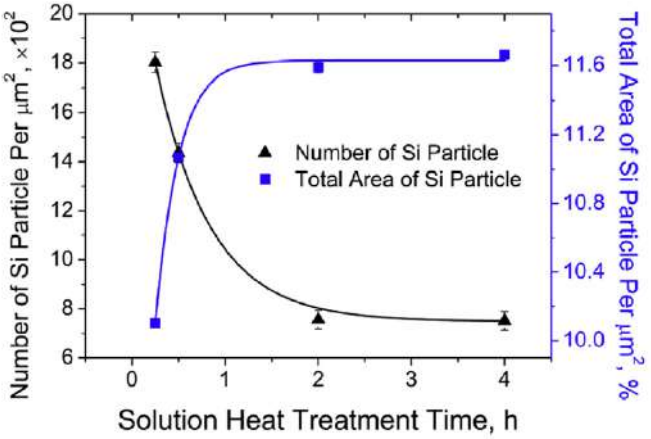

Figure 18: The Si particle number and total Si particle area as a function of solution treatment time based on SEM images [9].

In Figure 19 is plotted the concentration of Si in Al measured by EDX in as-built condition and after different solution heat treatment time at 500 °C [10]. Notice that the concentration of Si in Al in the as-built condition is about 7 wt% which is much higher than the maximum Si solubility given by the phase diagram (1.6 wt%). However, upon solution treatment the Si content in the Al drops rapidly to about 2 wt% after just 15 min and then to the maximum equilibrium concentration of 1.6 wt% after 30 min, as shown in Figure 19. Longer solution treatment time durations have no influence on the Si content in Al, which remains about 1.6 wt% which corresponds to thermodynamic equilibrium.

In Figure 20 are plotted the tensile properties of AlSi12 according to different solution heat treatment times at 500 °C. Notice that a large increase in ductility and decrease in strength is observed after only 15 minutes. Tensile properties reach a plateau after only 30 min. The variation of elongation, from a brittle to a ductile fracture mode has been confirmed by dimples coarsening on the fracture surface. It can be argued that mechanical properties are drastically changed due to the disruption of the Si-enriched phase network and to the precipitation of Si from the super saturated α-Al matrix, reducing the solid solution strengthening. The cellular morphology no longer acts as a barrier for dislocation motion and as the Si particles get coarser, they no longer contribute to the mechanical properties. It is important to note that samples were built at 200 °C so there should not be residual stresses in the as-built condition. It means that the differences in mechanical properties observed between as-built and after solution heat treatment are only due to a microstructure evolution.

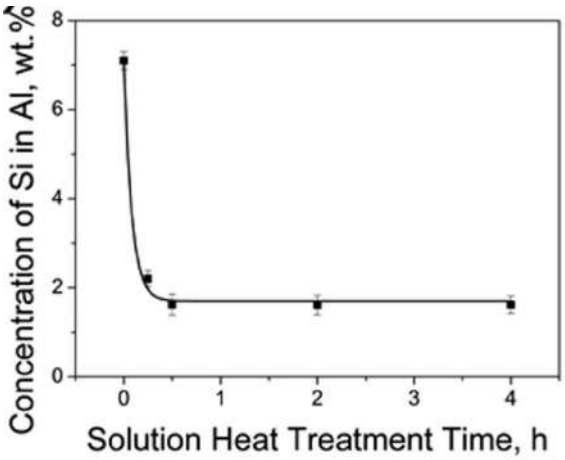

Figure 19: Concentration of Si in Al at different solution heat treatment times at 500 °C [9]

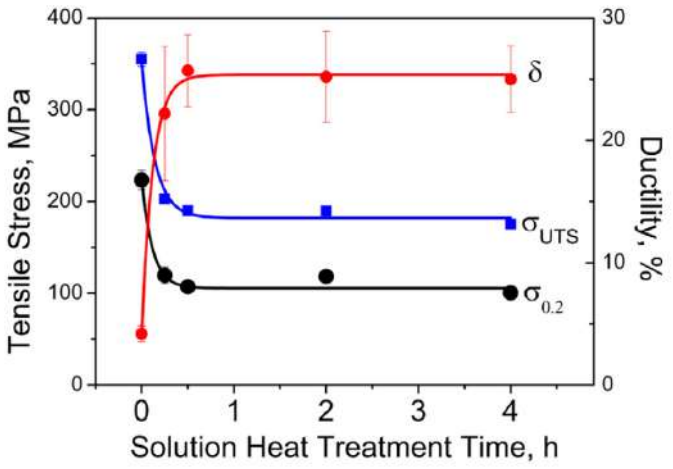

Figure 20: Variation of mechanical properties of the Al–12Si alloy upon solution heat treatment at different times [9]

Li *et al.* studied the effect of different solution heat treatments and artificial ageing temperatures on AlSi10Mg microstructure and properties [10]. Specimens were built with a base plate temperature of 100 °C. XRD patterns were used to determine the amount of Si retain in solution. In Figure 21 are plotted the concentration of Si in α-Al, at.% in as-built condition and after different solution heat treatment temperatures (SHT) for 2 h and after artificial ageing (AA) at 180 °C for 12 h. A trend similar to the discussed previous papers has been observed, with a very high Si amount retained in the supersaturated α matrix in the as-built condition. This amount is progressively reduced during SHT and further diminished after AA. Note that in [9], a plateau was reached at 500°C for only 30 min whereas here, a heat treatment at 550 C for 2 h can still decrease the amount of dissolved Si.

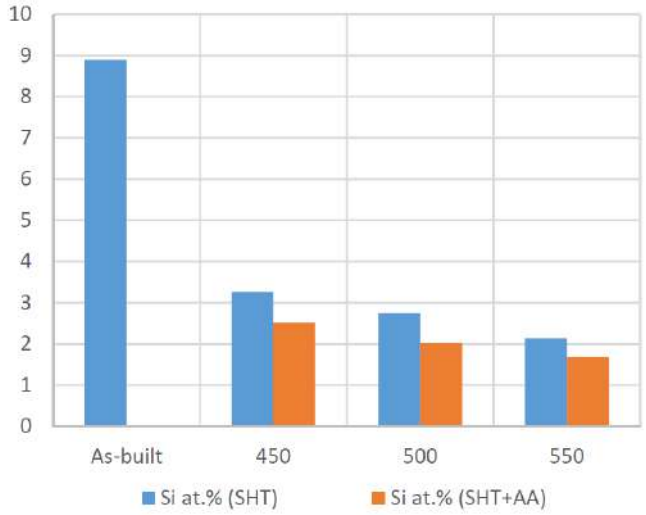

Figure 21: Concentration of Si in Al, at.% in as-built condition and after different solution heat treatment temperatures (2 h) [10]

As already shown, a particle coarsening is observed for Si particles. This is illustrated in Figure 22. It can be observed how the eutectic Si-enriched network is disrupted into small particles which then progressively grow as the temperature is increased. Notice that after artificial ageing, particles grow further.

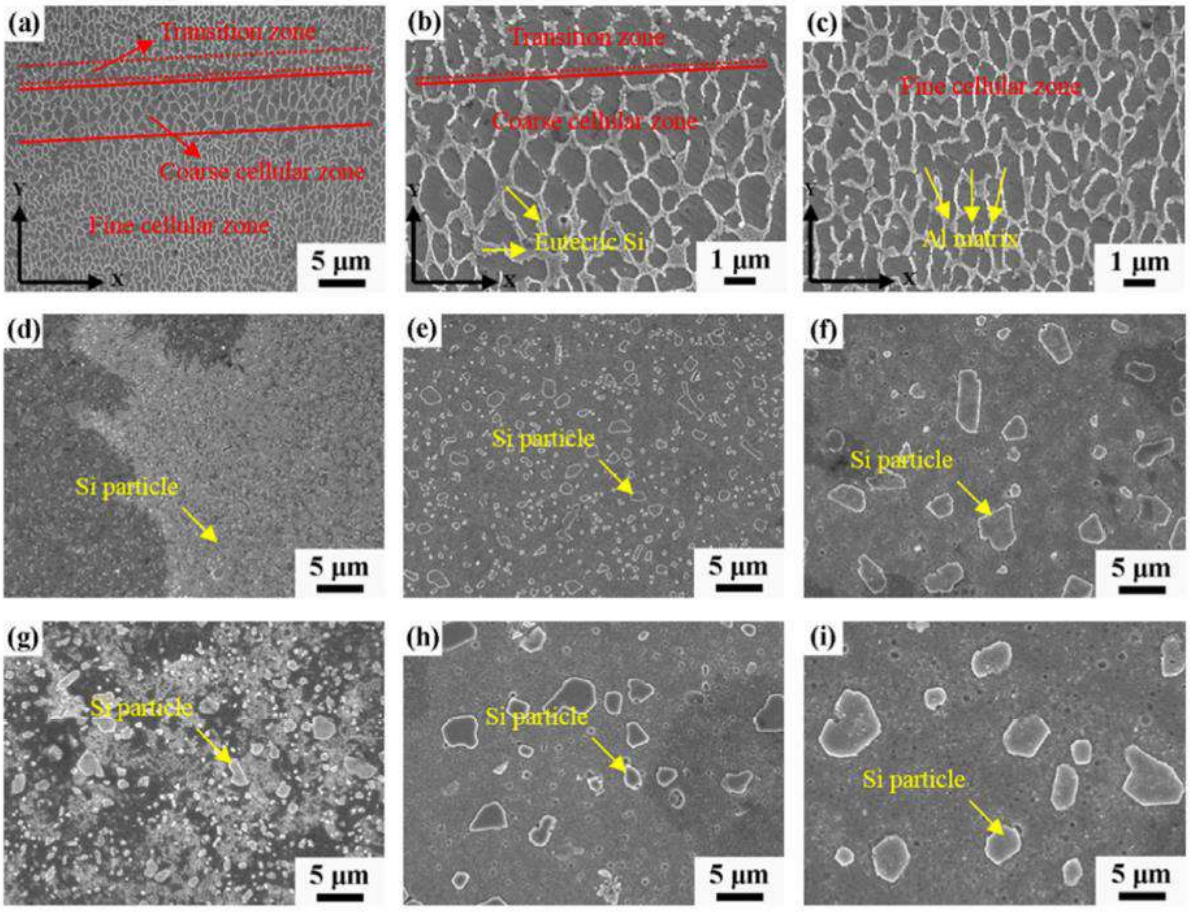

Figure 22: Micrographs of the as-built and heat-treated LBM AlSi10Mg specimen microstructures after etching with Keller's reagent: (a) single melt track with three distinctive regions; (b) boundary of melt track with coarse cellular region and transition region; (c) interior of melt pool with fine cellular microstructure. SEM images of the eutectic microstructures of the LBM-built AlSi10Mg after different heat treatment conditions: (d) 450 °C for 2h; (e) 500 °C for 2h; (f) 550 °C for 2h; (g) 450 °C for 2h + 180 °C for 12h; (h) 500 °C for 2h + 180 °C for 12h; and (i) 550 °C for 2h + 180 °C for 12h [10]

(Yang, Rometsch, Davies, et al. 2018) evaluate the amount of free Si in AlSi7Mg0.6 made by LBM samples according to different heat treatments. Results are given in Figure 23. Heat treatments at high temperatures release Si from α. Direct ageing at low temperature 160 °C leads to a small amount of precipitation. Longer solution heat treatment do not increase the amount of free Si [8].

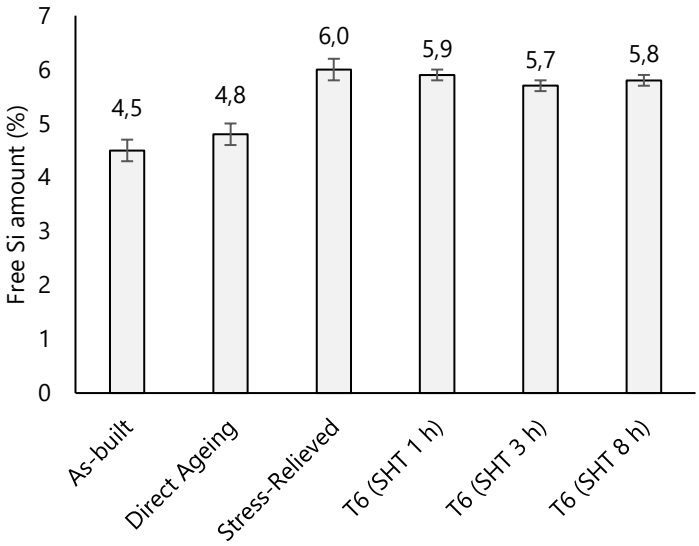

Figure 23: Free Si Amount according to different heat treatments.

Li *et al.* describe the precipitation and coarsening of Si when subjected to solution heat treatment in a three phases process as presented in Figure 24 [10]. Phase A is obtained in the as-built condition, where α cells supersaturated in Si are surrounded by a network of Si-enriched phase. Then, when subjected to solution heat treatment, Si begin to precipitates from the α cells and the network starts to disrupt. Then, particle coalescence and Ostwald ripening occur, leading to coarser Si particles in the α matrix.

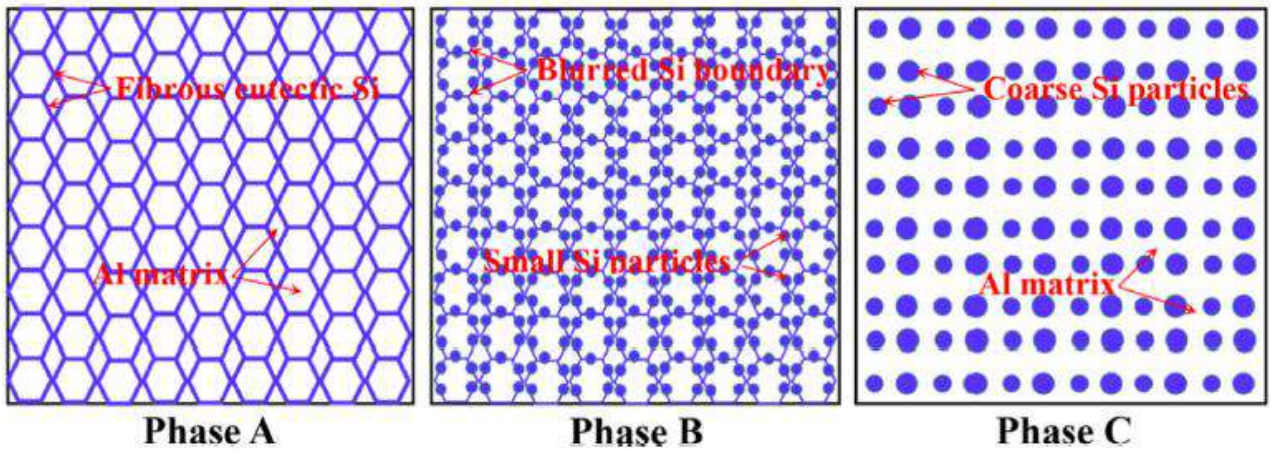

Figure 24: Schematic of the microstructure evolution of the LBM-produced AlSi10Mg samples during the solution and artificial ageing heat treatment. Blue features represent Si- rich areas, while white features represent Al-rich areas [10]

Rao *et al.* studied the microstructure and tensile properties of A357 (AlSi7Mg0.6 by LBM) according to different heat treatment [11]. Two batches of samples were produced. One was stress relieved at 300 ± 1 C with air cooling, and the others were solution heat treated (SHT) at 535 ± 3 C in salt bath for 0.25 h, 1 h, 4 h, 24 h, and 150 h, followed by water quench. For both types of heat treatments, a disruption of the eutectic Si network was observed, with a different range of particles coalescence according to the temperatures used. As seen previously, a decrease in the concentration of Si in α-Al has been observed by XRD analysis according to stress relief and SHT as shown in Figure 25. Note that values are different from what has been seen previously but the trend is similar, showing a much higher Si amount in solution in the as-built state (5.4 wt%) than the equilibrium, which decreases as the temperature gets higher and time gets longer.

Residual stresses have been evaluated and were high in as-built sample but were almost zero both after 2 h at 300°C or 1 h at 535 °C.

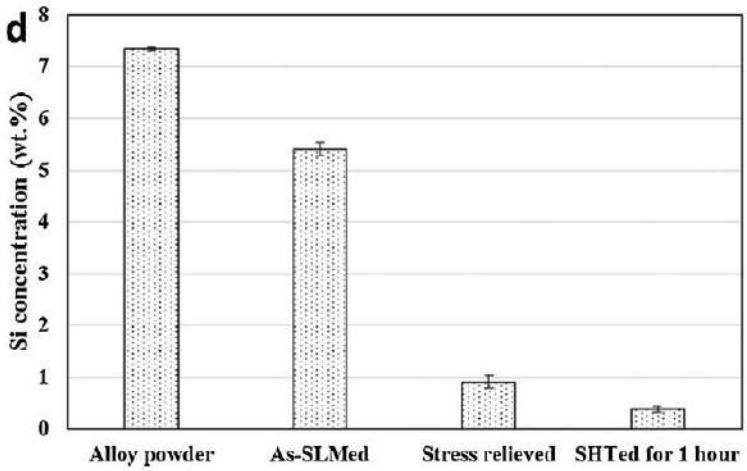

Figure 25: The solid solute content of silicon measured by STEM of LBMed A357 at different conditions [11]

Takata *et al.* studied the effect of stress relief and SHT on microstructure and mechanical properties of AlSi10Mg [12]. Samples were treated either at 300 C for 2 h or at 530 C for 6h, followed by water quenching in water. Macrostructure of as-built and stress-relieved sample were similar ash shown on Figure 26. On both optical micrographs at low magnification melt pools are visible. At high magnification, on the as-built structure, a fine elongated cellular microstructure can be observed, with cells being primary α-Al saturated in Si surrounded by an eutectic α/Si Si-enriched. After annealing at 300 °C for 2 h, the observed microstructural characteristics changed slightly. The melt pools can still be observed but the Si particles became coarser and the network has been disrupted. Note that fine Si particles can be observed within the columnar α-Al grains, indicating that the Si phase precipitates in the α-Al matrix during annealing. After the solution treatment at 530 °C for 6 h, no melt pools are observed in the optical micrograph. SEM observations revealed a significant coarsening of the Si particles and the formation of a Fe-containing intermetallic phase (β-AlFeSi) with a rod-shaped morphology.

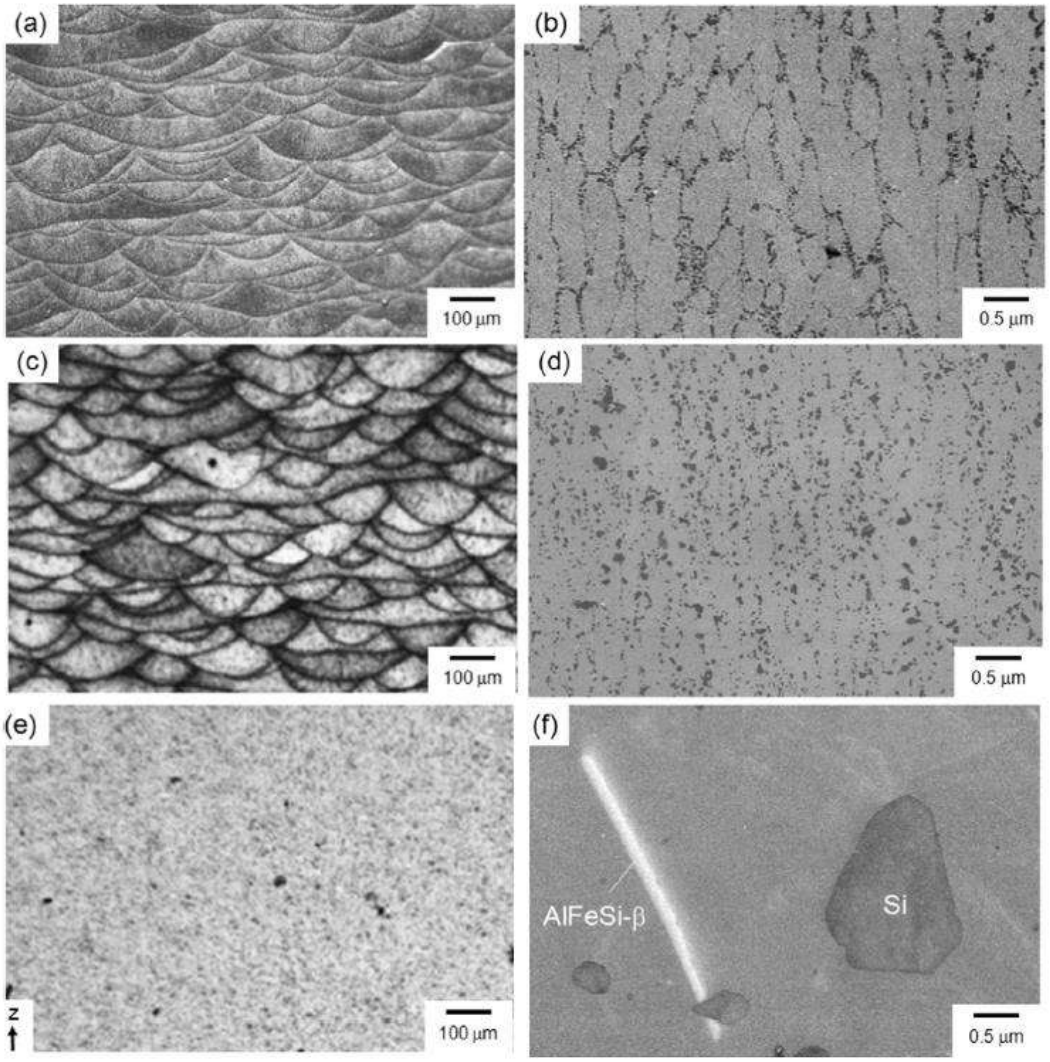

Figure 26: (a, c, e) Optical micrographs and (b, d, f) SEM images showing microstructures of the AlSi10Mg alloy samples: (a, b) as-fabricated, (c, d) annealed at 300 °C for 2 h, (e, f) heat-treated at 530 °C for 6 h [12]

Takata *et al.* also performed EBSD analysis on different metallurgical states [12]. Figure 27 shows that elongated grains with a mean width of approximately 10 µm grows inside melt pools. In the vicinity of the boundaries between the melt pools, smaller (several µm) equiaxed grains appear. It is interesting to note that no significant differences were observed on the crystallographic texture according to the different heat treatments. Many of the elongated grains have a <001> orientation along the Z direction. The <001> -oriented grains (assuming that the <001> direction varies from that parallel to the Z direction by no more than 15°) constitute 20% of the area, resulting in the development of a {001} texture in the as-fabricated sample. These microstructural features remain unchanged after annealing at 300 C and even after the solution treatment at 530 °C for 6 h as well, whereas the width of the elongated grains becomes slightly larger [12].

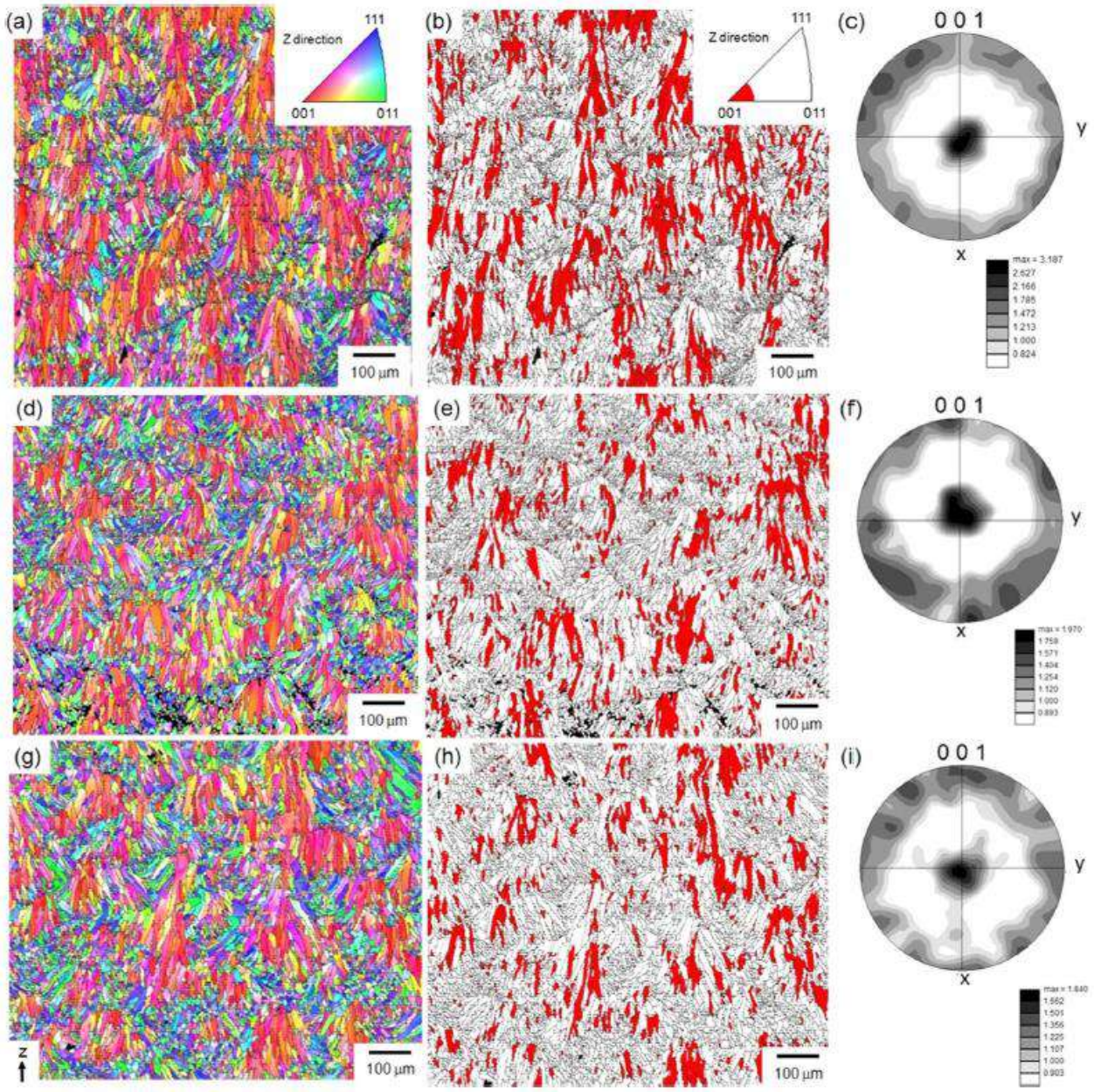

Figure 27: (a, d, g) Orientation color maps, (b, d, f) distribution maps of [001] oriented regions (less than a 15° deviation was tolerated from the [001] direction parallel to the Z direction) and (c, f, i) 001 pole figures of the AlSi10Mg alloy samples: (a, b) as-fabricated, (c, d) annealed at 300 °C for 2 h, (e, f) heat-treated at 530 °C for 6 h [12]

Figure 28 shows the microstructure evolution mechanism proposed by Takata *et al.* [12].

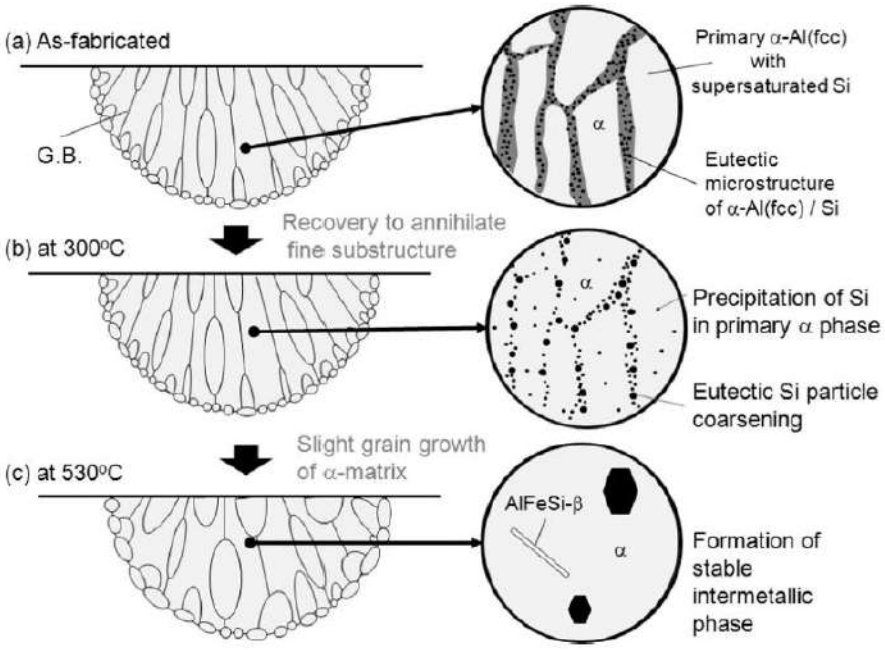

Figure 28: (Takata, Kodaira, Sekizawa, et al. 2017) *[12]*

Fousova *et al.* studied the microstructure and mechanical behaviour of specimens subjected to different heat treatments [13]. These were as-built, stress-relief, T6 and direct ageing. Direct ageing has been studied due to the supersaturated structure obtained in as-built condition, leading to a potential precipitation when bringing heat. Figure 29 shows the microstructure according to the different heat-treatments tested. First, it can be noticed that as-built, stress-relief and T6 microstructure are identical to previously observed microstructures in other papers. Secondly, no significant changes can be observed between specimens in as-built condition and after annealing at 160 °C during 5 h. At 300 °C for 2 h, the Si-enriched network has is disrupted.

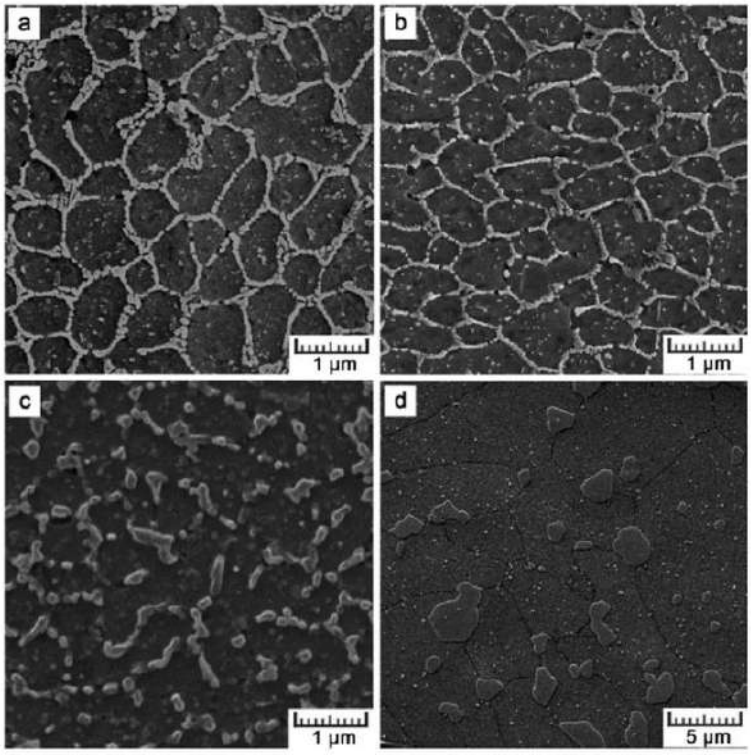

Figure 29: Microstructures of the AlSi10Mg alloy: (a) as-built state, (b) annealed at 160 °C (5 h), (c) stress-relieved, (d) after T6 heat treatment [13]

Because no changes were observable in SEM images, transmission electron microscopy was applied to demonstrate what happened in the material when exposed to the elevated temperature (160 C). In Figure 30 are shown TEM views of microstructure before and after annealing. After annealing, very small needles can be observed. They were up to 200 nm long and up to 5 nm thin. The small dots correspondent to needles seen from the top. These needles were surprisingly pure Si. No magnesium was found in them. This is unexpected as the usually encountered precipitates in a needle shape like this are Mg_xSi precipitates. Further research needs to be done to understand the reason why pure Si precipitates are formed after direct ageing.

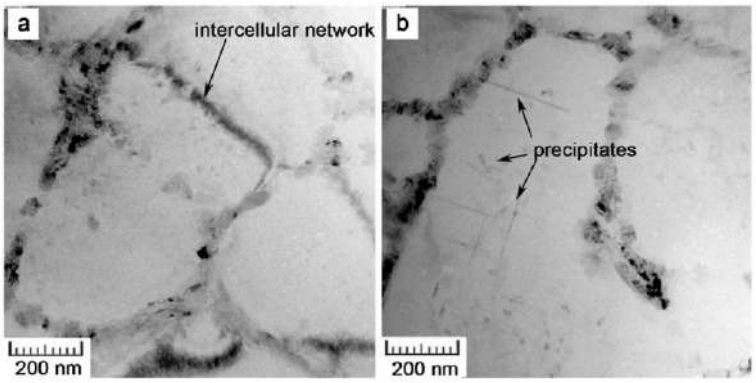

Figure 30: TEM views of microstructure: (a) before and (b) after annealing at the elevated temperature of 160 °C [13]

Uzan *et al.* studied the effect of stress relief and Hot Isostatic Pressing (HIP) on AlSi10Mg samples made by LBM [14]. In Figure 31 is given the typical macrostructure of printed specimens after various heat treatments. It can be observed that melt pool borders are still visible after stress-relief (300 °C 2 h) and stress-relief + HIP at 250 °C for 2 hours. Indeed, the temperature of the HIP is smaller than the stress-relief one, so no significant change is expected. However, these borders disappear when the sample undergoes a HIP at 500 °C during 2 hours. The macrostructure is totally changed.

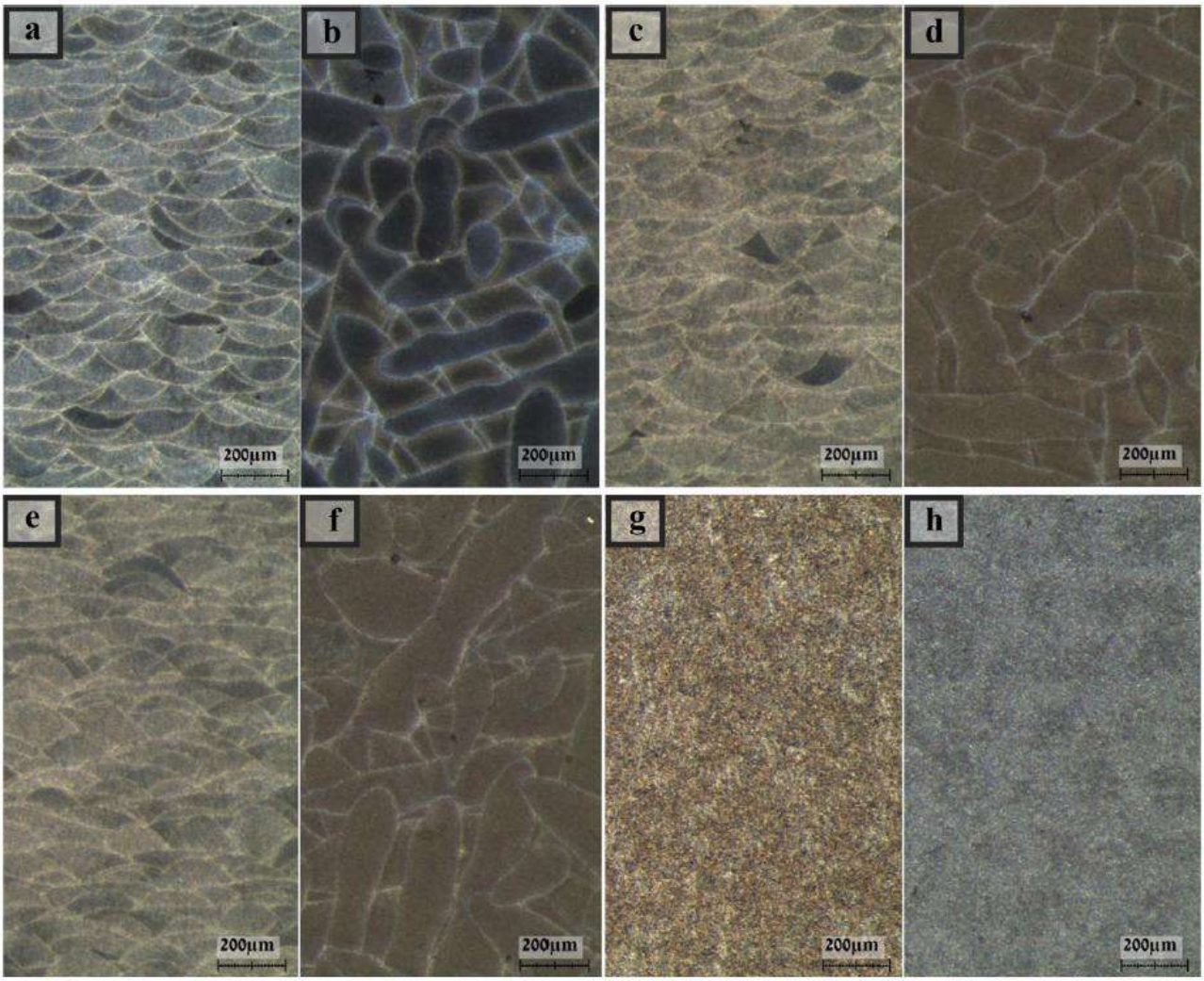

Figure 31: Typical macrostructure of printed specimens after various heat treatments; as-built, side (a) and top (b) views; after SR, side (c) and top (d) views; after SR+HIP at 250 °C, side (e) and top (f) views; after SR+HIP at 500 °C, side (g) and top (h) views [14]

In Figure 32, the detailed microstructure of theses samples are shown. Once again, the microstructure of as-built, stress-relief and stress-relieved + HIPed at 250 °C samples are very similar. The Si-enriched network is only disrupted, but the shape of the network and cells is still distinguishable. In case of the HIPed sampled at 500 °C, Si particles are much larger and separated. This microstructure is actually similar to one obtained after SHT.

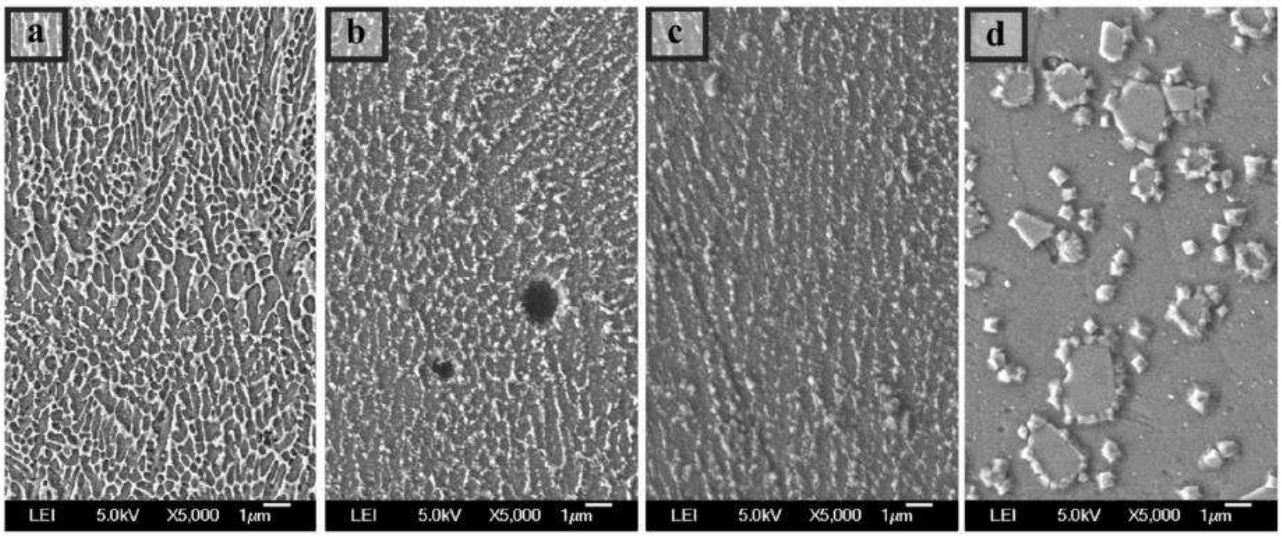

Figure 32: The typical microstructure of AM LBM specimens; a) as-built; b) after SR; c) after SR+HIP at 250 °C and after SR+HIP at 500 °C (d) [14]

Aversa *et al.* studied the influence of base plate heating on microstructure and tensile properties of A357 samples [15]. In Figure 33 are given the micrographs of A357 samples built at 100, 140, 170 and 190 °C. These microstructures are similar but a slight disruption of the Si-rich network and very fine Si particles precipitation occur as the baseplate temperature increases. The behaviour is similar to what is observed during stress-relief like treatments, where T°C is smaller or equal to 300 °C.

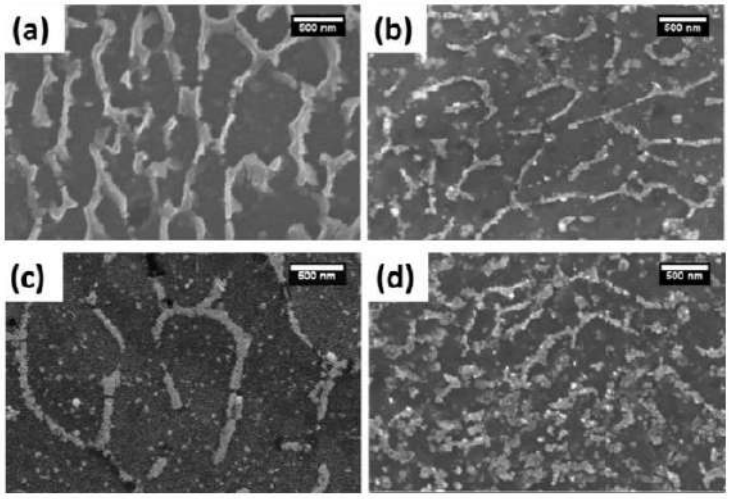

Figure 33: FESEM micrographs of A357 samples' cross-section built at (a) 100; (b) 140; (c) 170; and (d) 190 °C [15]

A slight increase in the intensity of silicon peaks in XRD patterns has been observed in the samples built with higher building platform temperature.

Mertens *et al.* [16] observed a slightly disrupted eutectic network on AlSi10Mg samples built at 200°C as shown on Figure 34.

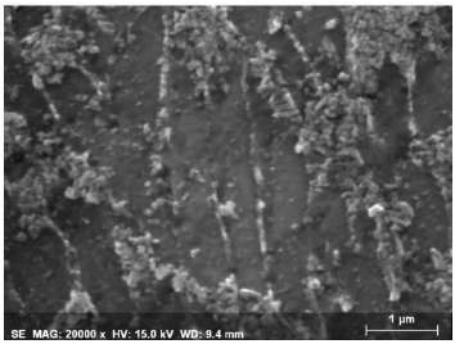

Figure 34: SEM micrograph of as-built LBM AlSi10Mg sample built at 200°C [16]

Partial conclusion on Microstructure:

- As-built samples show a very fine cellular microstructure with α-Al cells surrounded by Si-enriched eutectic.
- As built samples exhibit α-Al cells oversatured with Si (around 7 at.%). This oversaturation is lost after short exposure to SHT temperature to reach thermodynamic equilibrium (< 2 at.%).
- By exposure to 160°C (direct ageing temperature), a part of this Si included in a phase is transformed into pure Si needles in the α-Al cells.
- When heat treated at temperature lower than 300 °C, several phenomenon occur :
    - From 150°C to 250°C, a fine precipitation of Si particles inside α cells is observed,
    - In the range of 300°C, a slight disruption of the eutectic network is evidenced,
- The disruption of the eutectic network is confirmed during the SHT treatment (T>500°C) for every duration.
- The T6 treatment after SHT induces coarsening of Si particles coming from eutectic network destroyed during exposure at T>500°C.
- Residual stresses are confirmed in the as built samples; they are eliminated by exposure to 300°C during 2 hours which corresponds to classical stress relief treatment in cast alloys.
- From macrostructural aspect and when heated at SHT temperature, another significant change is observed, as the Si particles coarsening occurs. Melt-pool boundaries are no longer visible, and the microstructure appears identical according to the different observation planes. At time and temperature increases, Si particles size increases too. Diffusion of Si from supersaturated α and its rearrangement occurs very fast, as equilibrium is reached in about 30 min.
- From macrostructural aspect, the melt pool boundaries are not affected by a HIP treatment performed at T<300°C. On the contrary, the melt pool boundaries disappear by HIP at T>500°C.
- When built at high temperatures (up to 170°C), Al-Si samples show similar microstructure as when treated at low temperatures; however more work is needed on the influence of base plate temperature and the eventual interaction with low temperature direct ageing.
- At 300 °C, a significant change occurs: the eutectic network is disrupted, the α cells are no longer clearly defined. However, the melt pool boundaries are still visible. Indeed, the network track is kept when disrupted as Si particles rearrange where the network was previously. HIP at this temperature range does not provide any significant change on the microstructure.

5 Porosity

When heat treated, Al-Si samples manufactured by LBM generally do not only show changes in microstructure but also on porosity amount.

It is common to identify hydrogen porosities in Al-Si alloys manufactured by LBM; this is generally linked to insufficient powder drying prior manufacturing [17]. Hydrogen porosity generally coarsen when samples are heat treated, especially at high temperature and for long times such as during solution heat treatment. In Figure 35 is shown the porosity amount evolution according to the different heat treatments given in Table 2, that is to say as-built, directly aged, and stress-relieved and SHT at 543 °C for 1 h, 3 h and 8 h.

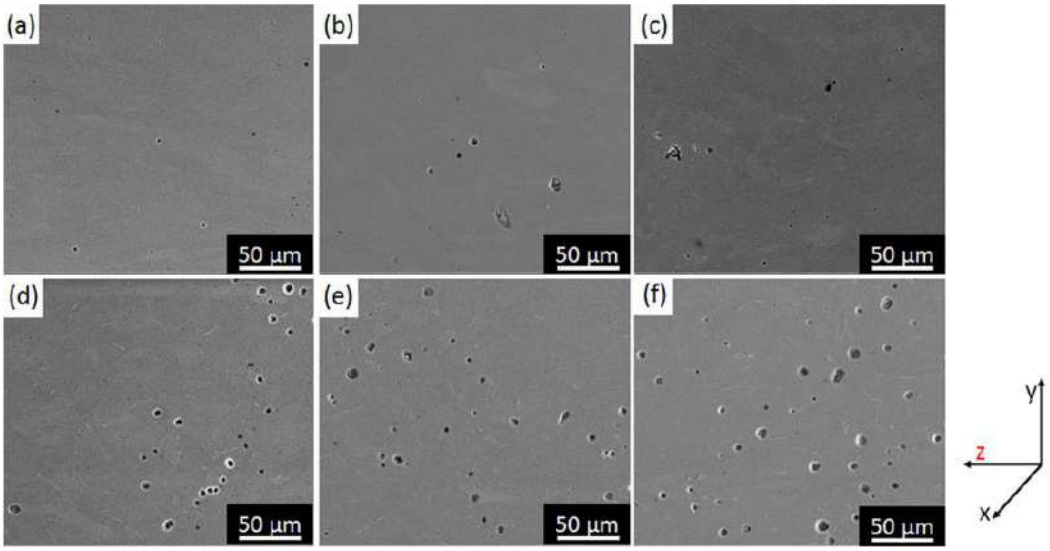

Condition	Heat treatment	Heat treatment Procedure
A	As SLM processed	N/A
B	DA	160 °C/8 h/Air Cool (AC)
C	SR	300 °C/2 h/AC
D	SR + SHT/1 h + AA	300 °C/2 h/AC + 543 °C/1 h/Polymer quench (PQ) + 160 °C/8 h/AC
E	SR + SHT/3 h + AA	300 °C/2 h/AC + 543 °C/3 h/PQ+ 160 °C/8 h/AC
F	SR + SHT/8 h + AA	300 °C/2 h/AC + 543 °C/8 h/PQ+ 160 °C/8 h/AC

Figure 35: Representative secondary electron images showing porosity development for Conditions (a) A, (b) B, (c) C, (d) D, (e) E, and (f) F, where the building direction (z) is parallel to the scale bar [8]

Yang *et al.* tested different ways to limit porosity enlargement during solution heat treatment of A357 samples [17]. Powder was pre-heated on the platform under an argon atmosphere at either 200 °C or 80 °C for 16 h, or simply kept in a vacuum chamber for 16 h, immediately before starting the build. As seen on Figure 36, gas pores enlarge significantly after solution heat treatment at 543 °C for 2 h when there is no pre-drying treatment applied. When powders are kept in the vacuum chamber under vacuum for 16 h before the build starts, samples show smaller and fewer gas pores. Samples built using powders having undergone an 80 °C pre-heat treatment under argon atmosphere for 16 h show a similar level of pore enlargement to the vacuum-treated samples. When powders are pre-dried at 200°C under an argon atmosphere for 16 h, samples show the smallest and least gas pores after solution heat treatment.

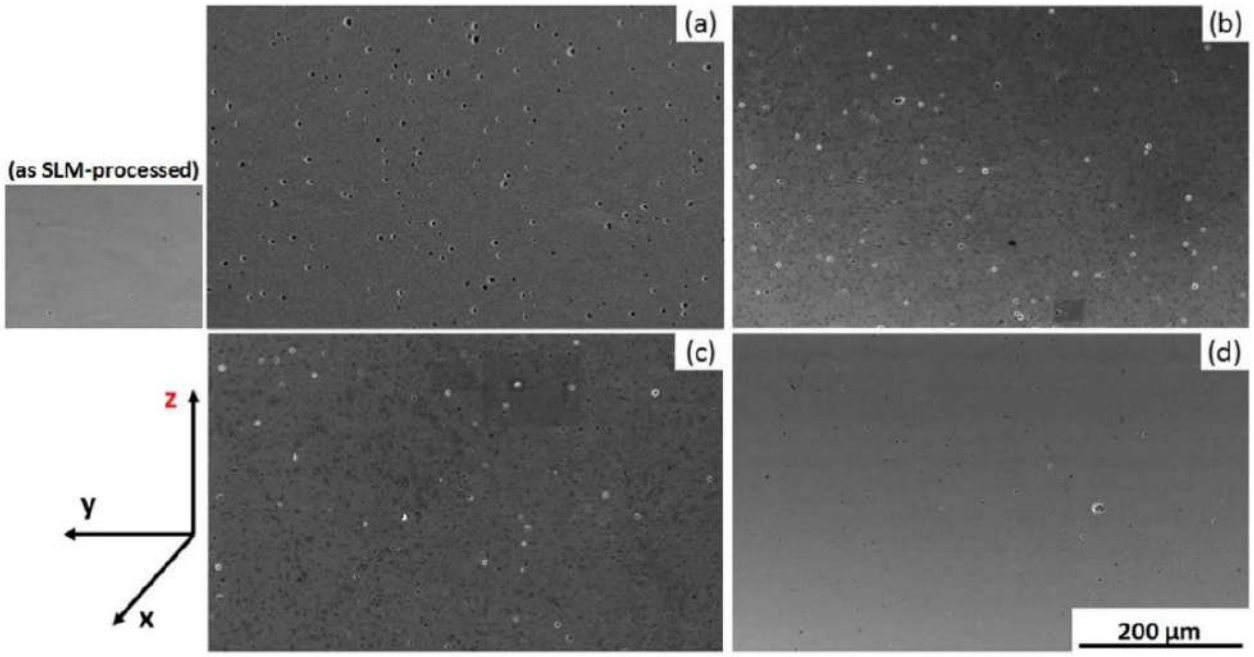

Figure 36: Secondary electron images of LBM-processed alloy A357 built using the optimised processing parameters with powder having undergone (a) no pre-treatment, (b) simple vacuum treatment, (c) pre-heat treatment at 80 °C and (d) pre-heat treatment at 200 °C for 16 h, after solution heat treatment at 543 °C for 2 h followed by warm water quenching. The as-LBM processed sample using powder with no pre-treatment is used as a reference [17]

(Delroisse et al. 2017) observed that hydrogen porosity amount could be function of the orientation of built features. Down-skin areas show higher amount of porosity due to lower cooling rate due to thermal insulation with powder. Microstructure is also coarser in the B area than in the A one [18]. The total hydrogen content in the powder material and in the inclined strut were measured to be 27.4 ppm and 27.0 ppm, respectively. Considering the hydrogen as an ideal gas at room temperature, this corresponds to 35 mL/100 g so 50 times the hydrogen solubility.

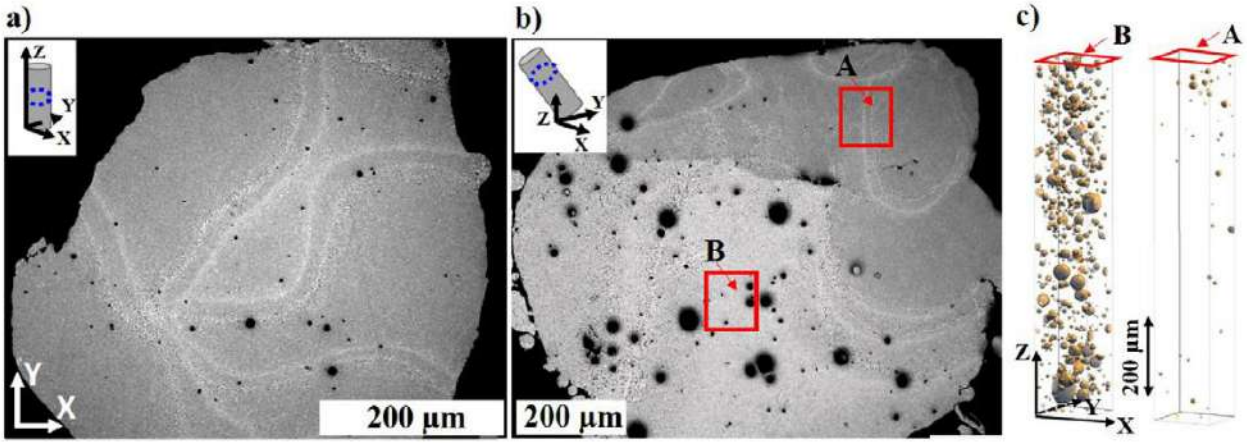

Figure 37: Comparison of the microstructure of (a) a vertical and (b) an inclined strut. The orientation of the observation plane is given by the blue dotted line (see also Fig. 2). (c) Porosity in zone A and B of (b) observed by 3D X-ray tomography along virtual parallelepiped oriented along the axis of the strut.

Mertens *et al.* performed T6 treatment on AlSi10Mg samples built with 200 °C base plate heating [16]. Solution heat treatment temperature has been selected to 510°C. Preliminary trials using a solutionizing temperature of 530°C had led to a significant deterioration of the surface of the samples (Figure 38).

Figure 38: Deterioration of the samples' surface following solutionizing heat treatment at 530°C for 6 hours [16]

Tradowsky *et al.* subjected AlSi10Mg samples to HIP and/or T6. Before HIP, samples showed irregular voids due to oxide films that were collapsed entirely after [19]. These were not gas entrapment pores or hydrogen ones. So there was no re-opening during the subsequent T6 heat treatment.

Partial conclusion on porosity:

- Hydrogen porosity tends to increase when samples are heat treated at high temperatures for long time duration. It is especially true when performing the solution heat treatment step.
- Porosity amount can vary according to the features built. It is generally greater in downskin area.
- Solution heat treatment can lead to deterioration on sample skin, where porosities coalesce and created bubbles on the surface.
- It is possible to limit these effects by drying the powder [17].

6 DTA/DSC profiles

DTA analysis is useful to determine the different transformations that occur into the material at different temperatures. For example, precipitation mechanisms or microstructure evolutions can be detected.

Fiocchi *et al.* performed DSC analysis on AlSi10Mg samples built at low base plate temperature (25°C) [6]. Two peaks were identified on the thermograms: the first one was related to the precipitation of Mg_xSi phase at 263°C, and the second one associated to diffusional and spheroidisation processes of Si at 294°C (see Figure 39 and Figure 40).

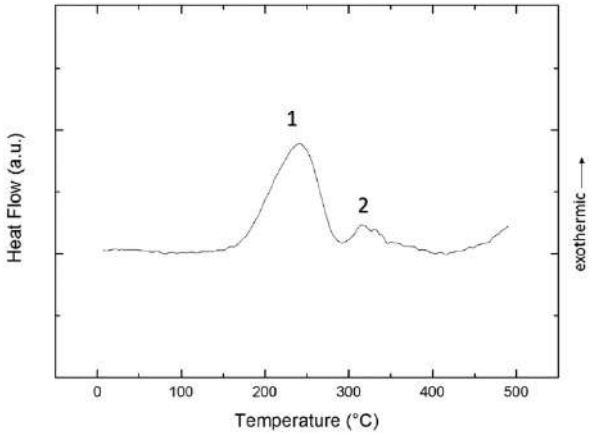

Figure 39: DSC curve recorded at 10 °C/min of as-built sample [6]

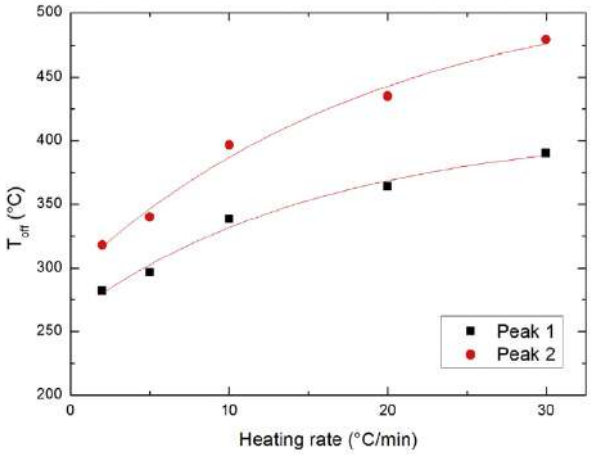

Figure 40: Offset temperatures of peak 1 and peak 2 plotted as function of heating rate applied during DSC experiments [6]

Samples were heat treated for 30 min and 2 h to the previously determined temperatures. DSC analyses were then performed after the heat treatments. These profiles are shown in Figure 41. At low temperature, even after only 30 min, the precipitation of Mg_2Si was complete (identified as the first transformation), whereas diffusion of silicon did not. On the other hand, at 294°C, both transformations have already occurred. Note that micrographs are available and confirm the spheroidisation of Si at high temperatures but do not provide information on the transformation occurring at the first peak. Indeed, only very fine Si precipitation in α cells can be observed on the micrograph of sample heat treated at low temperatures, and as Mg_xSi precipitates are very small, they are not observed. This means that the first peak identified here may not be related to Mg_xSi precipitation.

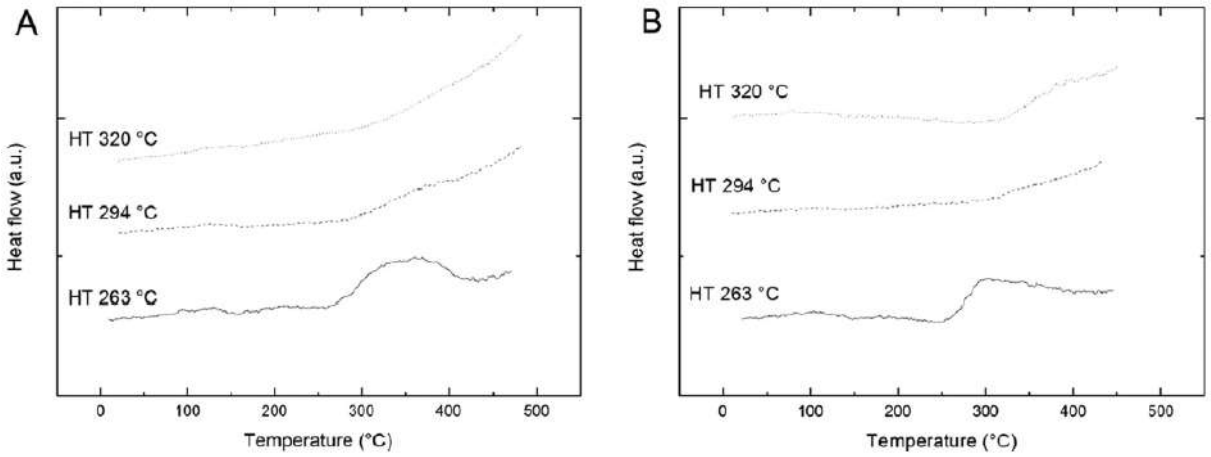

Figure 41: DSC curves recorded at 10 °C/min of samples heat treated for 30 min (a) and 2 h (b) [6]

Aversa *et al.* studied the influence of base plate heating arguing that it could act as an in-situ ageing heat treatment, therefore modify the microstructure and mechanical properties [15]. In Figure 42, the DTA measurement on A357 samples built at different build platform temperatures are shown. Two exothermic peaks are visible. The first one is supposed to be related to the precipitation of Mg_xSi, the second one to be correlated the diffusion of saturated Si in α-Al. It can be noticed that the higher the building platform temperature, the lower the intensity of the first peak. It is thus reasonable to suppose that samples built at higher temperatures should contain more Mg_xSi, whereas the process

is carried out at low temperatures, produced materials should contain Mg and Si in solid solution. However, no optical or TEM micrographs have been provided in order to confirm the presence of Mg_2Si.

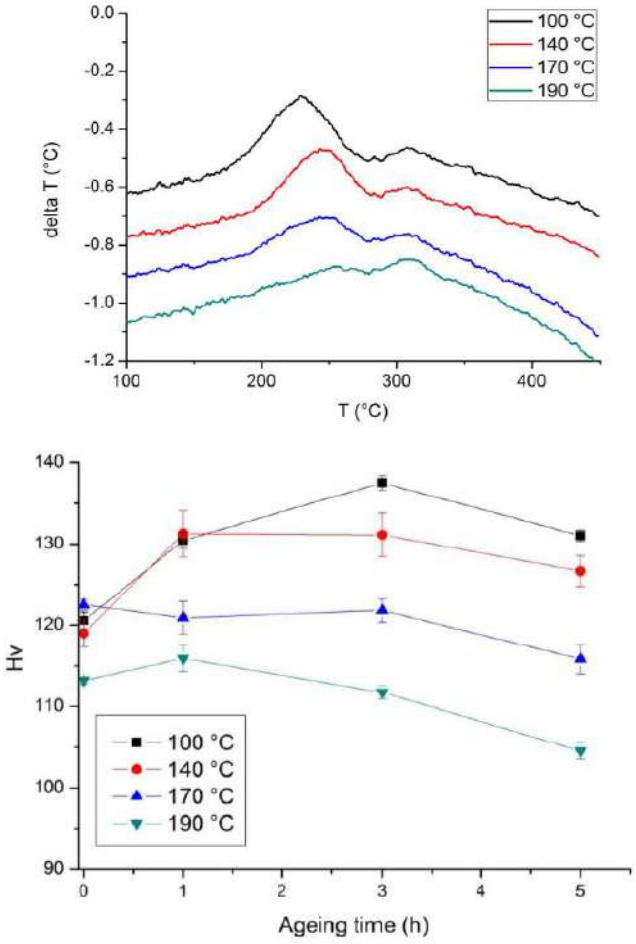

Figure 42: Differential thermal analysis (DTA) measurements of A357 samples produced with different building platform temperature and corresponding hardness values [15]

The Figure 42 shows the influence of the built platform temperature from 100°C to 190°C. The Vickers hardness is measured versus ageing time; the direct-ageing temperature is fixed at 170°C. Indeed, hardness increases during ageing at 170 C for samples built with a baseplate temperature of 100 and 140 °C. Whereas for samples built at 170 and 190 °C, ageing does not improve the mechanical properties, showing that ageing has already occur during the fabrication and no precipitation is possible anymore. However, in case of low temperature built samples, the phase that causes the hardening effect has not been clearly identified. It is supposed to be Mg_2Si but Fousova *et al.* showed on samples built without base plate heating that direct ageing at 160°C leads to fine needles of pure Si precipitation [13].

DSC analysis performed by Zhang *et al.* on cast AlSi7Mg0.4 (A356) samples after SHT and quench showed two exothermic peaks that where related to Mg_xSi precipitation [5]. The first one, beginning at about 217 °C was related to β'' precipitation and the second one at about 270 °C to β'. Peaks are sharper with lower quench rates for water quenching (Figure 43). With air cooling, only a broad peak is visible (Figure 44). TEM micrographs showed that at peak aged conditions, samples quenched at 250 °C and 110 °C showed fine β'' Mg_xSi precipitates (Figure 45). When quenched at 0.5 °C/s, peak aged samples showed both β'' and β' precipitates. When the quench rate is reduced from 250 °C/s to 110 °C/s, the density of the precipitates decreased and the size of the precipitates increased slightly.

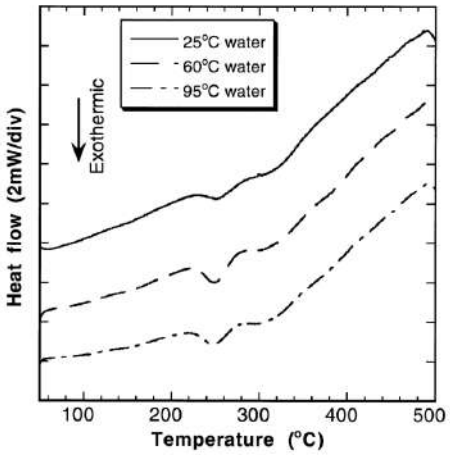

Figure 43: DSC traces during heating of as-quenched A356 alloy for different water-quenching condition [5]

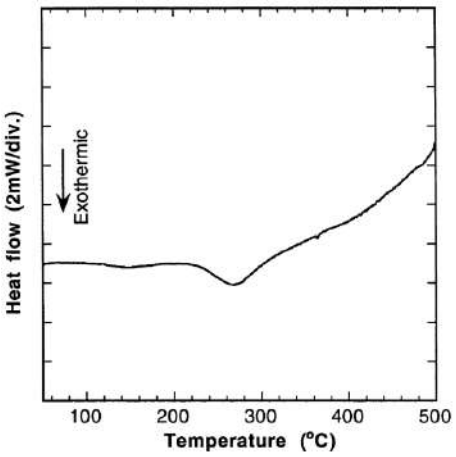

Figure 44: DSC trace during heating of air-cooled A356 alloy [5]

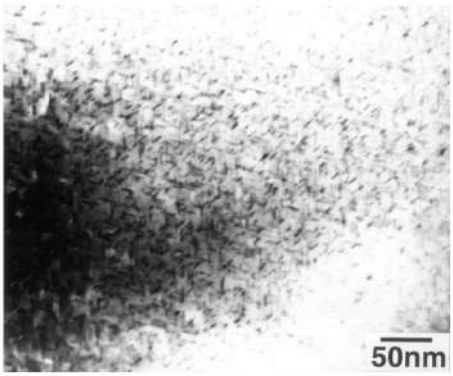

Figure 45: TEM micrograph showing β''-MgxSi precipitates in the α-Al matrix of peak-aged A356 alloy corresponding to an average quench rate of 250 °C/s. Beam direction: <112>$_{Al}$ [5]

In Figure 46 is given the DSC curve of an AlSi7Mg0.75 LBM as-built sample from [20]. A peak is clearly visible at around 210 °C. Samples were built without base plate heating. This graph shows that due to the fast solidification, some precipitation phenomenon can occur on as-built samples, without going through SHT and quench.

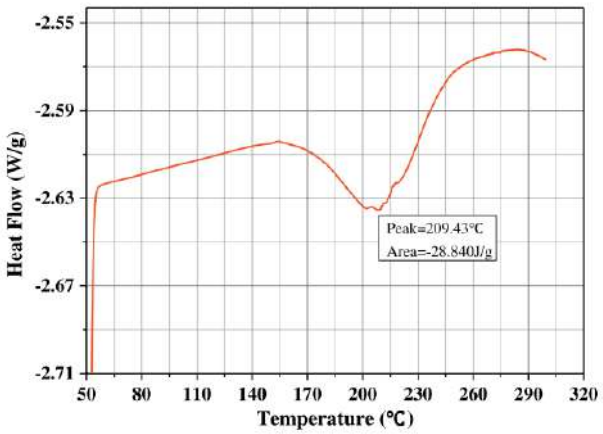

Figure 46: DSC curve of AlSiMg0.75 alloy manufactured by LBM [20]

Partial conclusion on DTA/DSC:

- As-built samples show potential precipitation of Mg_xSi hardening precipitates during fabrication and / or during direct ageing.
- Base plate temperature has an influence on the precipitation kinetic. If the base plate is maintained between 170°C and 200°C, no complementary direct ageing treatment is necessary to increase hardness.
- It is not clear if cast and LBMed precipitation mechanism are identical and occur in similar temperatures ranges.
- More work is needed on identifying the link between the precipitation observed by DSC and the corresponding microstructure in order to identify clearly the phases that precipitate. Furthermore, it is to consider that DTA/DSC is a dynamic measurement; therefore the temperatures evidenced with this method are higher than static values linked to a classical ageing treatment performed at constant temperature.

7 Hardness

Cabrini *et al.* show that after stress relieving (2h – 300 °C), micro-hardness drops from 124±4 HV0.1 to 110±4 HV0.1, indicating a softening of about 10% [21].

Fiocchi *et al.* studied the influence of low temperature annealing heat treatments on hardness [6]. As it can be seen on Figure 47, hardness decreases as time and temperature is increased. The hardness behaviour according heat treatment is coherent with the microstructure evolution and the stress relief as compared to as built samples. At 263 °C, time does not have a significant influence on both the microstructure and hardness. However, there is a significant drop from the as-built hardness. Since the microstructure is very similar to as-built, the reduction in hardness may be attributed to the relaxation of internal stresses or to the precipitation of Mg_2Si in β form, reducing the strength. Fine characterization at very high magnification would be needed to confirm this hypothesis. When the temperature is increased to 294 °C and above, the hardness is reduced and time plays an important role. Indeed, in this range of temperature, Si diffusion and globularisation occurs, leading to a decrease in strength. The Si enriched network is disrupted and as the particles grow due to longer times, hardness decreases.

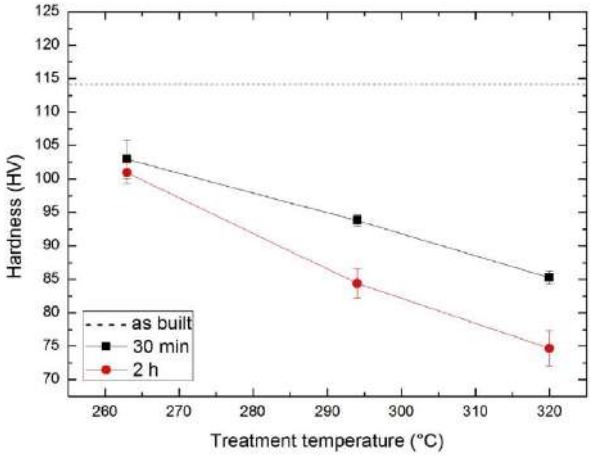

Figure 47: Evolution of hardness as function of the heat treatment temperature and time [6].

Mertens *et al.* studied the evolution of hardness according to three different configurations: as-built, stress-relief and T6 [16]. All samples were produced with a preheating at 200°C. Results are presented in Figure 48. The highest hardness is obtained in as-built condition. However, it is suggested that due to the preheating to 200°C, the value is lower than other studies where samples were built without pre-heating. In comparison with the as-built samples, heat treating at 250°C for 2 hours results in a decrease of the hardness by 10 %. No significant microstructural changes have been observed between as-built and stress-relief samples, so the decrease in hardness could be ascribed to the relief of internal stresses. However, due to the high baseplate temperature, residual stresses are limited. So the effect might be due to another mechanism, such has silicon diffusion and a reduction of solid solution strengthening. It would be relevant to have the measurement of the Silicon amount in α-Al before and after stress-relief for these samples or similar one, especially built at high base plate temperature.

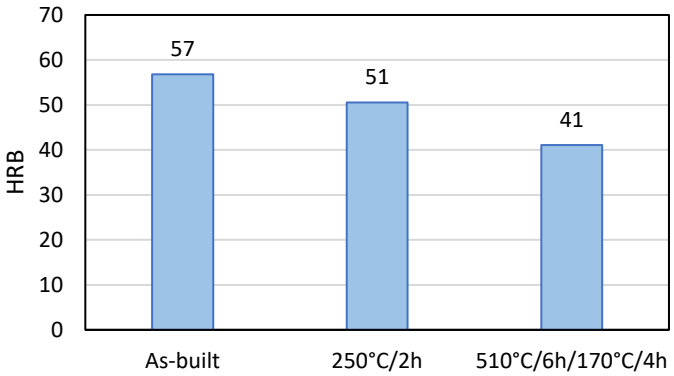

Figure 48: Hardness measurement on AlSi10Mg samples in three different configurations [16].

To go further, the hardness evolution according to temperature and time have been plotted for different ageing conditions after standard SHT. Three temperatures were tested: 150°C, 170°C and 190°C. Hardness profiles are presented in Figure 49 and recall the theoretical behaviour presented in Figure 1 for holding time shorter than 2 hours; for holding time higher than 2 hours, kinetic aspect is an additional parameter to consider.

When ageing at 150°C, the hardness increases slowly and steadily up to a value of 53 HRB after ageing for the longest investigated holding time of 10 hours. The hardness increases rapidly during the 4 first hours of ageing at 170°C. It then remains at a constant value of about 40 HRB for the following 6 hours at 170 C. When ageing at 190°C, the hardness goes through a maximum of 38 HRB after 1 hour, after which it decreases slowly and steadily (likely because of an excessive coarsening of the precipitates). In conclusion, among the investigated condition, the highest hardness is obtained after ageing at 150 C for 10 hours. However, a good compromise between hardness improvement and holding time can be reached when ageing at 170°C for 4 hours. It is these latter ageing conditions that have been further investigated in this study as they provide a fairly large processing window.

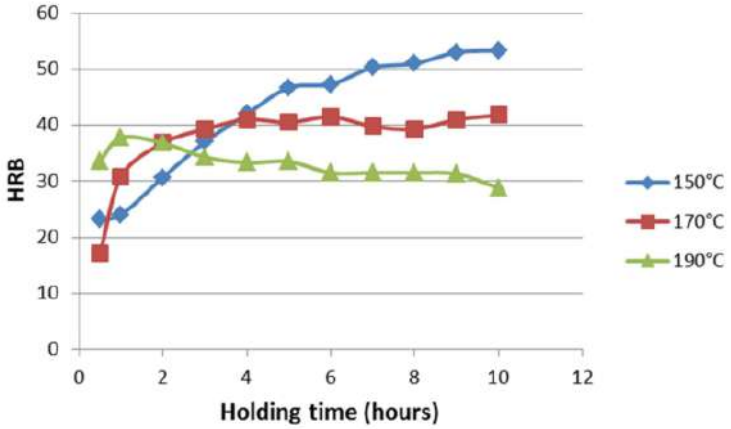

Figure 49: HRB hardness as a function of ageing temperature and time, after solutionizing at 510°C for 6 hours [16]

Takata *et al.* observed a natural ageing at room temperature after SHT at 530 C for 6 h followed by water quench as shown on Figure 50 [12]. The hardness of the as-fabricated sample significantly decreases from 132 HV to 88 HV after annealing at 300°C for 2 h. After the solution treatment at 530°C for 6 h, the hardness decreased to approximately 60 HV. The hardness increases with the natural ageing time, reaches 75 HV, and then nearly saturates after 10^3 ks (about 11 days). The natural ageing (commonly called T4) hardening is caused by the precipitation of the Mg_2Si phase.

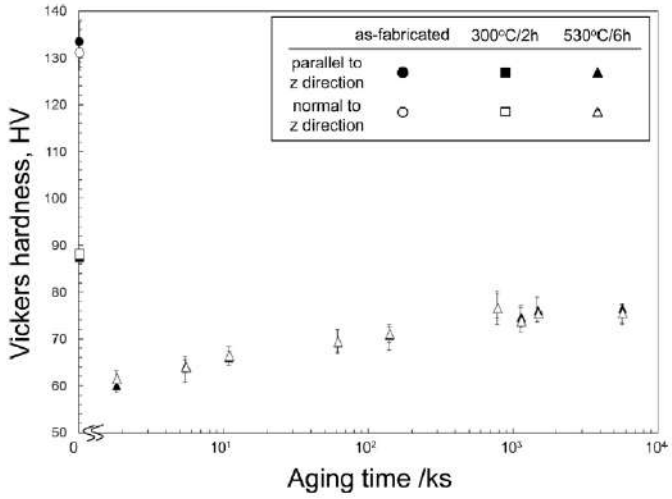

Figure 50: Change in hardness of solution-treated AlSi10Mg alloy (530 °C/6 h) with ageing time at room temperature, together with hardness of as-fabricated sample and subsequently annealed sample (Takata, Kodaira, Sekizawa, et al. 2017).

Fousová *et al.* observed the hardness evolution in time according to different direct ageing temperatures [13]. AlSi10Mg samples were built without base plate preheating, leading to a metastable state in as-built condition, and then directly

aged at different temperatures. Results are plotted in Figure 51. A typical behaviour is observed: the higher the temperature, the faster the hardening. In addition, as the temperature is increased, the over-aged condition is obtained quicker, potentially leading to a material softening. The maximum hardness reached is about 140 HV1.

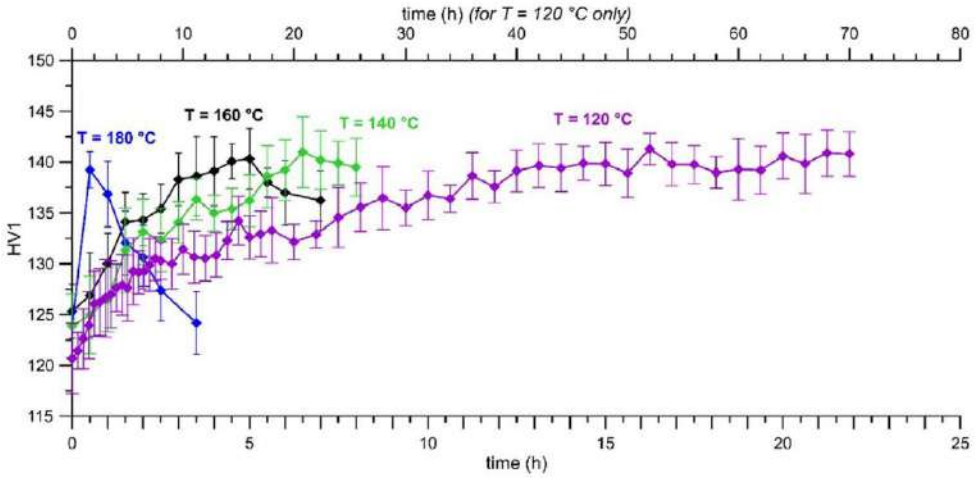

Figure 51 : Curves showing the time evolution of hardness when exposed to elevated temperatures (120 to 180 °C) [13]

In addition, the effect of conventional heat treatment on the material stability was tested too. T6 heat treatment led to a 16% reduction in hardness, whereas the stress-relief treatment resulted in a more significant decrease: 34%. Nevertheless, hardness remained almost stable during 24 h of exposure at 160 °C.

Fousová *et al.* performed direct ageing and plotted a simple TTT-type diagram in order to determine the time needed to reach the highest hardness at a given temperature. It is shown in Figure 52 [13]. For example, at 200 °C, the time necessary for reaching the maximum hardness is 7.1 min.

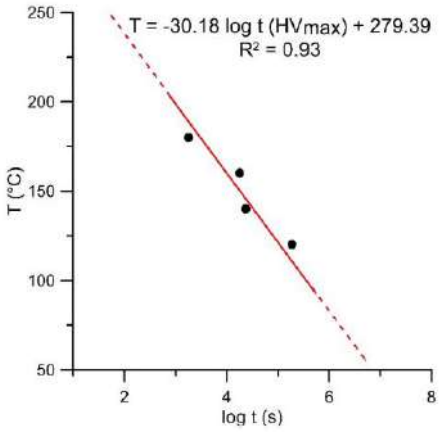

Figure 52 : TTT-type diagram for AM AlSi10Mg [18]

Rosenthal *et al.* evaluate the hardness after different heat treatments [22]. As seen before, stress relieving at 300 °C for 2 h and HIP at 500 °C for 2 h tend to reduce the hardness, Figure 53. In fact, the higher the temperature, and the longer the time, the lower the hardness. However, there is a unique phenomenon occurring at 200°C where hardness is higher than in as-built condition. However, the figure 53 shows that that a stress relief at low temperature/low time (2 h - 200 °C) has not a real negative impact on the hardness meaning that the silicon precipitates growing phenomenon is not really initiated with these too soft conditions.

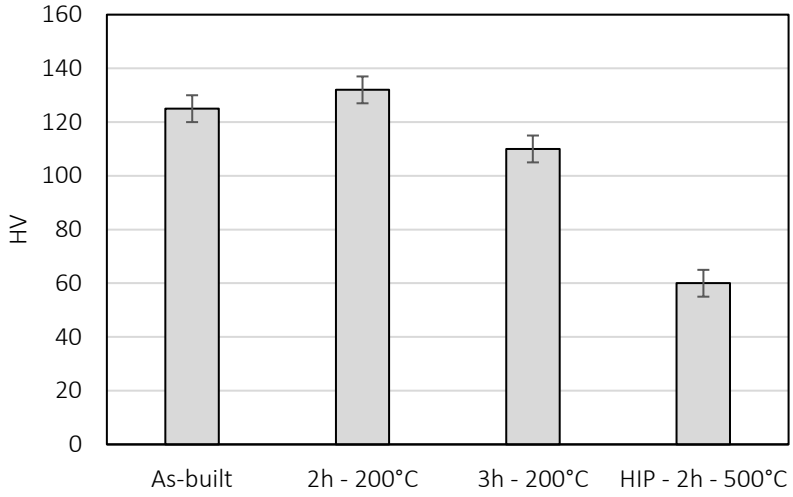

Figure 53: Hardness of AlSi10Mg samples according to different heat treatments [22]afenstein *et al.* studied the combined HIP and T6 heat treatment on cast A356 [23]. The idea is to perform the solution heat treatment at the same time than the pressing step instead of doing it separately. The main issue is that the equipment needs to be able to perform high cooling rates in order to obtain an oversaturated state with magnesium and silicon atoms dissolved in the aluminium matrix, that is to say be able to perform gas quenching.

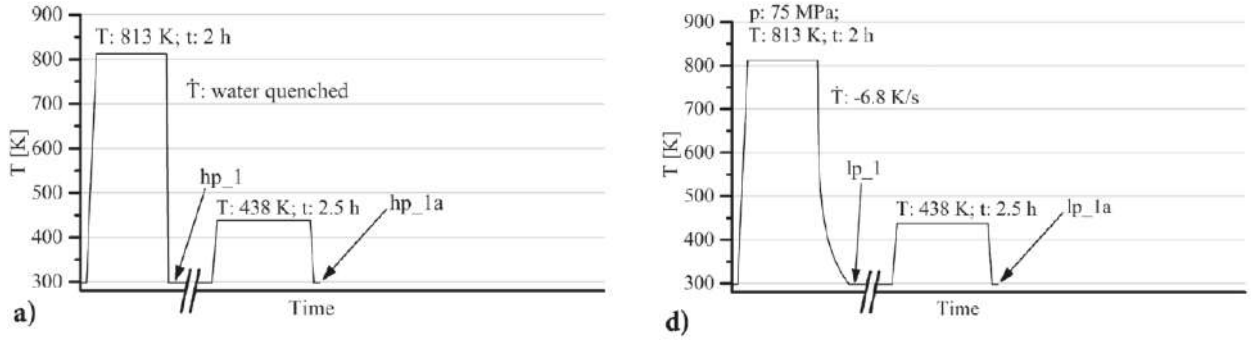

Figure 54: Examples of thermal cycles performed by Hafenstein. (a) Typical T6 treatment; (b) T6 treatment with combined HIP and SHT step [23]

	HIP			Cooling	SHT		Cooling	Ageing		Comment
	Temperature (°C)	Time (h)	Pressure (bars)	Speed (°C/s)	Temperature (°C)	Time (h)		Temperature (°C)	Time (h)	
hp-ac										As cast High porosities
lp-ac										As cast Low porosities
hp-1					540	2	Water			
hp-1a					540	2	Water	165	2,5	
hp-2	540	2	750	-0,32						
hp-2a	540	2	750	-0,32				165	2,5	
hp-3	540	2	750	-0,32	540	2	Water			
hp-3a	540	2	750	-0,32	540	2	Water	165	2,5	
lp-1	540	2	750	-6,8						
lp-1a	540	2	750	-6,8				165	2,5	

Tableau 3: summary of thermal treatments proposed by Hafenstein and al. [23]

Hardness measurements after different heat treatment are shown in Figure 55 for conditions schematized in Figure 54 and detailed in Table 3. Firstly, a significant increase in hardness can be noticed between the high and low porosity as-cast materials (lp_ac *vs* hp_ac). Secondly, the hp_1 and hp_1a samples, being respectively subjected to SHT + quench, and SHT + quench + ageing (see Figure 54) show higher hardness than as-cast material. Notice that the solution strengthening brought by the SHT + quench gives an irease in hardness, and the artificial ageing gives more due to the precipitation of Mg_xSi precipitates. hp_2 and hp_2a samples have been HIPed and quenched with a conventional equipment with a quench rate of 0.32 K/s. hp2_a has been artificially aged. It can be observed that the quench rate was not enough to give an oversaturated solid solution since hardness is not as high as hp_1 and because after artificial annealing, the hardness has not much increased, showing that precipitation mechanism could not occur. hp_3 and hp_3a have been subjected to a combination of cycles 2 and 1. Hardness measurements on theses samples show that it is possible to recover to a high hardness similar to T6-treated sample even after a HIP with a slow quench rate. However, this configuration is not suitable in economic terms. Finally, lp_1 and lp_1a are samples that underwent a combined HIP+T6 with the SHT being done during the HIP step. But in this case, the equipment used was able to perform a higher quench rate that in the 2nd configuration, being 6.8 K/s (see Figure 54). In this case the quench rate is sufficient to allow a supersaturated solution, as the hardness is much higher than in hp_2 condition, however, the gain in hardness after ageing is not as important as in the other conditions, but the hardness achieved is still in the range of classical T6 treatment, being about 82 HB. To conclude, the combination of HIP step and SHT+Quench can be performed as long as the equipment is able to perform a quench rate higher or equal to 6.8 K/s.

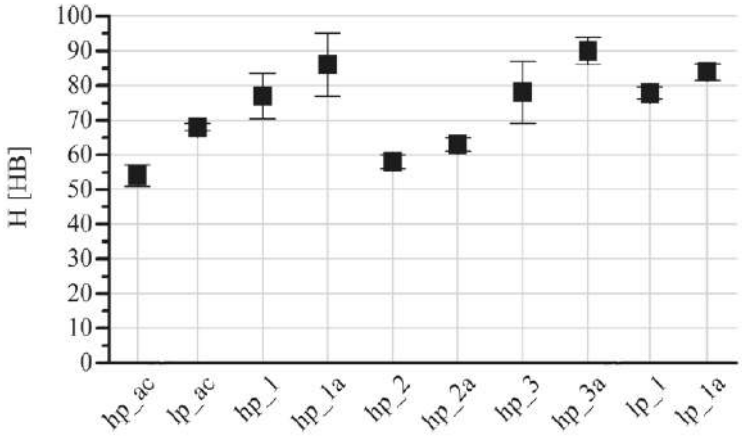

Figure 55: Hardness of the investigated samples depending on the performed thermal treatment.

Fracasso *et al.* studied the influence of quench rate on peak hardness achievable after annealing in case of a T6 treatment for cast AlSi7Mg0.3 [24]. In order to achieve different quench rates, different quench media have been used: 60 C water, 100 C water, sand, insulation material and furnace cooling. The corresponding quench rates were respectively 200, 26, 3, 0.6 and 0.08°C/s. Samples were solution heat treated and then quench (transfer time was shorter than 3 seconds). Then samples were aged at 170°C and the evolution of hardness according to time was plotted (see Figure 56). It is clear that below 3°C/s, the quench rate is not sufficient to obtain a fully saturated solid solution that as the potential to form precipitates. Indeed, for the sample let in the furnace, no precipitation occurs, and for the samples "quenched" in the insulation material, a typical trend is visible, showing that hardening particles precipitates but not sufficiently to achieve the highest hardness. However, for quench rates higher than 3°C/s, the peak hardness is similar whatever the quench rate. Note that still, the higher the quench rate, the higher the hardness. Notice that for a 3°C/s quench rate, the peak hardness is higher when ageing temperature is 170°C than 210°C.

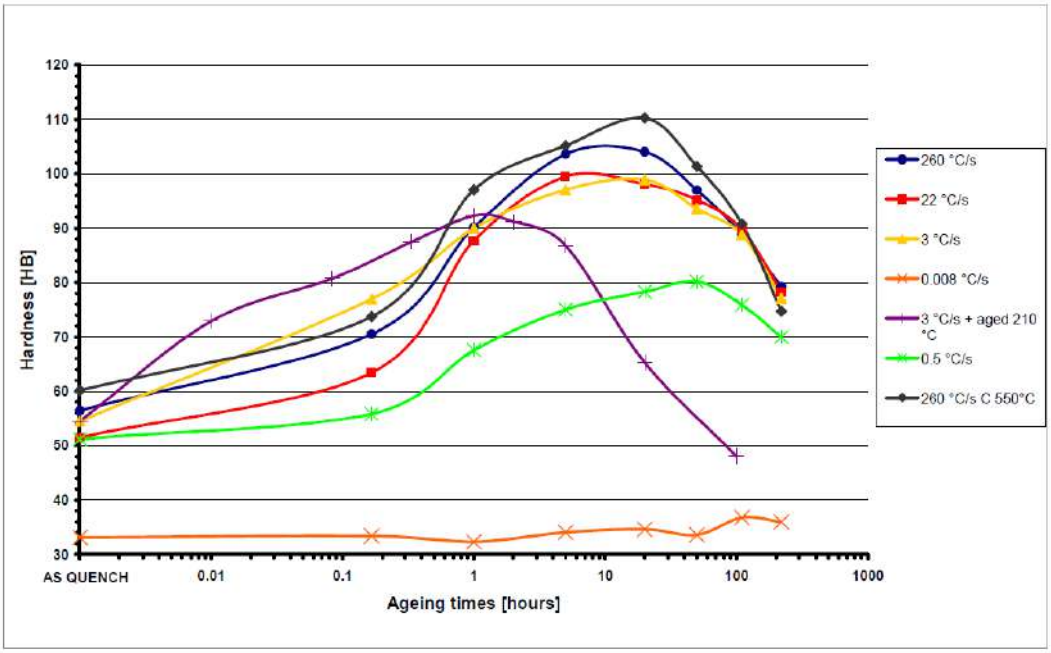

Figure 56: Hardness as function of ageing times for different quench rates [24]

Zhang *et al.* studied the quench sensitivity of cast AlSi7Mg0.4 alloy [5]. Quenching medium were 25 °C water, 60°C water, 95°C water and air. Samples were solution treated for 14 hours at 540 ± 3 °C, quenched and aged at 170°C. Figure 57 shows hardness evolution according to time during ageing. Air cooling (0.5°C/s) leads to lower peak hardness, reached at longer ageing time. At a quenching rate of 20 °C/s with 95°C water, peak hardness trend is similar to the one obtained at higher quenching rates and the peak hardness value reached is about 110HV. 110°C/s and 250°C/s quench rates gives the same behaviour with a slightly higher peak hardness at about 115 HV.

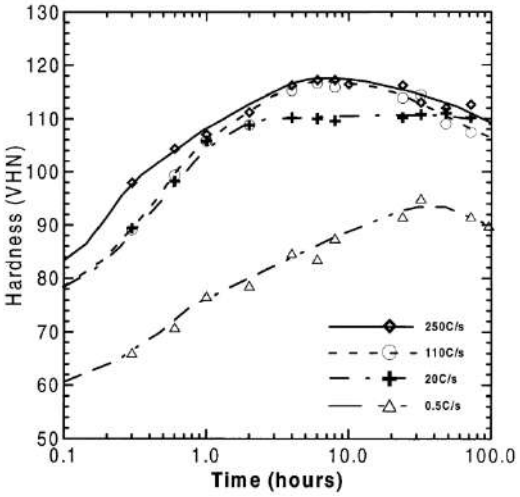

Figure 57: Hardness of A356 alloy as a function of aging time at 170 °C for different quench rates [5]

Partial conclusion on Hardness:

- Hardness is high in as-built condition, generally about 120 HV. This high value is partially induced by residual stresses induced by the process leading to strong deformations if no stress relief step is performed before removing parts from the built plate.
- Increasing the base plate temperature during manufacturing can reduce residual stresses and related harness levels.
- Heat treatments at high temperatures such as stress-relief at 300°C or solution heat treatment decrease the hardness.
- An optimum peak hardness value can be found depending on ageing time and duration.
- Reasonable time optimization can be carried out by making HIP and SHT at the same time. The same hardness value can be reached than the one obtained with classical SHT/Ageing but the porosity content is optimized.
- Low temperature direct ageing, at about 150°C to 200°C slightly increases the hardness. This must be due to a precipitation mechanism but the precipitates are not strictly identified. (One article shows TEM observation of pure Si needles – Fousova and al. 2018).
- High hardness can be obtained after T6 treatment as long as the quench rate is greater than 3 C/s.

8 Tensile Properties

Pedersen *et al.* studied the influence of solution heat treatment time on different AlSi cast alloys heat treated in T6 condition [25]. As seen on Figure 58, UTS is neither affected by SHT duration nor by the Silicon amount. However, higher Mg amount leads to higher mechanical properties after T6. In as-cast condition, there are similar. This demonstrates that Mg has an important role during the T6 treatment and does not play a role in the as-cast microstructure. Figure 59 shows that high level of Si amount leads to lower ductility confirming other findings [7].

Moreover, different quenching rates have been studied with air, oil and water in [7]. The greater the quenching rate, the higher the elongation for all the Al-Si alloys studied here. It is argued that elongation after quenching at different quenching rates is related to the amount of excess silicon in the α-Al. This amount is nearly twice as much in low-amount Mg alloys than in high ones.

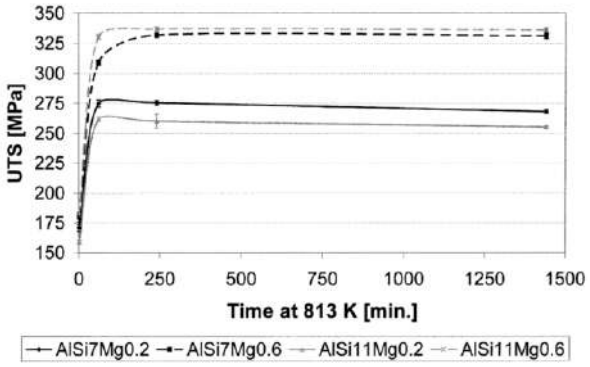

Figure 58: UTS of Al-Si alloys that have been solution heat treated at 540 °C, quenched in water, and aged at 150 °C [25]

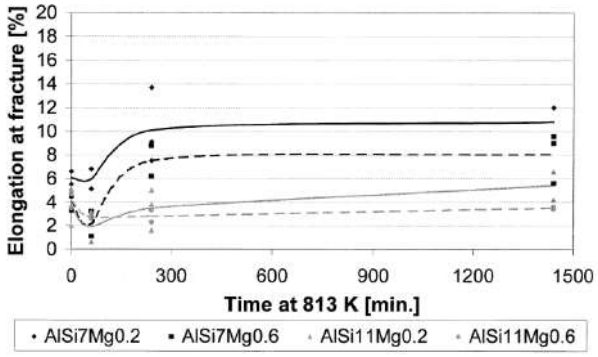

Figure 59: Elongation at fracture of Al-Si alloys that have been solution heat treated at 540 °C, quenched in water, and aged at 150°C [25]

Zhang *et al.* studied the quench sensitivity of cast AlSi7Mg0.4 alloy [5]. It has been observed that yield strength and heat evolution during precipitation were linked to the quench rate as shown on Figure 60 and Figure 61. Note that X axis is in logarithmic scale, so it is not necessary to go to very high quench rates in order to obtain good mechanical properties; this is in phase with the Fracasso's study concerning the influence of the quench rate on the hardness [24].

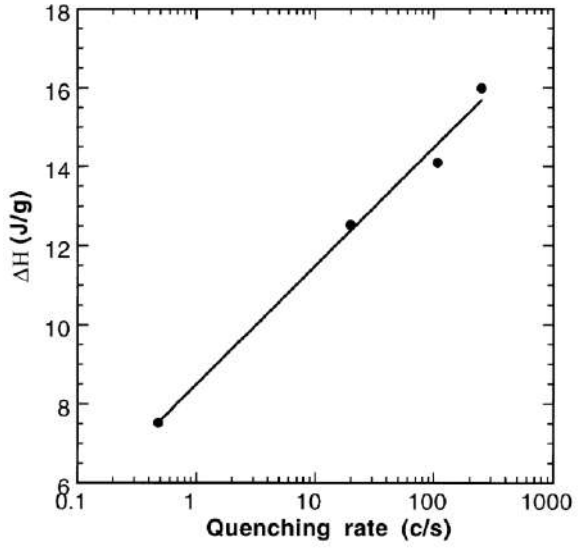

Figure 60: Heat evolution due to precipitation of β'' and β' precipitates, ΔH, during heating of as-quenched A356 alloy in the DSC, as a function of the average quench rate [5]

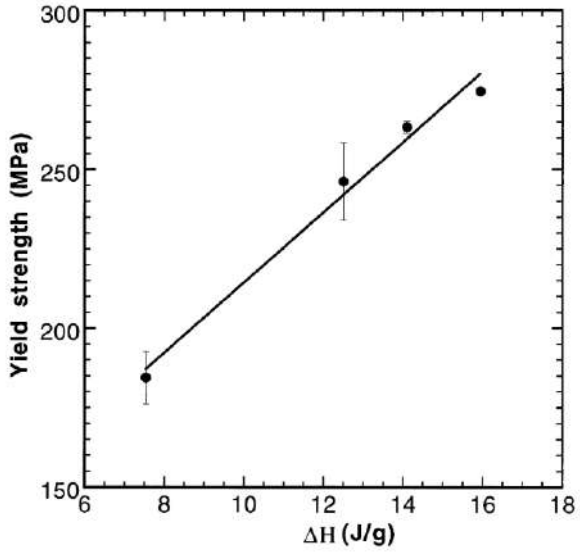

Figure 61: Yield strength of peak-aged A356 alloy as a function of the heat evolution due to precipitation of β'' and β' precipitates, ΔH, measured by DSC [5]

Annealing heat treatments tend to lower the strength and increase the elongation at break. In Figure 62 and Figure 63 are shown the evolution of strength and elongation of LBM specimen after annealing during 5 h at different temperatures [7]. It can be observed that there is a sudden variation after T5 treatment at temperatures equal or above 300°C (T5 correspond to annealing or direct ageing). This behaviour correlates with the microstructure observation, where the Si-enriched phase network disappear at these temperatures. It is suggested that the variation observed at low temperatures are due to a slight cells coarsening and the sudden evolution is related to the fact that there are no cells boundaries to act as dislocation barriers after high temperature annealing.

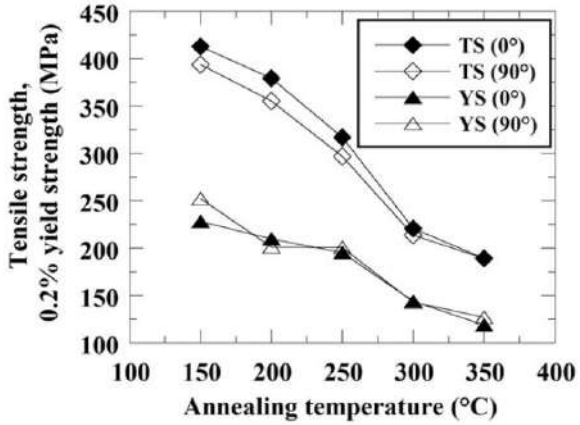

Figure 62: Change of tensile strength (TS) and yield strength at 0.2% nominal strain (YS) in T5 LBM specimens annealed at various temperatures [7]

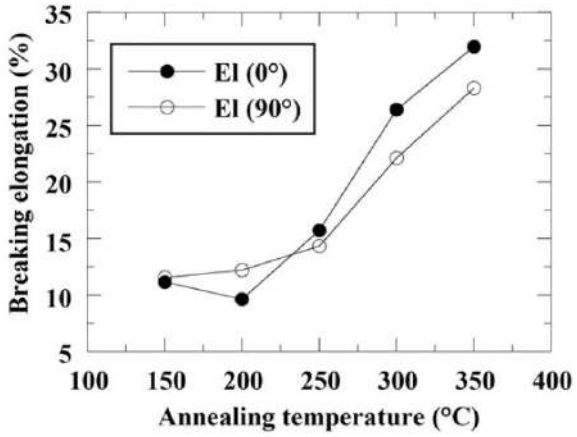

Figure 63: Change of breaking elongation (El) in T5 LBM specimens annealed at various temperatures [7]

Stress relief performed at 250°C for 2h does not have a significant influence on tensile properties of AlSI10Mg specimens built at 200°C as shown on Figure 64. No significant microstructure evolution has been observed between as-built and stress-relieved specimens [16]. It is suggested that the differences might be related to the relief of internal stresses only however with a base plate heated at 200°C, stresses are already minimised. Instead, it might be due to a diffusion of Si from the supersaturated α matrix which decrease the amount of solid solution strengthening, or eventually by the precipitation of Mg_xSi. After a T6 treatment, ductility is largely increased due to the globularised microstructure. In parallel, tensile strength is slightly decreased, but yield stress is largely increased due to precipitation hardening. According to these data, it seems that T6 treatment is relevant on parts printed with a baseplate temperature of 200°C.

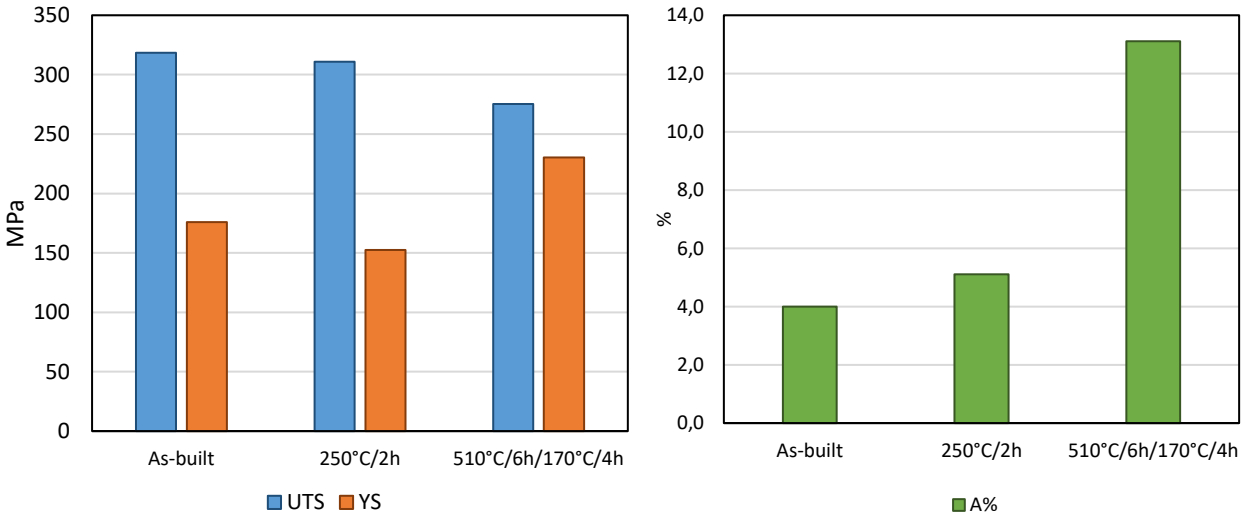

Figure 64: Tensile properties of AlSi10Mg samples in different conditions, adapted from [16]

On Figure 65 is shown typical tensile behaviour of heat treated samples built at 35°C [8]. Direct Ageing at low temperatures (160°C- purple) leads to brittle behaviour as already observed [13]. Stress-relief at 300°C (blue), leads to more ductile behaviour with decreased strength due to the disruption of the eutectic network. T6 treatment (red), with a solution heat treatment of only one hour, seems to be a relevant choice, as it increases the yield stress while maintaining acceptable level of elongation.

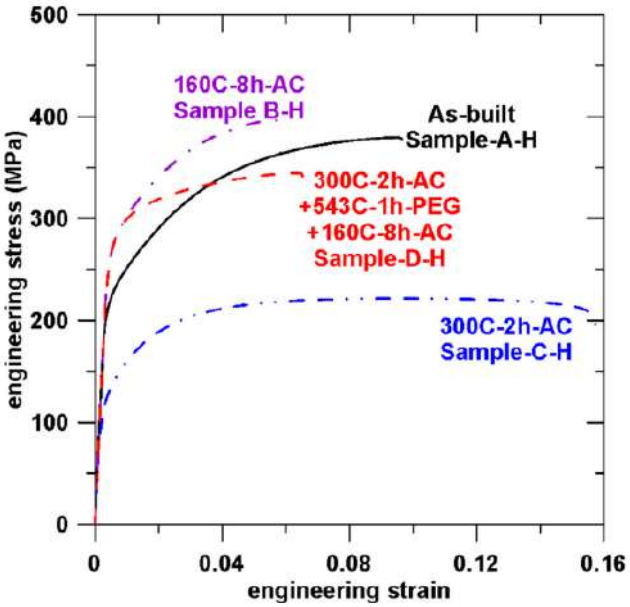

Figure 65: Engineering stress-strain curves for selected horizontally oriented samples [8]

Figure 66 shows the mechanical behaviour of the same batch of samples both in horizontal and vertical direction. The trend discussed before is confirmed here. First, it can be noticed that anisotropy is much more pronounced on elongation than on strength. Stress-relief at 300°C for 2 h, leads to a very large amount of elongation but does not reduce anisotropy. On the contrary, T6 treatment gives similar elongation to as-built samples but reduced anisotropy. Notice that anisotropy and elongation at failure reduces as solution heat treatment duration increases.

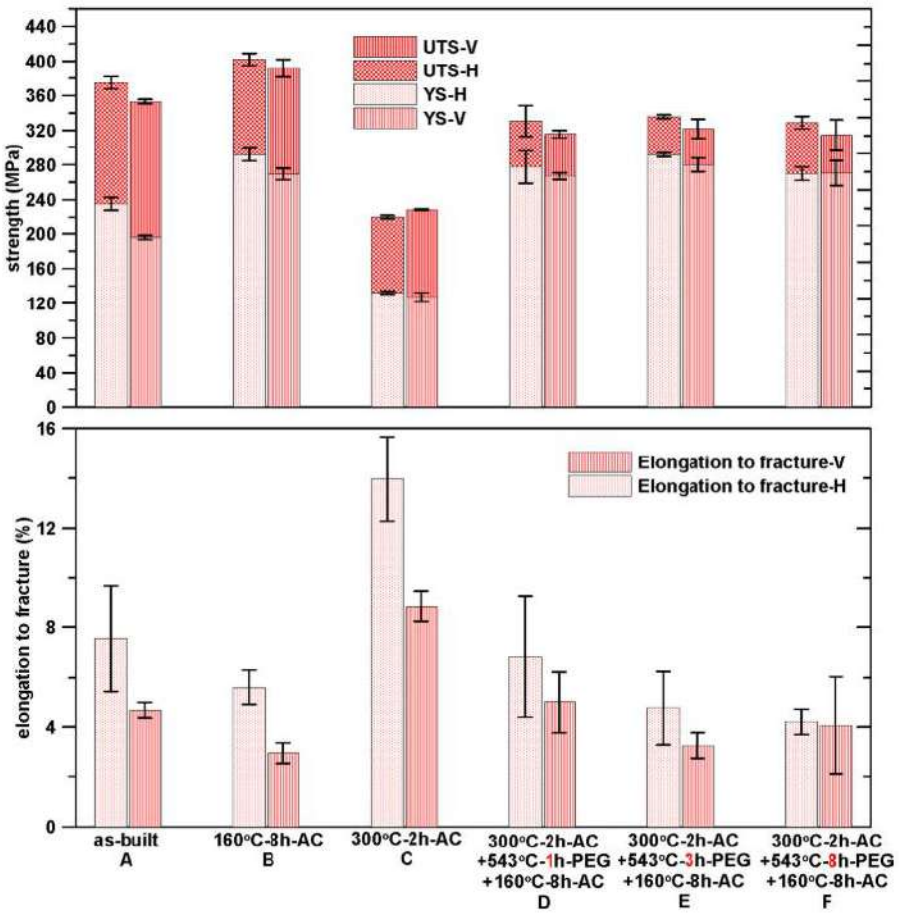

Figure 66: Bar charts showing yield strength (YS), ultimate tensile strength (UTS) and elongation to fracture of samples under different heat treatment conditions(V means vertically oriented samples and H means horizontally orientated sample) [8]

Yang *et al.* tried to identify the mechanisms that play a role in the mechanical behaviour observed for different heat treatments as shown on Figure 67; for that, they use thermodynamic considerations and calculate the effect of each hardening contributor using Thermocalc Software. However, the contribution of the cellular morphology is not taken into account although according to the literature, it is the main contributor to high strength especially in as-built specimens. The grain boundary strengthening presented here is related to the crystallographic grains, which indeed does not seem to play a role as it does not change with heat treatments. However, cellular morphology can largely be modified and even disappear when temperatures are above 300°C. This effect is not taken into account here, leading to incoherent interpretation, like the major role of natural ageing in as-built samples which is not so significant [12], and may be explained by the cellular morphology.

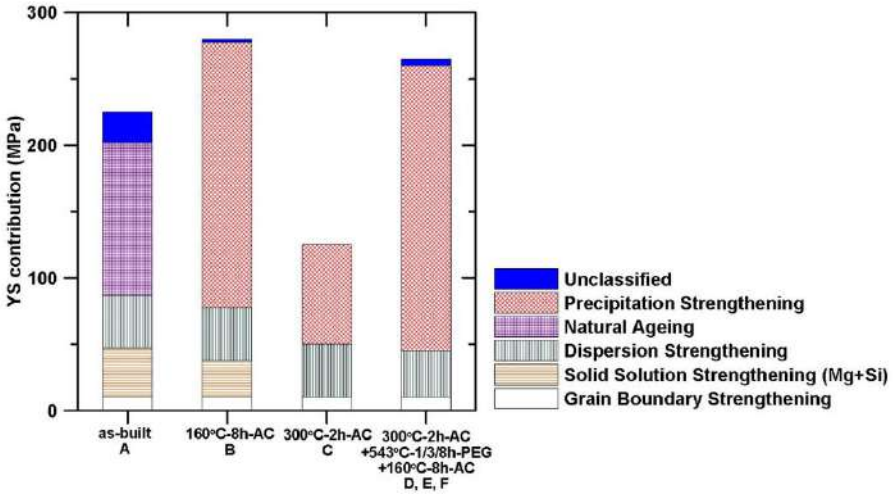

Figure 67: Bar chart showing YS contributions from each strengthening mechanisms, unclassified including contributions from dislocations, SSS from Fe solutes etc.

(Rosenthal, Shneck, and Stern 2018) [22] studied the impact of different heat treatments on tensile characteristics. The tensile behaviour for each of the configuration tested is shown in Figure 68. The different behaviours observed are typical from the ones already presented [22]. Stress-relief at 300°C for 2 h (green) leads to higher elongation than as-built condition but with lower yield strength. HIP at 500°C for 2 h (purple) gives the same trend but with more pronounced effect. As-built samples present a very high mechanical strength but with low elongation. When treated at 200°C for 2 h (blue), a similar behaviour to (Fousová et al. 2018) is observed, where the elongation is reduced and strength slightly increased [13]. This treatment leads to a more brittle behaviour. Before 300°C, the microstructure remains cellular, with only a precipitation of fine Si particles in the α matrix occurring. This precipitation reduces the amount of solid solution strengthening. According to the tensile properties, it seems that the effect of the morphology of the structure, that is a very fine sub-micron cellular cells, plays a major role compared to the solid solution precipitation brought by the supersaturated solution of Si in α.

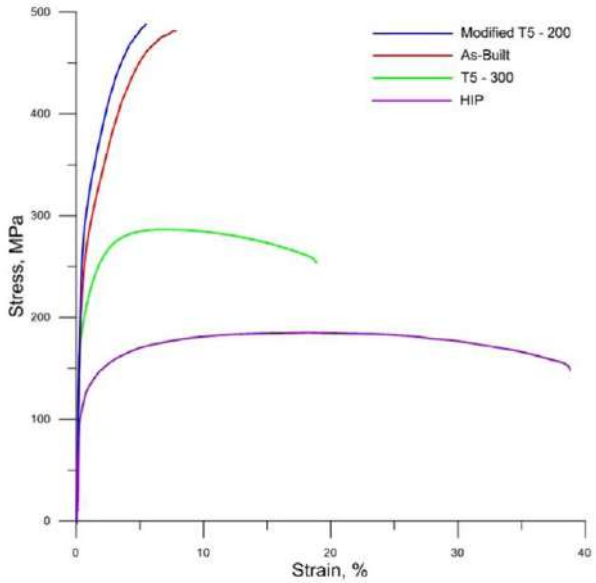

Figure 68 : Engineering stress-strain curves for AlSi10Mg samples under different conditions [22]

The surface fractures of these samples have been observed and showed different patterns according to the heat treatments performed. Samples were all manufactured in Z direction. As-built (figure 69-a) and directly aged at 200°C (figure 69-b) samples share similarities in the macro-features of the fracture surface. Both only contain short and discontinuous track segments with the direct ageing treatment resulting in a more irregular fracture. They also both consist in shallow dimples, reflecting the high strength and low ductility of the material at these states. The lower ductility of the directly aged specimens can be attributed to the precipitation of the nano-sized particles of Si that originate from the supersaturated solution at 200°C and their location is dispersed within the center of the cellular eutectic cells. In case of the sample stress-relieved at 300°C (figure 69-c), it is clear that fracture occurs along the melt pool borders which serve as weak points. Following the HIP treatment the whole meso-structure of the AM process is erased and the fracture surface reflects this by the lack of any visible segments (figure 69-d).

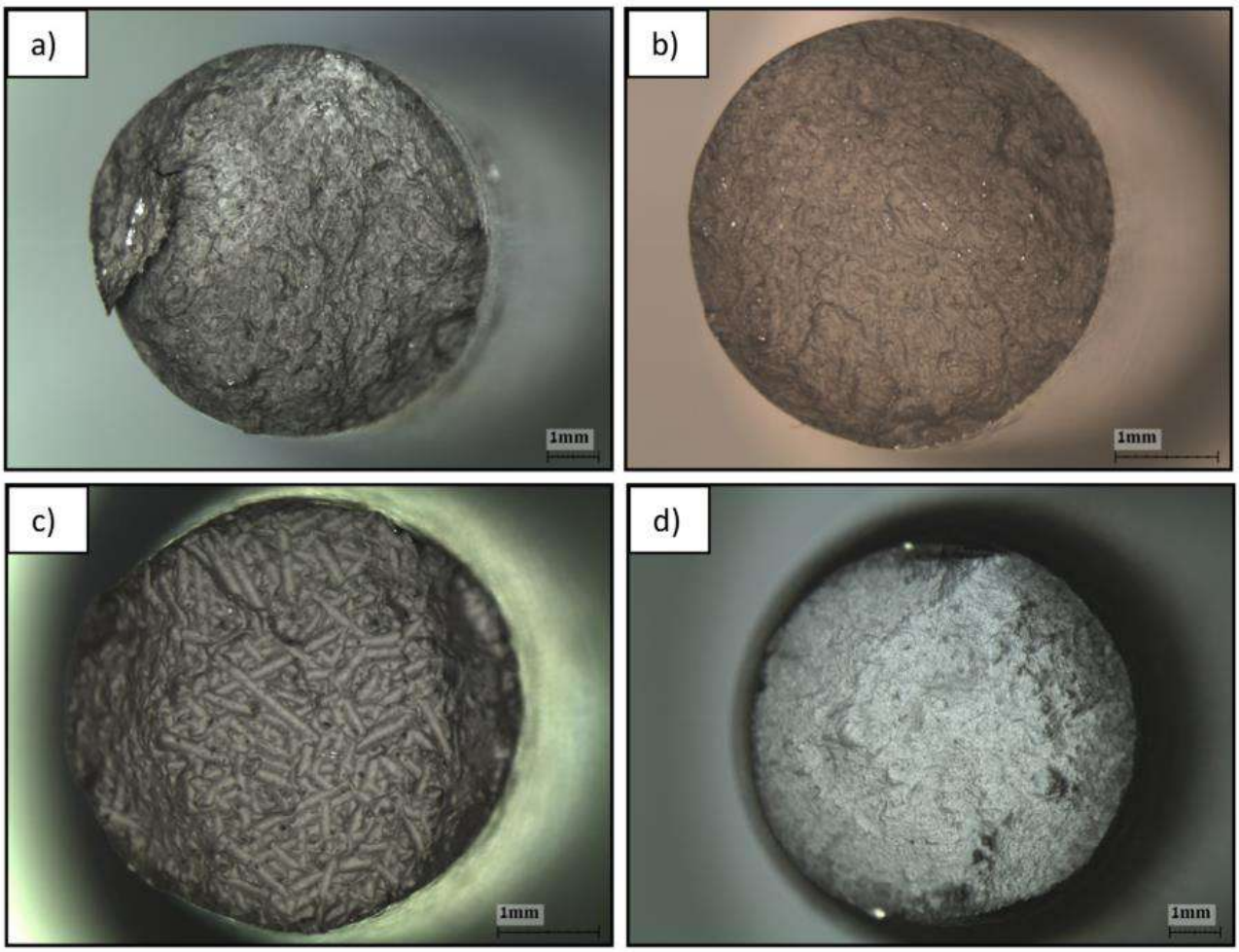

Figure 69: Optical images of the tensile fracture surface's macro-features of the AlSi10Mg LBM alloy; a) as-built with barely visible track segments; b) modified T5 treatment (200°C), barely noticeable track segments, shorter in nature and less ordered than the typical T5 treatment; c) typical T5 treatment (2 h at 300 °C), showing the track segments indicative of the hatching strategy and the 67° rotation of the laser; d) HIP treatment, completely "erased" the traces of the hatching strategy [22]

Li *et al.* studied the tensile properties of AlSi10Mg samples subjected to different SHT temperatures and after artificial ageing at 180°C for 12h [10]. Their results are presented in Figure 70.

As the samples are solution heat treated, there is a dramatic decrease in strength and a large increase in ductility (Figure 70a). The higher the SHT temperature the lower the strength and the higher the ductility. The increase in elongation to failure seems to occur mainly for SHT temperature below 500°C as elongation to failure is similar when treatment is performed at 500°C or 550°C.

It can be noticed that the artificial ageing performed here after different SHT gives almost the same behaviour whatever the previous state. It seems there is no need to heat samples above 500°C as the gain in ductility is very limited whereas the strength is still reduced. The chosen artificial ageing does not seem relevant as the mechanical characteristics are poor and identical between all the samples. 12 h at 180°C may be too high and long leading to an over-aged condition. As the tensile properties are identical after ageing, it is not possible to determine the influence of the different solution heat treatment temperatures. It would have been better to perform different ageing cycles and to plot the complete hardness curve according to time for a given temperature and compare the results. According to the different SHT, there may be a difference in peak hardness and time to reach this peak.

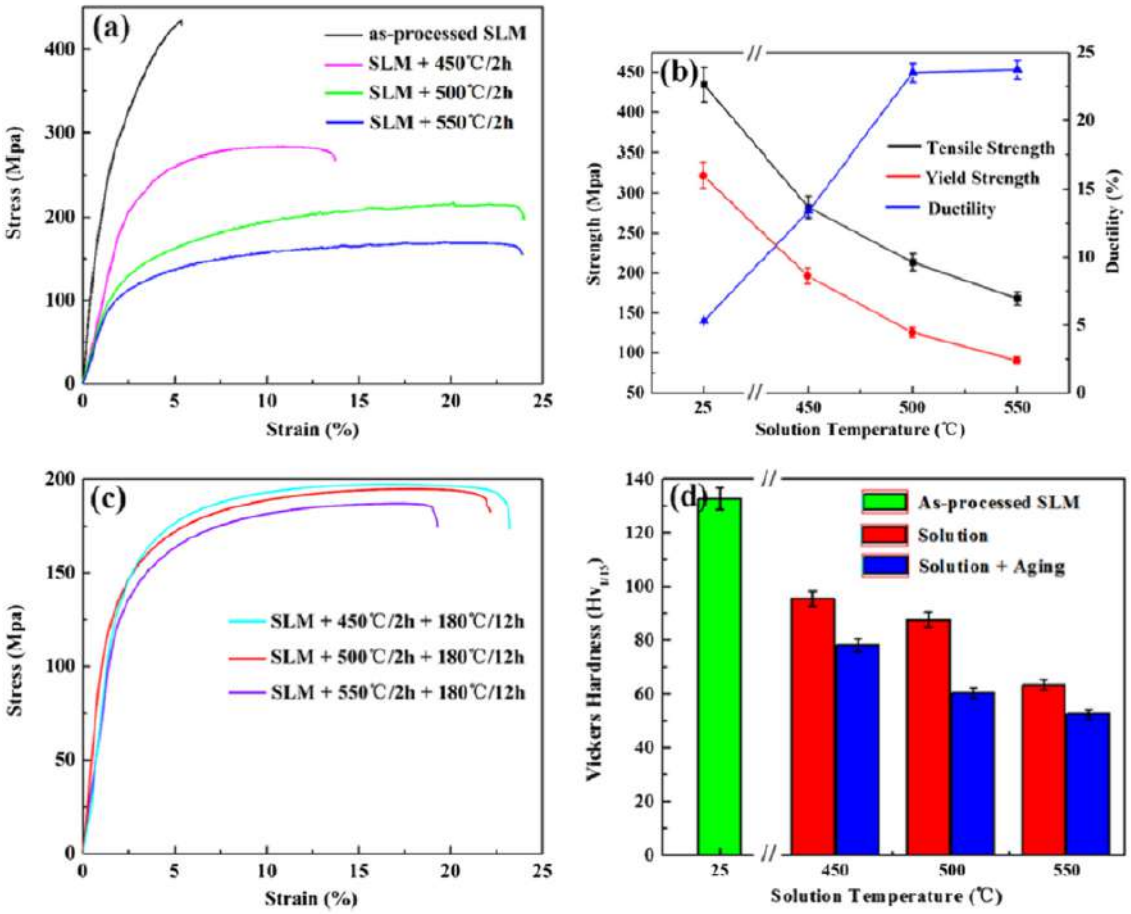

Figure 70: (a) Room temperature tensile stress-strain curves of the as-built LBM samples that solution heat treated at different temperatures; (b) corresponding mechanical data; (c) tensile test stress-strain curves of the solution + artificial ageing specimens; (d) the Vickers hardness of the as-built and heat-treated LBM specimens [10]

In Figure 71 are presented the results from Rao *et al.* where the effect of stress relief and different SHT on tensile properties were evaluated [11]. Stress relief or solution heat treatment leads to an increase in ductility and decrease in strength. After 2h at 300°C, there is a significant decrease in strength and a slight increase in ductility. It is argued these variation are due to the relaxation of internal stresses and to partial diffusion of Si from the supersaturated matrix. After 15 min of solution heat treatment, the ductility increases significantly to 23%. However, with further increase in solution heat treatment time, there is a steady drop in ductility to 16% after 150 h. Accompanying this the tensile stresses steadily decrease after solution heat treatment to around 200 MPa in UTS, and less than 100 MPa in yield strength after 150 h solution heat treatment. Residual stresses are negligible for all the heat treated configurations so they cannot explain the differences observed in tensile properties. However, both the amount of Si in α-Al and the morphology of Si particles are different. The differences between the stress-relived and SHT for 15min samples can be explained by the different amount of Si in α-Al, leading to a reduction of Yield strength in the second one. Note that the Si particles are also more numerous in case of the stress-relieved samples. However, for SHT samples, the amount of Si in solid solution is similar, so differences in tensile properties can only be explained by the Si particles morphology. As the SHT time increases, the Si particles network is dissolved and ductility is increased but up to a certain point. Indeed, when particles get coarser they act as initiation sites of failure, leading to a decrease in strength and ductility. Indeed, a correlation has been observed between particle size and ductility and strength as shown on Figure 72.

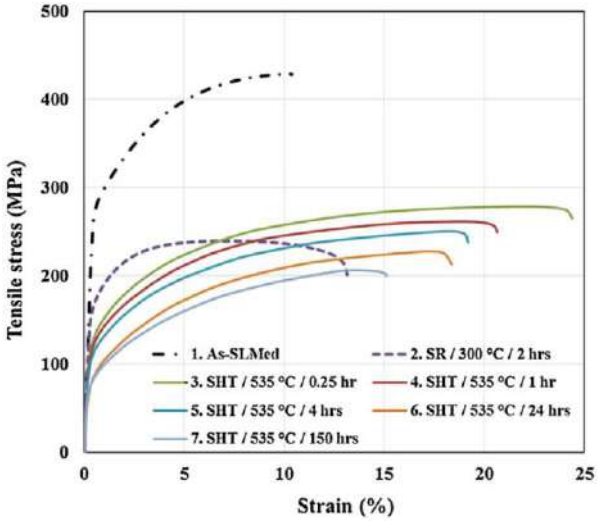

Figure 71: Engineering stress – strain curves of LBMed tensile samples in the as-built and different heat treated conditions [11]

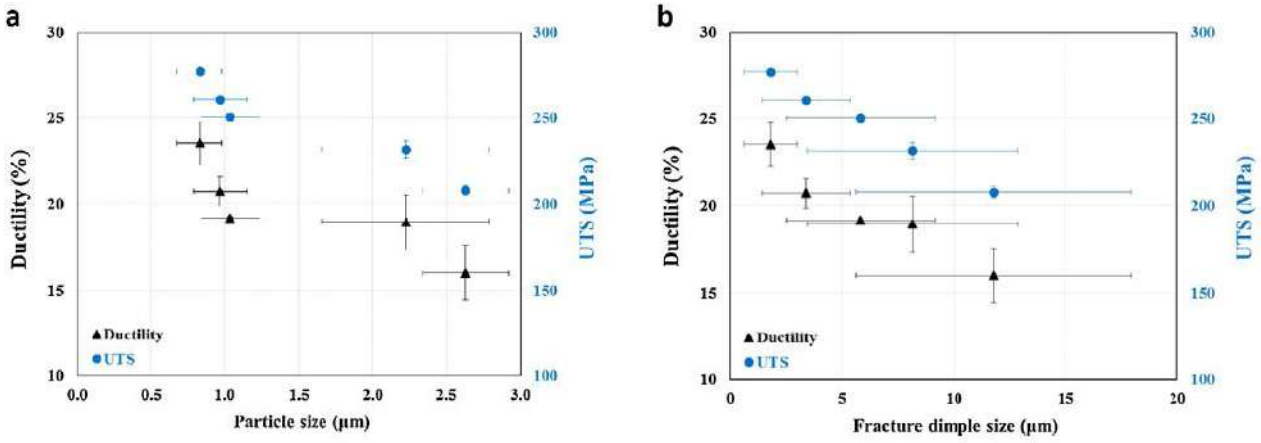

Figure 72: The relationship between tensile ductility with (a) Si particle size and (b) fracture dimple size of LBMed A357 samples [11]

Takata et al. evaluated the tensile properties of AlSi10Mg subjected to stress relief and SHT in XY and Z direction [12]. In Figure 73 are given the curves of these tensile tests. Firstly, it can be noticed that as seen previously, stress-relieved samples show a significant reduction in strength and a gain in elongation compared to as-built-samples although the microstructure are similar. Relief of internal stresses, precipitation of Si in α-Al leading to reduction in Solid Solution Strengthening and partial diffusion of Si from the eutectic network are involved in this change in behaviour. Secondly, a difference in ductility behaviour is observed between XY and Z specimens as-built and stress-relived. Elongation is lower in Z direction for these specimen and fracture along melt-polls boundaries has been confirmed by fractography. On the other hand, no difference in ductility is observed between XY and Z samples after SHT. The microstructure is homogenous and melt pools were not visible anymore.

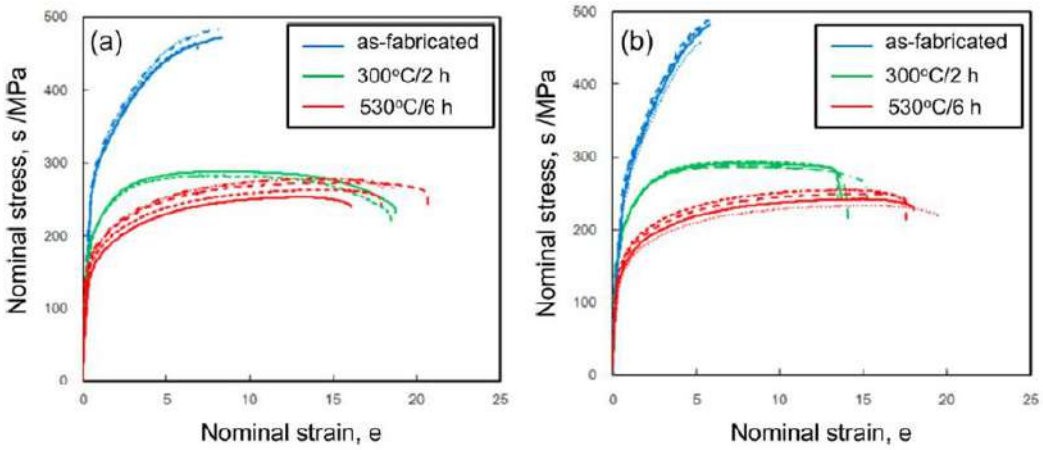

Figure 73: Nominal stress-strain curves of AlSi10Mg specimens measured by tensile tests at room temperature: (a) tensile direction normal to Z direction, (b) tensile direction parallel to Z direction [12]

In Figure 74 are shown the tensile properties of AlSi10Mg specimens in different configurations which are: as-built, HIP treated and T6 treated, in vertical and horizontal orientations and with a machined or rough surface. These configurations are summarised in Table. Note that specimens had generally a high level of porosity, about 1-2%. HIP was performed at 100 MPa for 2h at 530 C. T6 was defined as the following: solution heat treatment for 5 h at 520°C, followed by water quench and then ageing for 12 h at 160 C.

In the as-built condition, both strength and elongation are smaller in Z direction than XY plane. This contradicts the general trend observed in other studies where the strength is generally similar in both direction and the anisotropy is only identified on the elongation. Elongation for HIP only sample is very high for horizontal samples, around 20%. But the anisotropy is especially pronounced for these specimens as the elongation in Z direction is only about 3%.

After T6 treatment, there are still differences between XY and Z direction samples, both for strength and elongation. This might be due to the effect of defects rather than the microstructure since it is supposed to be homogenous after T6.

Finally, it can be observed that HIP+T6 tends to slightly increase the strength compared to T6 only samples but the anisotropy is not eliminated, showing that even if defects are collapsed by HIP, microstructure must play a role in the anisotropy of the tensile properties. As already seen, a longer SHT time might be needed in order to have complete disappearance of anisotropy [8].

Table 4: A summary of the conditions investigated using tensile testing.

Condition	Machined from rod (M)	As-fabricated dogbone (rough surface, R)
Vertical build orientation (V)		
As-fabricated (AF)	3 (AF-V-M)	3 (AF-V-R)
HIP-only (HIP)	3 (HIP-V-M)	3 (HIP-V-R)
T6-only (T6)	3 (T6-V-M)	3 (T6-V-R)
HIP plus T6 (HIP + T6)	3 (HIP + T6-V-M)	3 (HIP + T6-V-R)
As-fabricated fresh powder (FP)	3 (AF-V-M-FP)	–
As-fabricated recycled powder (RP)	3 (AF-V-M-RP)	–
Horizontal build orientation (H)		
As-fabricated (AF)	3 (AF-H-M)	3 (AF-H-R)
HIP-only (HIP)	3 (HIP-H-M)	2 (HIP-H-R)
T6-only (T6)	3 (T6-H-M)	3 (T6-H-R)
HIP plus T6 (HIP + T6)	3 (HIP + T6-H-M)	3 (HIP + T6-H-R)

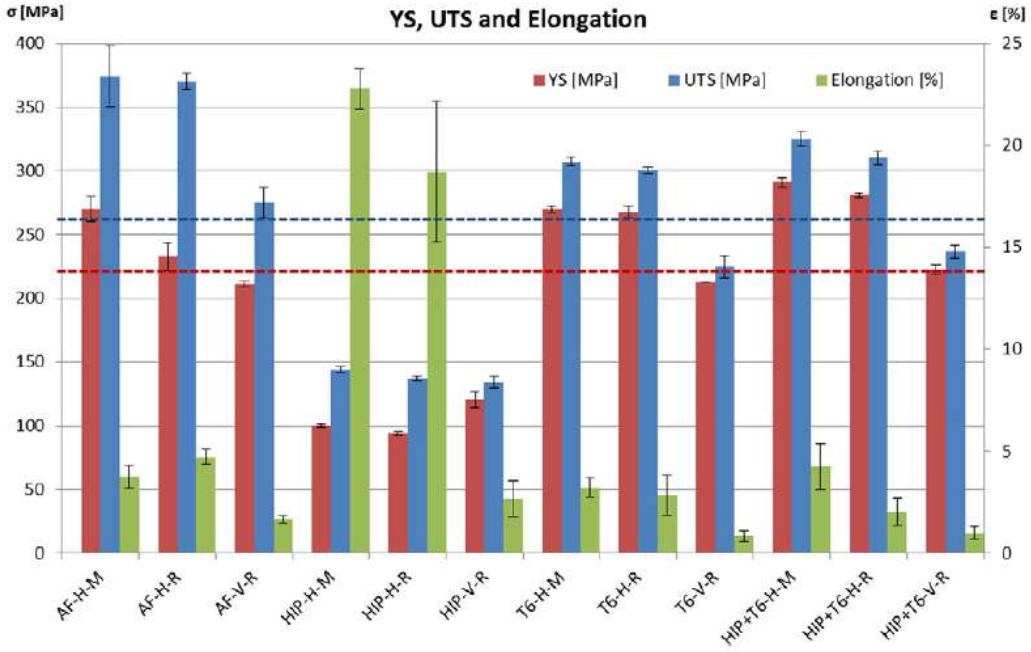

Figure 74: The mechanical properties of all conditions (sample code is shown by Table 4). Dashed lines indicate the standard values for cast + T6 AlSi10Mg [19]

Fousová et al. observed that a direct ageing at 160°C during 5 h of as-built AlSi10Mg samples gives the highest hardness in the minimum amount of time and was selected as the most suitable heat treatment in terms of hardness [13]. However, the tensile behaviour of these specimens was not satisfying. Indeed, the hardening goes hand in hand with a slight increase in the tensile yield strength. Nevertheless, a significant drop in elongation down to below 1% occurred as shown in Figure 75. Such embrittlement is very negative and may significantly reduce the lifetime of a considered part by a premature fatigue failure. On the other hand, T6 heat treated and stress-relived samples show a typical behaviour with increased elongation and reduced strength compared to as-built condition.

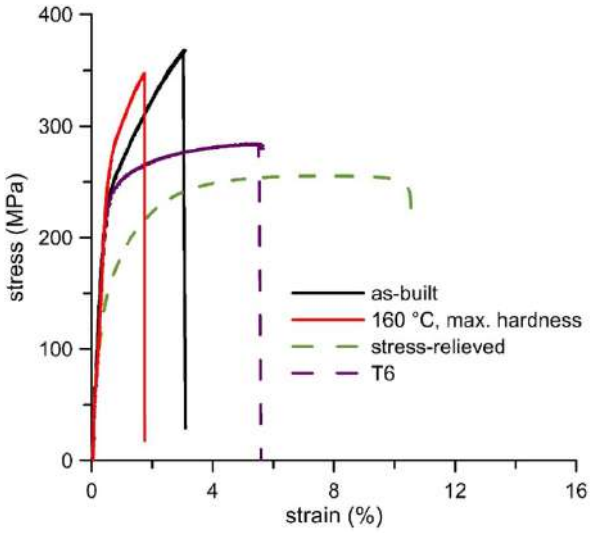

Figure 75: Tensile stress-strain curves for specimens in the as-built condition, after conventional heat treatment and after exposure to 160 °C/5 h [13]

Hafenstein et al. studied the potential to use a combined HIP with a SHT+Quench treatment, in order to perform a T6 like heat treatment but at lower cost by reducing the lead times (Hafenstein et al. 2016) [23]. The different configuration are described in the paragraph dealing with hardness. Tensile properties of these samples are given in Figure 76 to Figure 78. Hp_1a is the T6 reference condition. Lp_1a is the fully treated condition with combined HIP+SHT+Quench and ageing. It can be observed that the strength reached with combined treatment is not as high as T6 but still better than as cast material. It shows that with a sufficient quench rate, the precipitation hardening can occur and improve the characteristics. It is worth to notice that the elongation is four times higher for the HIP treated sample lp_1a than the T6 reference, certainly due to reduction of porosity amount. This compromise in strength, in accordance with a lead time reduction, can be a valuable opportunity for industrial applications. Again, the condition on quench rate in order to obtain a saturated solution was determined to be a quench rate of 6.9 K/s.

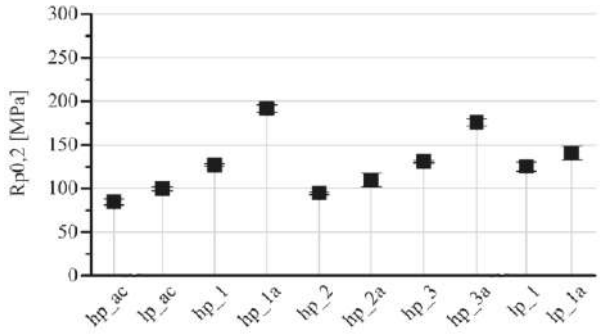

Figure 76: Yield stress of the investigated samples depending on the performed thermal treatment.

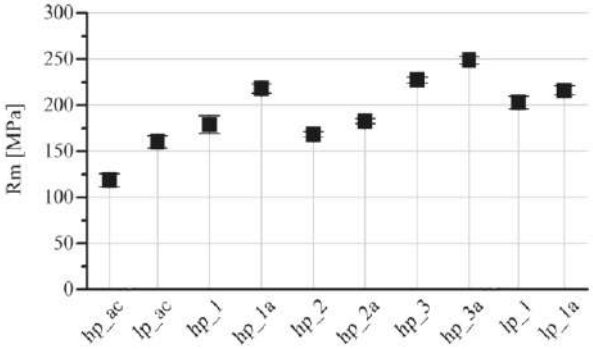

Figure 77: Ultimate tensile strength of the investigated samples depending on the performed thermal treatment.

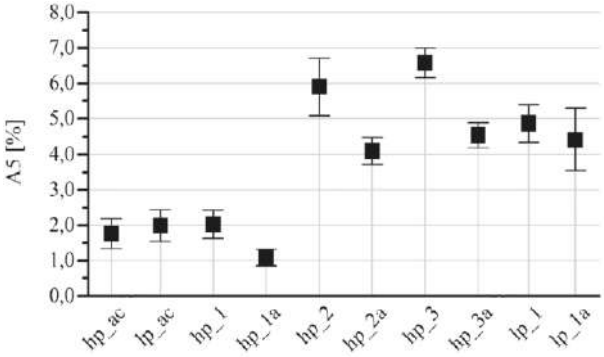

Figure 78: Elongation at fracture of the investigated samples depending on the performed thermal treatment.

Finally, they observed that room temperature pre-ageing greater than 48h and the absence of pressure during the SHT step do not significantly affect the hardness after ageing at high temperature.

Uzan et al. evaluated the tensile properties of AlSi10Mg samples built at 35°C in different configurations: as-built, stress-relieved and HIPed [14]. Tensile curves are shown in Figure 79. As seen previously, the as-built condition gives the highest strength but with le lowest elongation. Stress-relief and SR+HIP at 250°C show a similar behaviour where Ultimate tensile strength is dramatically reduced compared to as-built condition, whereas Yield Strength is not much affected. However, the elongation is dramatically increased. This behaviour can be explained to a combination of different factors : the release of internal stresses (recall that the baseplate was kept at 35°C for building these samples), the precipitation of Si from saturated α, reducing the solid solution strengthening, and the disruption of the eutectic network, leading to less resistance to the motion of dislocations. After HIP at 500°C during 2 h, the strength is significantly reduced but the elongation is increased. The material has become very soft, with no more strength. Indeed, the microstructure is made of very large Si particles that play no role in the mechanical properties and the ductility is inherited from the aluminium matrix.

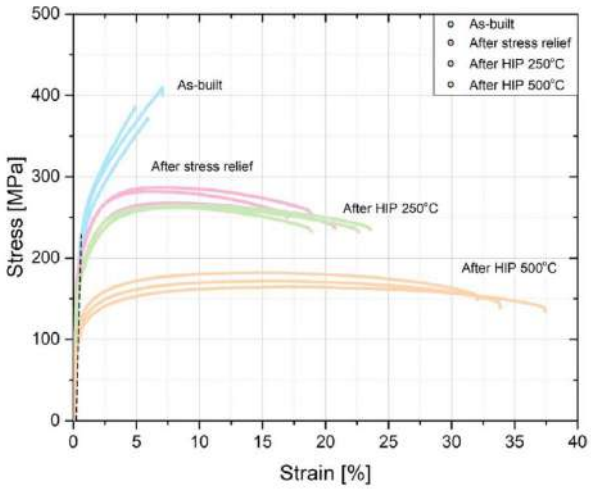

Figure 79: Engineering stress-strain curves of LBM AlSi10Mg specimens after various treatments. The slope of the dash line corresponds to Young modulus of AlSi10Mg alloy (65 GPa) [14]

Aversa et al. studied the influence of baseplate heating on tensile properties [15]. Tensile strength tends to increase when base-plate temperature is between 140°C and 170 C. At 100°C and 190°C base plate heating, tensile behaviour is similar. This might be explained by the following: an in-situ ageing is performed when building specimens at high temperatures. When temperature is too low, precipitation hardening cannot be performed as the energy is not sufficient. Whereas in case of 190°C pre-heating, the effect may be opposite and over-ageing is performed. Between the two, the right temperature can achieve precipitation hardening during the fabrication.

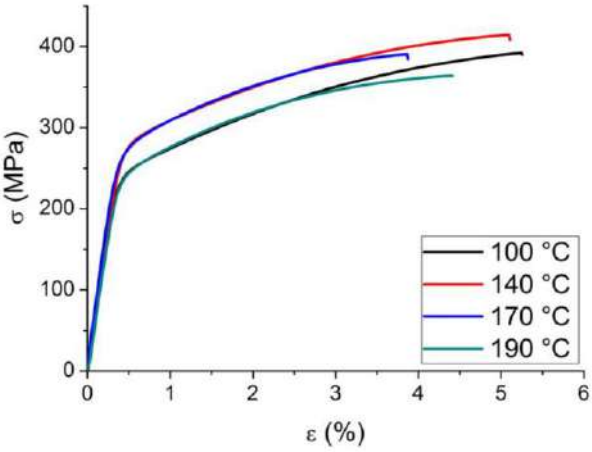

Figure 80: Stress–strain curves of A357 samples [15].

Partial conclusion on tensile properties:

- Tensile strength is high in as-built components due to manufacturing residual stresses, but elongation is generally low.
- A direct ageing at temperature up to 200°C does not allow improvement neither of the strength nor of the ductility of the material but can be performed for medium-structural applications.
- When the material is exposed to high temperature during a long time (e.g. during SHT or stress relief), strength decreases and elongation increases, leading to a material softening.
- The same observation can be done for the HIP process temperature. High HIP temperature is generally required to reduce the porosities number; in this case, a post-T6 treatment will be necessary to get acceptable yield strength.

- During the SHT/quench step, the quenching rate must be higher than 3°C/s if a post T6 treatment is envisaged. Therefore, a sufficient quantity of hardening element can be maintained in solution and an optimized yield strength can be reached.
- T6 treatment can bring a good compromise between strength and elongation. Yield stress is generally about the same as in as-built condition, but elongation is increased. However, an increase in porosity is generally observed during the solution heat treatment, as long as the distortion during quenching. So SHT combined with HIP, and quenching at lower rates could potentially increase the properties while avoiding such problems. Solution heat treatment step can be shorter than on cast alloys since microstructure is very fine on as-LBMed samples.
- If high base plate temperature strategy is selected to limit internal stresses, a temperature range typical of Artificial Aging must be selected (140/180 °C) to avoid under or over aging. If the machine is not equipped with a base plate heater, the same method can be put in place after manufacturing: in this case, the treatment is called Direct Aging.

9 Fatigue behaviour

Influence of heat treatment on fatigue behaviour has been studied by Aboulkhair *et al.* [26]. A base plate preheating of 180°C has been used in order to minimise residual stresses and reduce scatter. Batches were either machined or let as-built and T6 heat treated or not (SHT 1h 520°C, AA 6h 160°C). Uniaxial load-controlled at 30Hz tests were performed with R=0.1. Resultant S-N curves are presented in Figure 81. It shows that the influence of heat-treatment is greater than the surface profile one. T6 treatment significantly improves the fatigue resistance, especially at low stress levels. It is suggested that the increase in fatigue strength is due to a more ductile structure after T6 compared to as-built one.

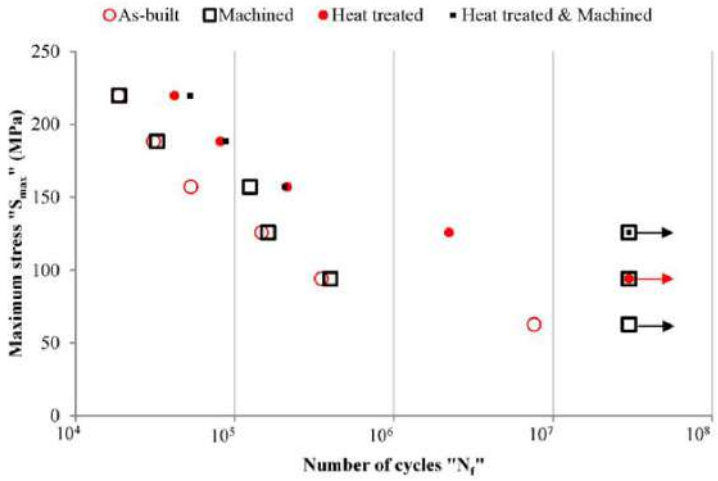

Figure 81: S-N curves superimposed for all the investigated conditions, namely, (1) as-built, (2) heat treated, (3) machined, and (4) heat-treated & machined. Results on this plot are average values determined from three replicates at each data point [26]

The influence of combined HIP+T6 on cast samples was performed by Hafenstein et al. [23]. The different configurations are given in the paragraph dealing with the hardness. Results are shown in Figure 82. First, it can be observed that the porosity amount has a very significant effect on the fatigue life as shown by the difference between high and low porosity as cast samples. However, the effect of thermal treatment, especially T6 is negligible as compared to as cast material. This shows that the first mechanism of failure is the porosity. However, when porosity amount is reduced the effect of heat treatment is much more pronounced. Indeed, hp_3 configurations, which are after HIP and separate SHT and ageing are greater. The best fatigue limit is obtained for samples subjected to combined HIP+SHT+Quench and separated ageing. This may be due to a combination of factors: porosity reduction and precipitation hardening.

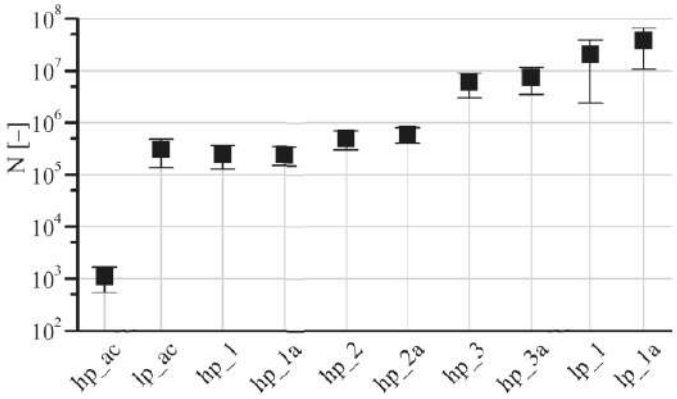

Figure 82: Fatigue resistance of the investigated samples depending on the performed thermal treatment [23]

Uzan et al. studied the fatigue behaviour of samples in as-built, stress-relief and HIP conditions [14]. Tests were performed using a rotating beam machine at 50 Hz and R=-1. Wohler curves are shown in Figure 83. Firstly and considering only as-built and stress relief samples (figure 83), it can be observed that the fatigue resistance is greater for as-built condition than stress-relief. Note that the density of stress-relieved sample was lower than for as-built specimens (respectively 2.616 g/cm^3 and 2.645 g/cm^3). However, this effect shouldn't be the major one, but the difference might be due to the difference in residual stresses amount. Polishing has no significant influence compared to machining when working with as-built samples. However, both as-built and stress-relief conditions lead to a lower fatigue resistance than Al 6061-T6. It can be concluded that amount of porosities has higher impact on Fatigue than initial residual stresses. Note that the stress relief samples present a lower density than as-built specimen; this may be attributed to thermally induced porosities due to coarsening of hydrogen porosities at high temperature.

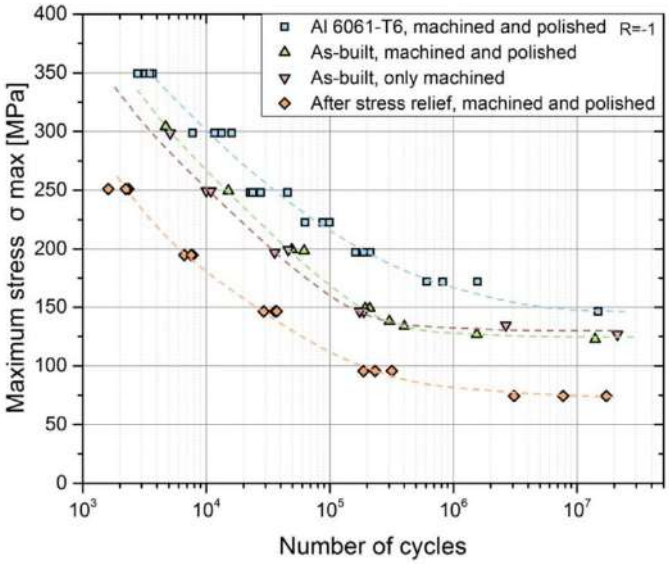

Figure 83: S–N curves of LBM AlSi10Mg specimens (machined and polished and only machined) in as-built and heat-treated conditions. Data for Al-6061-T6 are shown for comparison [14]

Uzan et al. also performed fatigue tests on HIPed samples. The formation of specific surface defects (depressions or dimples) was observed in the HIP-treated specimens [14]. The formation mechanism of such defects was attributed to a plastic deformation of the metal into subsurface pores (figure 84). These dimples cause considerable roughening of the surface after HIP, such that additional machining or grinding is required to restore surface smoothness.

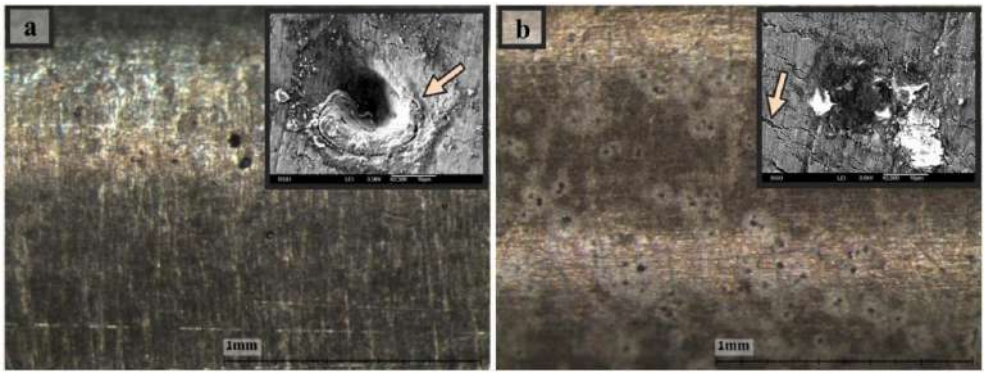

Figure 84: OM images and HRSEM magnification (inserts) of the surface after SR+HIP at 250 °C (a) and 500 °C (b) [14]

S-N curves are presented in Figure 85. It is interesting to note than even if samples HIPed at 250 °C have more defects than at 500 °C (density is respectively 2.622 g/cm3 vs 2.656 g/cm3, which is greater than the as-built density2.645 g/cm^3), the fatigue resistance is greater for these samples. The surface defects seem to induce a slight reduction of fatigue life. HIP at 250 °C gives fatigue limit similar to stress relief, and HIP at 500 C gives the lowest fatigue limit to around 50 MPa at 10^7 cycles.

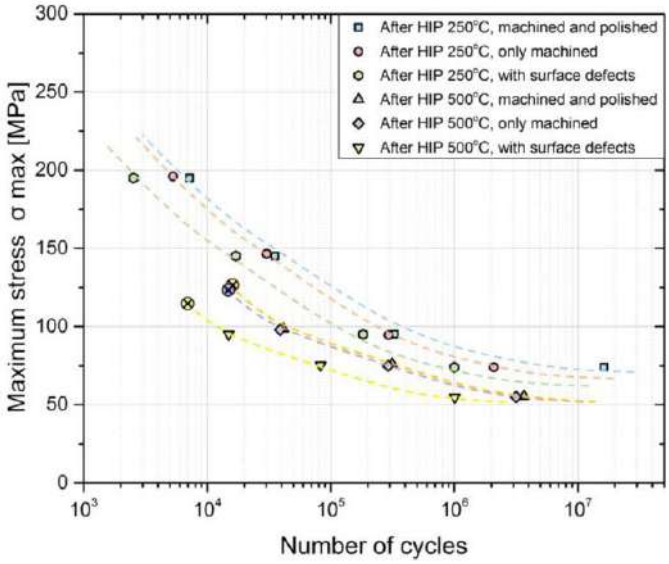

Figure 85: S–N curves of AM AlSi10Mg specimens after SR+HIP treatments [14]

Fracture surfaces of these samples in the overload zone are presented in Figure 86. In as-built specimens the overload fracture showed shallow dimples with their scale was similar to the cellular eutectic microstructure. For SR samples, the final fracture area displayed a ductile fracture with relatively deep dimples, as compared to the as-built specimens. Pores were clearly observed in the fracture surface. This type of overload (catastrophic) fracture was also observed for stress-relieved specimens printed in the Z direction after tensile tests. The crack propagation in SR+HIP-treated samples at 250 °C displayed the same morphology as seen in the SR specimens. Nevertheless, the size of the pores observed in the final fracture area of the former was significantly larger than in the latter specimens. This is very surprising since HIP is meant to reduce porosity amount and defect size. A significant difference was observed for samples that underwent SR +HIP at 500 °C. Huge dimples were apparently initiated by large Si precipitates of average size in the 2–5 µm range.

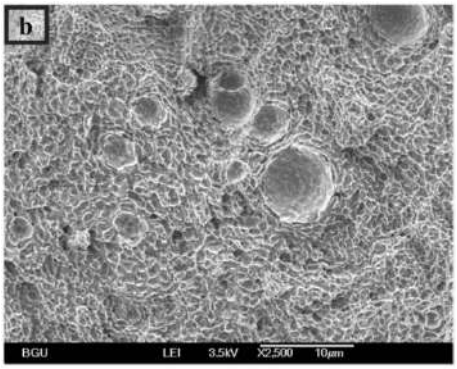

(a) As-built condition

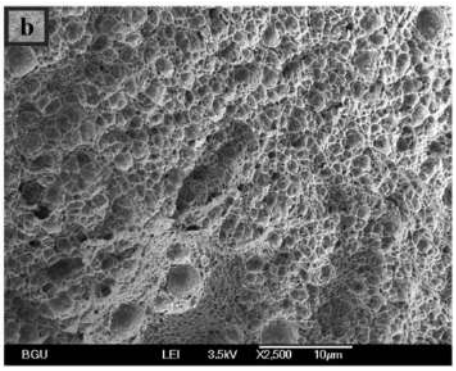

(b) Stress-relieved

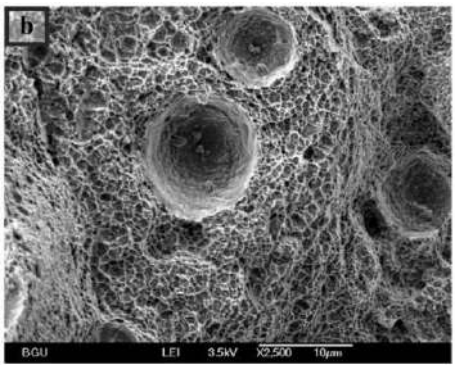

(a) SR + HIP 250 °C

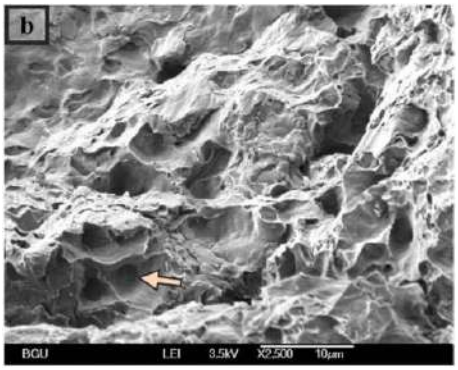

(a) SR + HIP 500 °C

Figure 86: HRSEM images of the overload fracture surface of AlSi10Mg specimens after different heat treatments [14]

Zhang *et al.* studied the fatigue property of selective laser melting AlSi10Mg samples with different heat treatments [27]. The samples were tested in the state of as-built condition, stress relief treatment (300°C for 2 h), solution treatment (530°C for 1h) and solution + artificial aging treatment (170°C for 12 h). Fatigue tests were performed with uniaxial sinusoidal cyclic loading with a stress ratio of R=-1 and a frequency of 15 Hz.

The results presented in Figure 87 show that the fatigue performance of as-built samples is the highest compared with that of heat treatment samples i.e., the heat treatments reduce the fatigue life. The fatigue life of the samples after T6 treatment is slightly lower than that of samples after SR treatment, samples after ST treatment exhibit the lowest fatigue life. The fatigue limitation of as-built samples is 90 MPa. Authors highlight that these results are lower than other published studies [26][28]in which different stress ratios are used.

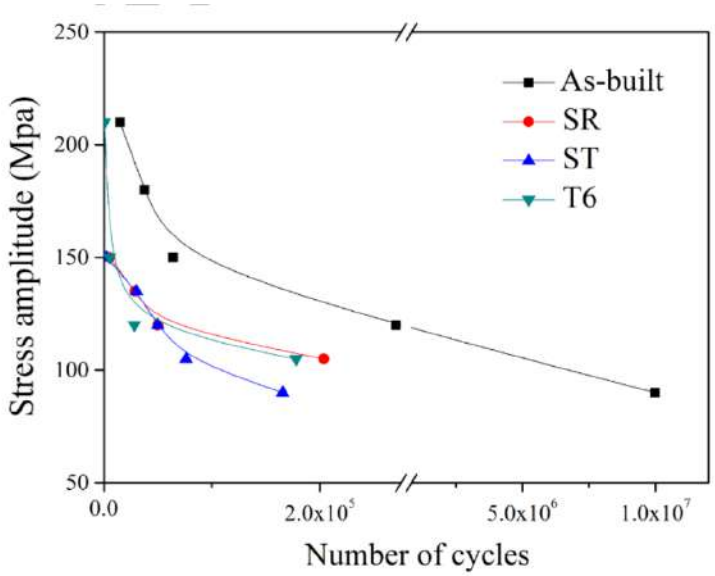

Figure 87 : S-N curves of AlSi10Mg samples [27]

It was found that the fatigue property was closely related to the yield strength as shown in Figure 88.

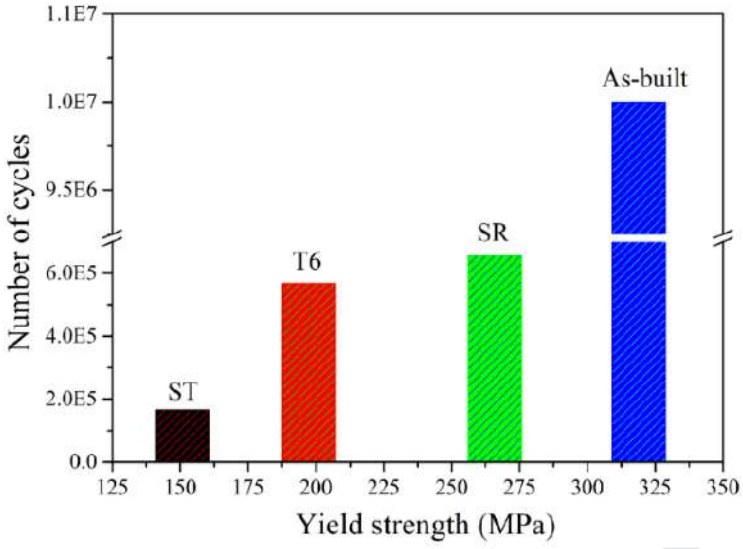

Figure 88: Correlation between fatigue life and yield strength of LBM AlSi10Mg [27]

A link was made between microstructure and fatigue resistance. As-built samples display the highest fatigue property due to the continuous network dendrite Si. Heat treatments change the microstructure, dendrite Si breaks into separated particles. The formation and coarsening of separated Si particles result in the decrease of fatigue property. During the heat treatment, Si particles precipitate, gather and grow up, which cause the increase of size and decline of number of Si particles. It is assumed that the dendrite width is the Si particle size of as-built sample. The correlation between fatigue property and Si particle size is presented in Figure 89. With the increase of Si particle size, the fatigue property gradually decreases. However, after artificial aging, the fatigue property of the sample increases. This is mainly due to the precipitation of MgxSi.

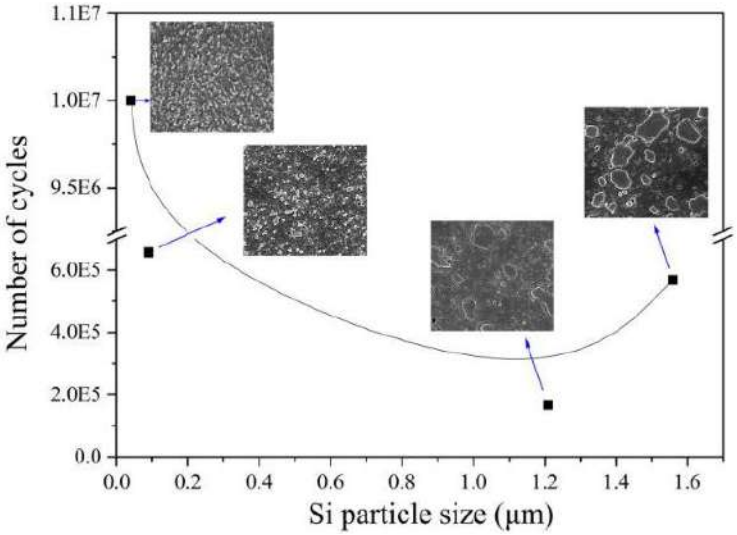

Figure 89: Correlation between fatigue property and Si particle size [27]

Brandl *et al.* studied the fatigue behaviour of printed AlSi10Mg according to different orientations (0°, 45° and 90°), base plate temperature (30°C and 300°C) and heat treatment (as built or T6) [28]. T6 heat treatment was as the following: Solution heat treatment for 6 h at 525 C, room temperature water quench and artificial ageing for 7 h at 165°C. A test frequency of approximately 108 Hz and a stress ratio of R = 0.1 were used. The HCF tests were terminated at $3x10^7$ cycles. Tension-tension was the solicitation mode. S-N curves are plotted in Figure 90 to Figure 92.

Main results are the followings:

- For samples built with a base plate at 30°C and subjected to a T6 heat treatment, the fatigue resistance is higher for the ones built at 0° than at 45° and at 90° direction.
- For samples built with a base plate at 300°C: T6 increases the fatigue resistance considerably whatever the orientation considered. Additionally, no impact on orientation can be highlighted in this configuration.
- Among all the specimens submitted to a T6 heat treatment, if the baseplate is fixed to 30°C better fatigue resistance is found for specimens built at 0° whereas if the base plate is fixed to 300°C fatigue resistance follow similar trends for specimens built in the 3 different directions

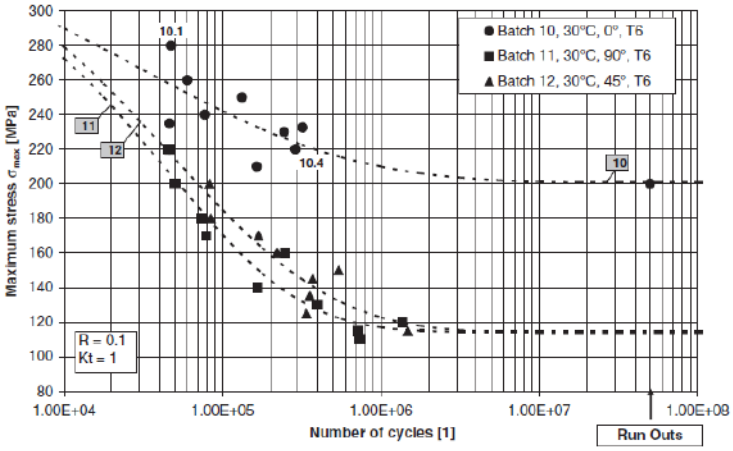

Figure 90: Influence of building direction on fatigue behaviour of 30°C / T6 samples [28]

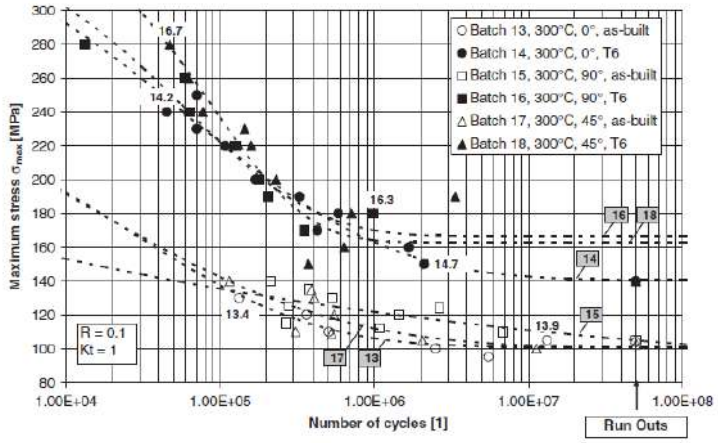

Figure 91: Influence of building direction and T6 treatment on fatigue behaviour of 300°C [28]

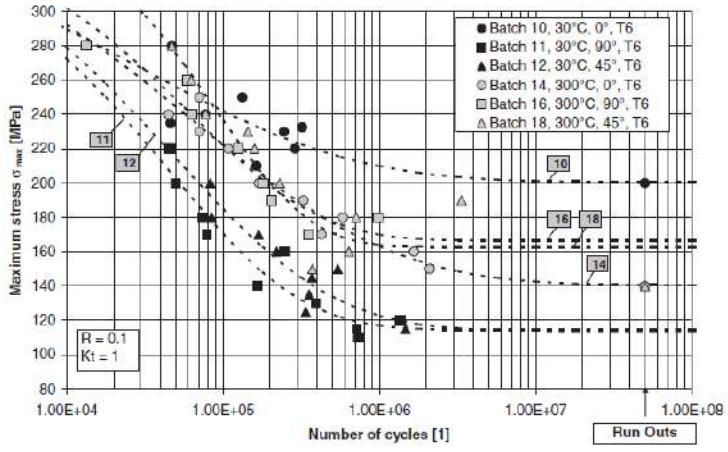

Figure 92: Comparison of T6 samples built at different base plate temperatures [28]

Brandl *et al.* indicates that porosity has the most detrimental effect on fatigue properties of$AlSi_{10}Mg$ made by LBM, especially when pore size and amount exceed certain values [28]. When either pore size or amount of porosity is reduced below a critical level, the next mechanism in the hierarchy becomes operational and dominates fatigue behaviour, e.g. microstructural features. This contributes to an explanation of why T6 has the most considerable impact on the fatigue resistance. The microstructure was homogenized, microstructural differences (e.g. heat-affected zones) were eliminated, the interdentritic eutectic Si-particles have become spheroidal. T6 also seems to increase ductility as the area of forced fracture showed dimples in contrast to the as built samples. The elongation of failure in the static

tensile tests, however, did not significantly increase or decrease at the 300°C samples after T6, but increased considerably at the 30°C samples. A further observation was that the fatigue resistance of the 300°C samples is comparable in the 0°, 45°, and 90° direction, in contrast to the 30°C samples. The building direction, however, showed the least considerable impact compared to the other factors. It can be imagined that the 300°C platform heating leads to fewer imperfections (e.g. non-melted spots), as the laser beam can heat up to higher temperatures and the cooling rate and distortion is reduced. Furthermore, the 300°C heating leads to fewer residual stresses, which might also contribute to a higher fatigue resistance. Fewer imperfections can also be the reason for a higher fatigue resistance in the 45° and 90° direction at 300°C platform temperature than at 30°C. A positive effect of fewer imperfections becomes especially evident in the 45° and 90° direction. In the 0° direction, the effect cannot be seen as clearly as imperfections are aligned parallel to the load (smallest notch-effect). As already mentioned above, additive manufactured components generally show the highest static and dynamic strength in the 0° direction for that reason. The presented fatigue results verify this common tendency as the 30°C samples showed the highest dynamic strength in the 0° direction. It was also figured out that static tensile strength and fatigue limit significantly correlate with each other.

The following main results were obtained:

- After T6 treatment, the microstructure is homogenous, i.e. dendrites, laser traces, and heat affected zones dissolved, and Si-particles formed to a globular shape. As no significant microstructural difference between 0°, 45°, and 90° can be highlighted, no difference in fatigue behaviour has been found in the case of hot platform temperature (300°C) during manufacturing.
- The area of forced-fracture of the T6 samples showed pronounced dimples in contrast to the as-built samples.
- The fatigue limit and static tensile strength significantly correlate with each other.
- In contrast to samples built at 300°C, samples built at 30°C show a higher fatigue resistance in 0° than in 45° and 90° direction.

From the results, the following main conclusions can be drawn:

- The combination of 300°C baseplate heating and T6 post treatment is a valuable approach to increase the fatigue resistance (and static tensile strength) and neutralize the differences in fatigue life for the 0°, 45°, and 90° directions.
- Despite the porosity and imperfections observed, the fatigue resistance of the samples is very high compared to the standard EN 1706. Indeed, according to EN 1706, the fatigue resistance to rotating bending of AlSi10Mg(Fe) at $5x10^7$ cycles is 60–90 MPa. Whereas here, fatigue limit was about 140-160 MPa in the best condition, *ie* built at 300°C and T6 heat treated.

Domfang and al. investigated the influence of the defects size on the Fatigue limit using the Murakami/Kitagawa methodology [29] [30]. In the Kitagawa diagram of Figure 93, the Fatigue limit is assessed versus the defects size represented by the Murakami's parameter (square value of area). A comparison of as-produced samples versus samples after classical T6 treatment was assessed. Moreover, the Figure 93 exhibits results for specimen parallel to the built plate (XY) and perpendicular to the built plate (Z). It is to note that in order to extend the range of this study, artificial spherical defects were introduced by electro discharge machining (EDM) to describe the part of the curve exhibiting the largest defects.

The Fatigue samples were prepared using a EOS M400 machine with the following strategy:

- Samples MA: stress relief treatment (300°C – 2 hours) and machining,
- Samples T6: stress relief treatment (300°C – 2 hours) + T6 treatment and machining.

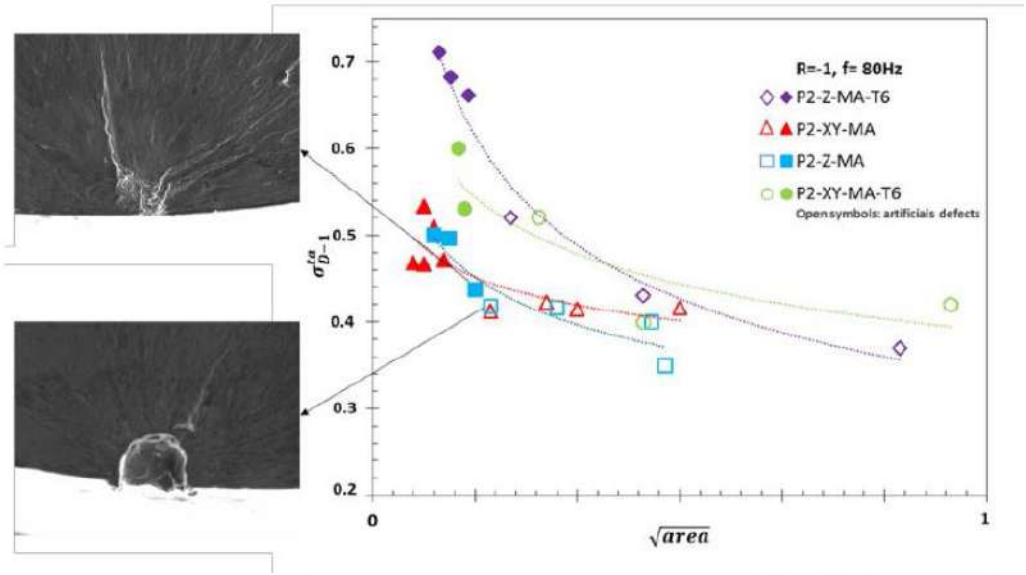

Figure 933: Kitagawa diagram for AlSi10Mg samples produced by LBM for as-produced specimen (MA) and specimen after classical T6 treatment [29] [30]. For a given condition, curves with and without artificial spherical EDM indentation are proposed

The Figure 93 led to the following conclusions:

- For the same defects size for non-heated material (MA samples), there is no anisotropy effect due to the direction of production,
- The fatigue resistance improvement (after T6 treatment) is less pronounced in presence of big defects (right side of the curves), but is significant in presence of small defects.

The impact of defect size have been quantify Through the Kitagawa type diagrams. It was observed that:

- It exists a value of defect size beyond that the fatigue limit is controlled only by the defect size, below that size, the fatigue limit is controlled by the defects size and the microstructure (right side of the curve).

Partial conclusion on Fatigue behaviour:

- Fatigue resistance is high in as-built components.
- Stress-relief decrease the fatigue limit by breaking the eutectic network.
- SHT/T6 tends globally to increase the fatigue behaviour with the following remarks:
  - If the built plate is not heated, the samples present a strong anisotropy with a significant deceasing of Fatigue properties in the z direction (25% for 10^5 cycles),
  - With a heated baseplate (300°C), the anisotropy disappeared. As compared to a non-heated in the XY direction, we can note a knock down of 10% in stress for 10^5 cycles.
- The defects size and the thermal treatment have a strong influence on the Fatigue limit. For a large quantity of defects, the sampling direction and the thermal treatment have a limited influence on the Fatigue limit.

10 Impact resistance

Rosenthal *et al.* studied the impact resistance of AlSi10Mg according to different heat treatments [22]. The evolution of impact energy is very well correlated to the elongation (see Figure 68). Generally, the higher the temperature, and the longer the treatment, the more ductile the material so the higher the impact energy. However, a semi-fragile behaviour is observed for the sample treated at 200°C. It is supposed that the mechanism involved here is the fine precipitation of Si needles like it was evidenced on Figure 30.

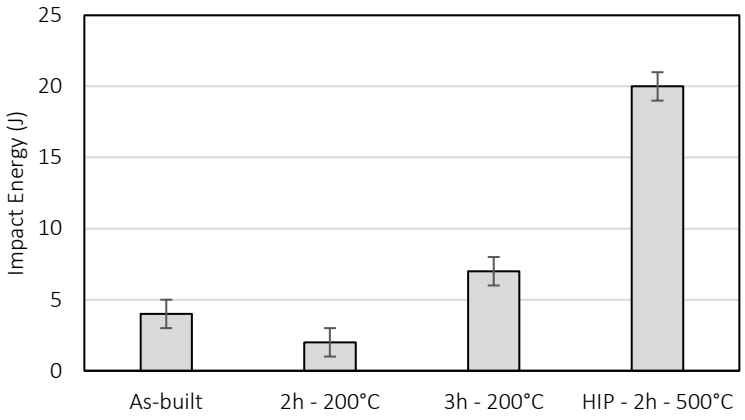

Figure 94 : Impact energy of AlSi10Mg samples according to different heat treatments [22]

Surface fracture of Charpy test samples have been observed. Samples were built vertically. Contrary to tensile samples, melt pools tracks are visible on as-built and heat treated to 200 °C samples, whereas on heat treated to 300°C and HIP samples there are not. It means that the fracture mode, namely the fracture speed, has an influence on how the material behaves and breaks. In case of Charpy tests, melt pools borders acts as weak points separating layers and detaching segments; this is very clear for the typical T5 treatment and less evident for the modified T5 treatment (less ductile specimen).

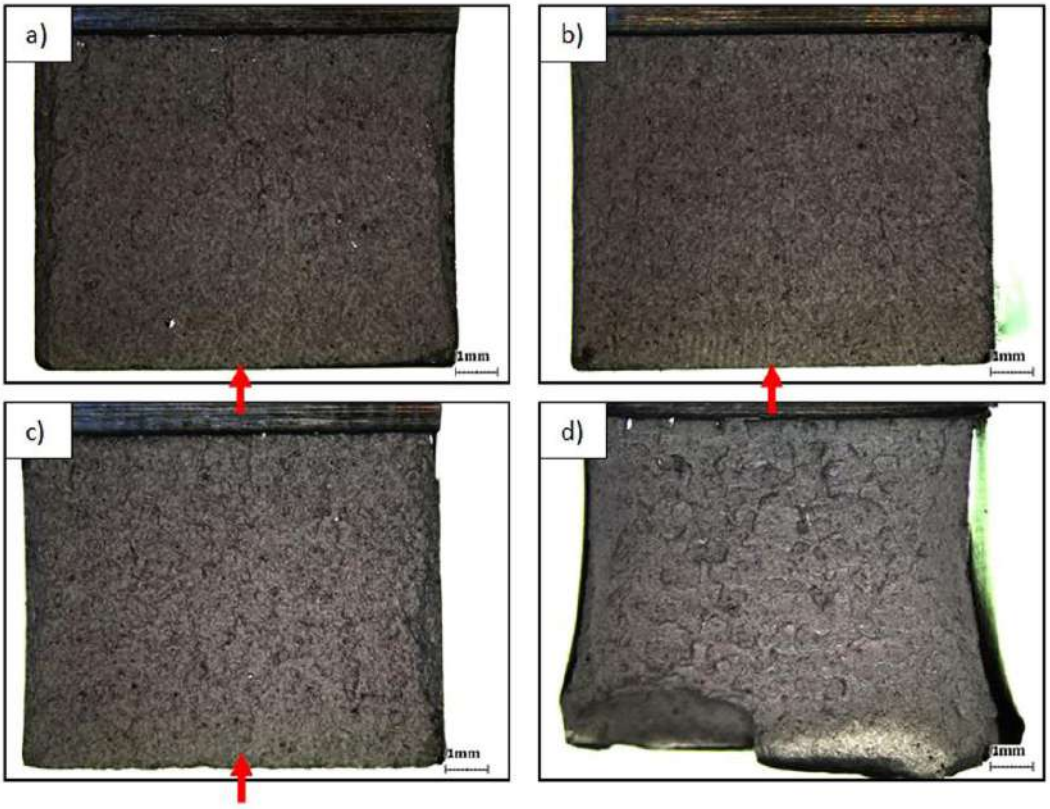

Figure 95 : Optical images of the Charpy fracture surface's macro-features of the AlSi10Mg LBM alloy; a) as-built, showing the track segments at the end of the Charpy fracture (marked by red arrows), unlike the tensile fracture; b) modified T5 treatment, noticeable track segments, but less than in the as-built condition; c) typical T5 treatment, barely showing any track segments; d) HIP treatment, completely "erased" the traces of the hatching strategy.

11 Conclusion

- As-built fine cellular microstructure gives high strength with low ductility and high anisotropy on elongation. However, the Fatigue resistance is high with this condition.
- The main microstructure evolution happens at 300 °C where the eutectic network is disrupted. Below this temperature, only slight disruption is observed with fine Si precipitation in α-Al. Above 300°C, Si particles start to grow and rearrange and α-Al cells disappear to form a matrix where large Si precipitates are found.
- Stress-relief leads to fine cellular microstructure disruption and Si coarsening; therefore, there is a material softening where mechanical properties are low but elongation is high. However, the stress relief induces a significant reduction of manufacturing residual stresses. It is to note that stress relief reduces the Fatigue behaviour by breaking the fine cellular eutectic network.
- Direct ageing at low temperatures leads to a brittle behaviour that is not fully understood. No data of direct ageing behaviour on Fatigue properties has been identified.
- T6 treatment seems to be the best option in order to have high tensile properties with good elongation. However, the cycle needs to be improved in order to be more relevant according to the microstructures deriving from LBM. It is to note that the quench rate must be higher to 3°C/s to optimize the T6 treatment. As compared to samples just stress relieved, the T6 samples exhibit also good Fatigue properties; the anisotropy can be reduced by heating the base plate during manufacturing.
- The duration of the SHT (included in the T6 treatment) has a strong influence on the quantity of gas porosities.
- The base plate can be heated up to 170°C without influence on the fine cellular microstructure morphology. However, the manufacturing residual stresses are reduced.
- (HIP+T6) does not change the microstructure as compared to a (T6) treatment. However, the HIP or the combined HIP/T6 in the same furnace needs further investigation to check their real influence on the Fatigue properties.

12 Suggestion for new heat treatment

It was evidenced that there is a lack of information concerning the following items in literature data and the impact of each of them on microstructure. As a consequence, it is really necessary to firstly investigate these points on sample coupons before going to complex shape parts.

1. SHT conditions: influence of the SHT temperatures and/or time duration in order to limit the increase of porosity while maintaining acceptable elongation values.
2. Quenching conditions: influence of quenching rate in order to avoid distortion and while creating a metastable state with saturated Si in α-Al.
3. Aging conditions: find the most relevant ageing after SHT + quenching in order to obtain quickly the peak hardness.
4. New aging method: characterize direct ageing at low temperatures which can sufficient for some applications in spite of samples brittleness.
5. New thermal treatment: evaluate the relevance of HIP+SHT combined in order to perform a T6 treatment directly in a HIP furnace. Compare with classical separate HIP treatment.
6. Manufacturing conditions: Understand the role of base plate temperature and/or stress relief at low temperature on potential direct ageing and on the potential reduction of manufacturing residual stresses.

After investigations on sample coupons, different manufacturing strategies will be proposed but additional tests will be necessary to verify their applicability on real parts or on representative coupons.

It will be necessary to investigate the following aspects of parts specificities on the microstructures homogeneity, porosities (number & size) and deformations:

1. Thickness variation
    a. Adapt the quenching strategy: transfer time, cooling rate,

   b. Verification of HIP + SHT combined conditions,
   c. Verification of residual stresses on thicker sections.
2. Edge and radius effect
   a. Influence on the quenching strategy,
   b. Verification of HIP + SHT combined conditions,
3. Homogeneity from the bottom to the top of parts
   a. Verification of the manufacturing conditions influence,

As a consequence, the proposed strategy for the experimental investigations to perform will follow the chronologic following sequences:

1. Sample coupons
   a. Optimization of SHT conditions on both T4 and T6 conditions,
   b. Influence on deformation due to quenching conditions,
   c. Determination of a costly effective aging parameters,
   d. Assessment on HIP + SHT combined treatment,
   e. Assessment on direct aging,
   f. Manufacturing conditions influence.
2. Representative coupons
   a. Parts thickness variation effect,
   b. Parts shape influence,
   c. Microstructure disparities depending on position in the parts.

End

13 References

[1] ASM International, «Elements of Metallurgy and Engineering Alloys,» 2008.

[2] M H Jacobs, «TALAT Lecture 1204 Precipitation Hardening,» 1999.

[3] G. A. Edwards, K. Stiller, G. L. Dunlop et M. J. Couper, «The precipitation sequence in Al-Mg-Si alloys,» *Acta Materialia,* vol. 46, pp. 3893-3904, 1998.

[4] B. BARLAS, «Bruno BARLAS Etude du comportement et de l ' endommagement en fatigue d ' alliages d ' aluminium de fonderie Remerciements,» 2004.

[5] D. L. Zhang et L. Zheng, «The quench sensitivity of cast Al-7 Wt Pet Si-0.4 Wt pct Mg alloy,» *Metallurgical and Materials Transactions A: Physical Metallurgy and Materials Science,* vol. 27, pp. 3983-3991, 1996.

[6] J. Fiocchi, A. Tuissi, P. Bassani et C. A. Biffi, «Low temperature annealing dedicated to AlSi10Mg selective laser melting products,» *Journal of Alloys and Compounds,* vol. 695, pp. 3402-3409, 2017.

[7] T. Kimura et T. Nakamoto, «Microstructures and mechanical properties of A356 (AlSi7Mg0.3) aluminum alloy fabricated by selective laser melting,» *Materials and Design,* vol. 89, pp. 1294-1301, 2016.

[8] K. V. Yang, P. Rometsch, C. H. J. Davies, A. Huang et X. Wu, «Effect of heat treatment on the microstructure and anisotropy in mechanical properties of A357 alloy produced by selective laser melting,» *Materials and Design,* vol. 154, pp. 275-290, 2018.

[9] X. P. Li, X. J. Wang, M. Saunders, A. Suvorova, L. C. Zhang, Y. J. Liu, M. H. Fang, Z. H. Huang et T. B. Sercombe, «A selective laser melting and solution heat treatment refined Al-12Si alloy with a controllable ultrafine eutectic microstructure and 25% tensile ductility,» *Acta Materialia,* vol. 95, pp. 74-82, 2015.

[10] W. Li, S. Li, J. Liu, A. Zhang, Y. Zhou, Q. Wei, C. Yan et Y. Shi, «Effect of heat treatment on AlSi10Mg alloy fabricated by selective laser melting: Microstructure evolution, mechanical properties and fracture mechanism,» *Materials Science and Engineering A,* vol. 663, pp. 116-125, 2016.

[11] J. H. Rao, Y. Zhang, X. Fang, Y. Chen, X. Wu et C. H. J. Davies, «The origins for tensile properties of selective laser melted aluminium alloy A357,» *Additive Manufacturing,* vol. 17, pp. 113-122, 2017.

[12] N. Takata, H. Kodaira, K. Sekizawa, A. Suzuki et M. Kobashi, «Change in microstructure of selectively laser melted AlSi10Mg alloy with heat treatments,» *Materials Science and Engineering A,* vol. 704, pp. 218-228, 2017.

[13] M. Fousova, D. Dvorsk, A. Michalcov et D. Vojtch, «Changes in the microstructure and mechanical properties of additively manufactured AlSi10Mg alloy after exposure to elevated temperatures,» *Materials Characterization,* vol. 137, pp. 119-126, 2018.

[14] N. E. Uzan, R. Shneck, O. Yeheskel et N. Frage, «Fatigue of AlSi10Mg specimens fabricated by additive manufacturing selective laser melting (AM-LBM),» *Materials Science and Engineering A,* vol. 704, pp. 229-237, 2017.

[15] A. Aversa, M. Lorusso, F. Trevisan, E. Ambrosio, F. Calignano, D. Manfredi, S. Biamino, P. Fino, M. Lombardi et M. Pavese, «Effect of Process and Post-Process Conditions on the Mechanical Properties of an A357 Alloy Produced via Laser Powder Bed Fusion,» *Metals,* vol. 7, p. 68, 2017.

[16] J. Mertens, A., Dedry, O., Reuter, D., Rigo O. and Lecomte-Beckers, «Thermal Treatments of AlSi10Mg Processed By Laser Beam Melting,» *Solid Freeform Fabrication Symposium,* vol. 1, pp. 1007-1016, 2015.

[17] K. V. Yang, P. Rometsch, T. Jarvis, J. Rao, S. Cao, C. Davies et X. Wu, «Porosity formation mechanisms and fatigue response in Al-Si-Mg alloys made by selective laser melting,» *Materials Science and Engineering A,* vol. 712, pp. 166-174, 2018.

[18] P. Delroisse, P. J. Jacques, E. Maire, O. Rigo et A. Simar, «Effect of strut orientation on the microstructure heterogeneities in AlSi10Mg lattices processed by selective laser melting,» *Scripta Materialia,* vol. 141, pp. 32-35, 2017.

[19] U. Tradowsky, J. White, R. M. Ward, N. Read, W. Reimers et M. M. Attallah, «Selective laser melting of AlSi10Mg: Influence of post-processing on the microstructural and tensile properties development,» *Materials and Design,* vol. 105, pp. 212-222, 2016.

[20] Y. Bai, Y. Yang, Z. Xiao, M. Zhang et D. Wang, «Process optimization and mechanical property evolution of AlSiMg0.75 by selective laser melting,» *Materials and Design,* vol. 140, pp. 257-266, 2018.

[21] M. Cabrini, S. Lorenzi, T. Pastore, S. Pellegrini, E. P. Ambrosio, F. Calignano, D. Manfredi, M. Pavese et P. Fino, «Effect of heat treatment on corrosion resistance of DMLS AlSi10Mg alloy,» *Electrochimica Acta,* vol. 206, pp. 346-355, 2016.

[22] I. Rosenthal, R. Shneck et A. Stern, «Heat treatment effect on the mechanical properties and fracture mechanism in AlSi10Mg fabricated by additive manufacturing selective laser melting process,» *Materials Science and Engineering A,* vol. 729, pp. 310-322, 2018.

[23] S. Hafenstein, M. Brummer, M. Ahlfors et E. Werner, «Combined hot isostatic pressing and heat treatment of aluminum A356 cast alloys,» *HTM - Journal of Heat Treatment and Materials,* vol. 71, pp. 117-124, 2016.

[24] F. Fracasso, «INFLUENCE OF QUENCH RATE ON THE HARDNESS OBTAINED AFTER ARTIFICIAL AGEING OF AN Al-Si-Mg ALLOY,» 2010.

[25] L. Pedersen et L. Arnberg, «The Effect of Solution Heat Treatment and Quenching Rates.pdf,» *Metallurgical and Materials Transactions A,* vol. 32A, p. 525, 2001.

[26] N. T. Aboulkhair, I. Maskery, C. Tuck, I. Ashcroft et N. M. Everitt, «Improving the fatigue behaviour of a selectively laser melted aluminium alloy: Influence of heat treatment and surface quality,» *Materials and Design,* vol. 104, pp. 174-182, 2016.

[27] C. Zhang, H. Zhu, H. Liao, Y. Cheng, Z. Hu et X. Zeng, «Effect of heat treatments on fatigue property of selective laser melting AlSi10Mg,» *International Journal of Fatigue,* 2018.

[28] E. Brandl, U. Heckenberger, V. Holzinger et D. Buchbinder, «Additive manufactured AlSi10Mg samples using Selective Laser Melting (LBM): Microstructure, high cycle fatigue, and fracture behavior,» *Materials and Design,* vol. 34, pp. 159-169, 2012.

[29] J. N. Domfang Ngnekou, Y. Nadot, G. Henaff, J. Nicolai et L. Ridosz, «Influence of defect size on the fatigue resistance of AlSi10Mg alloy elaborated by selective laser melting (LBM),» *Procedia Structural Integrity,* vol. 7, pp. 75-83, 2017.

[30] J. N. D. Ngnekou, G. Henaff, Y. Nadot, J. Nicolai et L. Ridosz, «Fatigue resistance of selectively laser melted aluminum alloy under T6 heat treatment,» *Procedia Engineering,* vol. 213, pp. 79-88, 2018.

End of document

